Enhancing microbial self-healing of cementitious materials using natural fibre-based carriers

By

Tingxuan Yao

A thesis submitted in fulfilment of the requirements for the degree of Doctor of Philosophy

Supervisor: Professor Luming Shen

Co-Supervisor: Associate Professor Daniel Dias-da-Costa

School of Civil Engineering

Faculty of Engineering

The University of Sydney

2025

Contents

Acknowledgements

I have walked a long road, weathered storms, and endured quiet trails, just to place this thesis before you. Twenty-two years of learning have passed like a dream, sometimes heavy with rain, sometimes light with hope. In these humble words, I express my gratitude to those who have accompanied me along the way.

I would like to express my deepest gratitude to my supervisor, Professor Luming Shen, for his unwavering guidance and encouragement throughout this journey. His support not only shaped this research but also inspired me to pursue an academic path. At no point during my PhD did I feel alone or lost, thanks to his mentorship. I am also sincerely thankful to my co-supervisor, Associate Professor Daniel Dias-da-Costa, for his insightful suggestions and thoughtful discussions. His guidance was essential to the completion of this work. I would also like to thank Professor Abhijit Mukherjee of Curtin University for his generous advice and support, especially during the early stages of this research. His input and encouragement were deeply appreciated. I am deeply grateful for you all patient teaching. As a student dull as decayed wood, I could only grow through your tireless guidance.

I am deeply grateful to my family for their unwavering support and for granting me the freedom to explore my own path. Your trust has always given me the courage to step back when needed. And your unconditional acceptance has allowed me to grow into a confident person. My thanks go especially to Ms. Wan and Gu, my love and gratitude for you remain steadfast as enduring as ink on canvas.

I am grateful to the friends who walked alongside me, no one is an island, and this journey has not always been smooth. Your presence made all the difference. Thank you to Ethan Cao for your support and encouragement in every mountain and river we crossed, I count it a blessing to have met you. To Ricky Cheng, my companion throughout this journey, I could not have comet his far without you. To my friend Jiaming, in your words: until we meet again, may our reunion wash away the sorrows of a thousand years. To Nancy Tan, thank you for your constant support and companionship along the way. To someone whose name I do not write-like a quiet sun that never sets, or a soft-winged kiwi in the sky, you've been part of my journey in ways no page can hold.

To all who have walked beside me, supervisors, friends, and loved ones, your presence has shaped this journey in ways no words can truly capture. My gratitude is quiet but enduring.

Statement of Originality

I, Tingxuan Yao, hereby declare that to the best of my knowledge, the content of this thesis is my own work. This thesis has not been submitted for any degree or other purposes.

I, Tingxuan Yao, hereby declare that the intellectual content of this thesis is the product of my own work and that all the assistance received in preparing this thesis and sources have been acknowledged.

Signature:

Tingxuan Yao

Date: 17 July 2025

List of Publications

Submitted Manuscript:

T. Yao, Y. Cao, D. Dias-da-Costa, A. Mukherjee, L. Shen. *Synergistic effects of natural fibres as bacteria carrier and scaffold for bio-cementation*. Submitted to *Cement and Concrete Composites* (Manuscript ID: CCC-D-25-01934) on July 5, 2025.

Preparation Manuscript:

T. Yao, Y. Cao, D. Dias-da-Costa, A. Mukherjee, L. Shen. *A comparative evaluation of natural fibres and high porosity minerals as bacterial carriers for self-healing mortar*. Prepared to be Submitted to *Construction and Building Materials* in July 2025.

Conference Presentation:

T. Yao, D. Dias-da-Costa, A. Mukherjee, L. Shen (2025). Enhancing Self-Healing in Concrete Using Natural Fibers as Bacterial Carriers. 14th International Conference on Structural Integrity and Failure (SIF2025). UNSW Sydney Australia.

Authorship Attribution Statement

Chapter 4 of this thesis is submitted to "Cement and Concrete Composites" journal under the title "Synergistic effects of natural fibres as bacteria carrier and scaffold for bio-cementation". For this study, I carried out the experimental program, result collection and formal analysis. Moreover, the original draft of the publication was prepared by me.

Chapter 5 of this thesis is prepared to be submitted to "Construction and Building Materials" journal under the title "A Comparative Evaluation of Natural Fibres and High Porosity Minerals as Bacterial Carriers for Self-Healing Mortar". For this study, I carried out the experimental program, result collection and formal analysis. Moreover, the original draft of the manuscript was prepared by me.

Signature:

Tingxuan Yao, School of Civil Engineering, The University of Sydney, NSW 2006, Australia

Date: 10 July 2025

As the primary supervisor for the candidature upon which this thesis is based, I can confirm that the authorship attribution statements above are correct.

Signature:

Professor Luming Shen, School of Civil Engineering, The University of Sydney, NSW 2006, Australia

Date: 10 July 2025

Use of Generative Artificial Intelligence Statement

During the preparation of this thesis, ChatGPT was used to assist with text enhancement. Where text was modified by generative AI, I reviewed the resulting content for any errors, inaccuracies, or biases, and made further modifications as necessary. I take full responsibility for the submitted thesis, confirms that the work is my own, and has used generative AI in accordance with appropriate use parameters.

Abstract

Cracks in cement-based materials pose a significant threat to long-term durability and service life, especially under harsh environmental exposure. To address this, bacteria-based self-healing systems have been developed, leveraging microbial-induced calcium carbonate precipitation (MICP) to autonomously repair cracks. However, achieving effective healing particularly in wider cracks requires the use of suitable carrier materials that protect bacterial viability and facilitate consistent calcium carbonate deposition. This thesis investigates the role of different carrier types in enhancing self-healing efficiency. Three carriers -jute fibre, flax fibre, and expanded perlite aggregate (EPA)—were systematically evaluated for their ability to serve as bacterial protective carrier in mortar, focusing on their influence on crack closure, water permeability, and mechanical performance under practical conditions.

The research is structured in two main parts. The first examines the interaction between the bacterium *Sporosarcina pasteurii* and each carrier material. Through bacterial growth analysis, scanning electron microscopy (SEM), and Fourier-transform infrared spectroscopy (FTIR), it was found that natural fibres, especially jute, support stronger bacterial colonisation and more extensive biopolymer formation than EPA. These biopolymer layers act as scaffold structures, enhancing bacterial retention and enabling more effective and sustained calcium carbonate precipitation. The improved microbial compatibility observed in jute and flax fibres is attributed to their rougher surfaces and higher water absorption capacities, which promote the development of bio-mineralisation networks critical to the healing process.

The second part of the study evaluates the healing performance of mortar specimens embedded with the three carriers under controlled crack formation and curing conditions. Bacterial spores

were immobilised on the carriers at 1% and 1.5% volume dosages, and healing was monitored over 56 days. Crack healing was assessed using image analysis, permeability testing, and mechanical property evaluation. Jute-based specimens achieved the highest performance, successfully healing cracks up to 1.23 mm wide and demonstrating significant reductions in water permeability. Flax specimens showed moderate effectiveness, particularly in cracks under 1 mm, while EPA consistently underperformed across all metrics due to its smoother surface and weaker microbial interaction. SEM images revealed denser and more continuous $CaCO_3$ deposition in fibre-based specimens, with jute outperforming flax in both surface and depth healing.

Additional factors such as crack depth and dosage effects were also analysed. Carriers not only facilitated microbial attachment but also acted as bridges across crack faces, enhancing stability and guiding mineral deposition deeper into the crack zone. Interestingly, increasing the fibre content beyond 1% did not always result in better healing and occasionally reduced mechanical properties, likely due to fibre agglomeration and uneven distribution. These findings suggest that an optimal balance between carrier concentration and matrix integration is necessary for reliable self-healing.

In conclusion, this thesis demonstrates that the synergy between bacterial activity and natural fibre carriers, particularly jute, significantly enhances the self-healing capacity of mortar. By providing both mechanical support and favourable microenvironments for microbial growth and biopolymer formation, jute enables robust and repeatable healing even under challenging crack conditions. In contrast, EPA's limited surface interaction restricts its healing potential, underscoring the importance of surface roughness, shape and aspect ratio retention in carrier design. Together, the insights from microbial interaction and healing performance evaluations

provide a comprehensive framework for developing more effective, sustainable, and application-ready self-healing cementitious systems.

Chapter 1: Introduction

1.1 General Introduction

Concrete is globally recognised for its high compressive strength, durability, and cost-effectiveness (Kumar 2023) . Although concrete is among the most widely used building materials, its inherent brittleness and susceptibility to cracking present significant challenges (Althoey, et al. 2023). These cracks weaken structures and make them last shorter. Cracks in concrete damage mechanical performance (Golewski 2023). They also allow harmful substances like water, chlorides, and carbon dioxide to penetrate. This accelerates structural degradation (Li, et al. 2024, Zhao, et al. 2021, Liu, et al. 2023). This process leads to the corrosion of steel reinforcement (Bidari, et al. 2024), which weakens the bond between concrete and steel (Capacci, et al. 2022). Over time, this results in spalling, where sections of concrete detach from the structure. Infrastructure such as bridges and highways is continuously exposed to harsh environmental conditions (Capacci, et al. 2022, De Belie, et al. 2002). Freeze–thaw cycles and de-icing salts accelerate the development of cracks (Matalkah and Soroushian 2018). Cracking also reduces the ability of structures to withstand seismic activity and heavy loading (Choi, et al. 2022). Traditional repair methods typically address only visible damage and do not prevent the formation of new cracks (Balakrishnan and Seidlitz 2018). Consequently, cracks often reoccur, creating a cycle of repeated interventions (Amran, et al. 2022) which places ongoing strain on maintenance budgets and resources.

Self-healing concrete is an innovative approach designed to improve the durability of concrete structures by enabling autonomous crack repair. (Nair, et al. 2022). Among the various self-healing mechanisms, microbial-induced calcium carbonate precipitation (MICP) has attracted

considerable attention due to its effectiveness and sustainability (Xue, et al. 2023). This approach leverages uratolytic bacteria, such as *Sporosarcina pasteurii*, to precipitate calcium carbonate ($CaCO_3$) in cracks, effectively sealing them and restoring mechanical properties (Wang and Wang 2025). The success of this technique depends largely on the bacterial carriers used, as they influence bacterial survival, adhesion, and overall healing efficiency (Elgendy, et al. 2025).

1.2 Importance of Carrier Materials

The bacterial carrier plays a crucial role in MICP-based self-healing concrete. It protects bacterial spores from the harsh alkaline environment of concrete, facilitates their activation upon crack formation, and ensures efficient calcium carbonate precipitation (Tang and Xu 2021). Three key carrier materials investigated in this study include:

- Jute Fibres: This natural jute fibres exhibit high water absorption capacity. Jute fibres enhance self-healing concrete by providing a porous, bacteria-friendly environment that supports long-term microbial activity for crack sealing (Rauf, et al. 2020). Their biodegradability aligns with sustainability goals, while reinforcing concrete tensile strength to reduce crack formation.

- Flax Fibre: Flax fibres have excellent water retention to ensure continuous hydration of the bacterial process and resist concrete alkalinity to maintain the long-term integrity of the carrier (Adibinia, et al. 2025). They are cost-effective and renewable, providing reliable performance at a low material cost.

- Expanded Perlite Aggregate (EPA): A lightweight, porous material traditionally used for bacterial encapsulation (Zamani, et al. 2020). Their synthetic matrices protect bacteria from harsh conditions, improving durability, while eco-friendly polymers reduce environmental impact.

Comparative analysis of these materials will help determine the most effective carrier for enhancing self-healing performance in concrete structures.

1.3 Research Gaps and Challenges

Despite significant advancements in self-healing concrete technology, several challenges remain:

- Limited understanding of carrier property influence: The impact of carrier material properties, such as shape, morphology, porosity, surface roughness, and water absorption, on bacterial activity and healing efficiency is not fully understood.

- Unexplored Mechanisms in Bacteria-Carrier Interactions: Existing studies primarily focus on carrier performance metrics (e.g., porosity, durability) but lack mechanistic insights into how carriers modulate bacterial behaviour The impact of carrier chemistry on bacterial adhesion and gene expression remains unexplored.

- Lack of Comparative Studies on Carrier Performance: Most studies focus on individual carrier materials rather than direct comparisons between different carriers.

- Unresolved Challenges in Healing Capacity: MICP is highly effective for microcracks but remains limited in its ability to restore structural continuity in cracks beyond the micro-scale. Enhancing bacterial retention and promoting calcium carbonate precipitation to improve overall healing capacity remains a critical challenge.

Addressing these gaps will enable the development of more effective and practical self-healing concrete solutions.

1.4 Research Objectives

The primary objective of this research is to evaluate the effectiveness of different bacterial carriers in enhancing the self-healing capability of concrete. Key objectives include:

- To investigate the interaction mechanisms between bacteria and carrier materials by analysing microstructural characteristics and mineralisation patterns.

- To examine the formation and colonisation behaviour of *Sporosarcina pasteurii* on jute, flax, and expanded perlite aggregate (EPA), and evaluate their role in facilitating the MICP process.

- To evaluate and compare the crack-healing performance of mortar specimens incorporating different bacterial carriers by measuring crack closure efficiency.

- To evaluate the capacity of different bacterial carriers to promote effective healing, with a focus on improving bacterial retention and calcium carbonate deposition within large crack volumes.

By achieving these goals, this study aims to advance the understanding of bacterial carrier materials and optimise their application in MICP-based self-healing concrete. The results of the study will contribute to the development of more durable and sustainable concrete structures, ultimately increasing the resistance of the built environment.

This research will advance knowledge on bacterial carriers for self-healing concrete, paving the way for practical applications in modern construction and infrastructure development.

1.5 Layout of Thesis

This thesis investigated the performance of bacteria based self-healing concrete and its content. Five chapters are included:

Chapter 1: Introduces the general background of concrete crack formation, hazards, MICP based self-healing concrete and their components. The research motivation is introduced, along with the objectives.

Chapter 2: Reviews the existing knowledge of Microbial-induced calcium carbonate precipitation (MICP) technology with an emphasis on its application in self-healing concrete. The current research on various bacterial carriers, including expanded perlite aggregate (EPA) and natural fibers such as jute and flax, is examined to understand their role in enhancing

bacterial viability and crack-healing efficiency. Subsequently, a review of recent advancements in self-healing concrete under different environmental conditions is presented.

Chapter 3: Describes the experimental program throughout this research

Chapter 4: This chapter details the methodological approach to investigating the synergy between bacteria and carrier materials in self-healing concrete. The key factors influencing bacterial adhesion, biopolymer formation, and calcium carbonate precipitation on jute, flax, and expanded perlite aggregate (EPA) are identified. The bacterial growth assessment and bio-cementation process are analysed using OD600 measurements, SEM imaging, and FTIR. The experimental outcomes illustrate how natural fibers enhance bacterial retention and mineralisation efficiency compared to EPA, providing insights into optimising bacterial carriers for self-healing concrete applications.

Chapter 5: This chapter evaluates the comparative effectiveness of natural fibers (jute and flax) and expanded perlite aggregate (EPA) as bacterial carriers in self-healing concrete. The influence of carrier shape, porosity, and surface properties on bacterial adhesion and calcium carbonate precipitation is analysed. Crack-healing efficiency is assessed through experimental investigations, including crack closure measurements, water permeability reduction, and SEM imaging.

Chapter 6: Draws conclusions and proposes recommendations for future research.

References:

[1] Adibinia, A., H. Dehghan Khalili, M.M. Mohebbi, M. Momeni, P. Moradi, S. Ghouhestani, A. Poorkarimi, Biomaterial-Assisted Self-Healing for Crack Reduction in High-Performance Centrifugal Concrete Piles, Buildings 15(7) (2025) 1064.

[2] Althoey, F., W.S. Ansari, M. Sufian, A.F. Deifalla, Advancements in low-carbon concrete as a construction material for the sustainable built environment, Developments in the built environment 16 (2023) 100284.

[3] Amran, M., A.M. Onaizi, R. Fediuk, N.I. Vatin, R.S. Muhammad Rashid, H. Abdelgader, T. Ozbakkaloglu, Self-healing concrete as a prospective construction material: a review, Materials 15(9) (2022) 3214.

[4] Balakrishnan, V.S., H. Seidlitz, Potential repair techniques for automotive composites: A review, Composites Part B: Engineering 145 (2018) 28-38.

[5] Bidari, O., B.K. Singh, R. Maheshwari, Effect of corrosion on bond between reinforcement and concrete-an experimental study, Discover Civil Engineering 1(1) (2024) 67.

[6] Capacci, L., F. Biondini, D.M. Frangopol, Resilience of aging structures and infrastructure systems with emphasis on seismic resilience of bridges and road networks, Resilient Cities and Structures 1(2) (2022) 23-41.

[7] Choi, Y., D. Park, S. Kim, J.-W. Hong, Seismic performance of crack-damaged masonry wall structures via shaking table tests, Structures 45 (2022), 2272-2291.

[8] De Belie, N., J. Monteny, L. Taerwe, Apparatus for accelerated degradation testing of concrete specimens, Materials and Structures 35 (2002) 427-433.

[9] Elgendy, I.M., N.E. Elkaliny, H.M. Saleh, G.O. Darwish, M.M. Almostafa, K. Metwally, G. Yahya, Y.A.G. Mahmoud, Bacteria-powered self-healing concrete: Breakthroughs, challenges, and future prospects, Journal of Industrial Microbiology and Biotechnology 52 (2025) 51.

[10] Golewski, G.L., The phenomenon of cracking in cement concretes and reinforced concrete structures: the mechanism of cracks formation, causes of their initiation, types and places of occurrence, and methods of detection—a review, Buildings 13(3) (2023) 765.

[11] Kumar, R., Review on the mechanism and mitigation of cracks in concrete, Applications in Engineering Science 16 (2023) 100154.

[12] Li, P., X. Wang, J. Peng, D. Li, Chloride penetration and material characterisation of carbonated concrete under various simulated marine environment exposure conditions, Construction and Building Materials 429 (2024) 135885.

[13] Liu, D., C. Wang, J. Gonzalez-Libreros, T. Guo, J. Cao, Y. Tu, L. Elfgren, G. Sas, A review of concrete properties under the combined effect of fatigue and corrosion from a material perspective, Construction and building materials 369 (2023) 130489.

[14] Matalkah, F., P. Soroushian, Freeze thaw and deicer salt scaling resistance of concrete prepared with alkali aluminosilicate cement, Construction and Building Materials 163 (2018) 200-213.

[15] Nair, P.S., R. Gupta, V. Agrawal, Self-healing concrete: A promising innovation for sustainability-a review, Materials Today: Proceedings 65 (2022) 1410-1417.

[16] Rauf, M., W. Khaliq, R.A. Khushnood, I. Ahmed, Comparative performance of different bacteria immobilized in natural fibers for self-healing in concrete, Construction and Building Materials 258 (2020) 119578.

[17] Tang, Y., J. Xu, Application of microbial precipitation in self-healing concrete: A review on the protection strategies for bacteria, Construction and Building Materials 306 (2021) 124950.

[18] Wang, H., S. Wang, Applications of microbial induced calcium carbonate precipitation in historical architecture restoration–a mini review, Journal of Infrastructure Preservation and Resilience 6(1) (2025) 1-10.

[19] Xue, Z.-F., W.-C. Cheng, L. Wang, Y.-X. Xie, P. Qin, Effect of a harsh circular environment on self-healing microbial-induced calcium carbonate materials for preventing Pb2+ migration, Environmental Technology & Innovation 32 (2023) 103380.

[20] Zamani, M., S. Nikafshar, A. Mousa, A. Behnia, Bacteria encapsulation using synthesized polyurea for self-healing of cement paste, Construction and Building Materials 249 (2020) 118556.

[21] Zhao, G., M. Guo, J. Cui, J. Li, L. Xu, Partially-exposed cast-in-situ concrete degradation induced by internal-external sulfate and magnesium multiple coupled attack, Construction and Building Materials 294 (2021) 123560.

Chapter 2 Literature Review

2.1 Introduction

Concrete is one of the most widely utilised construction materials due to its high compressive strength, cost-effectiveness, and durability. However, its brittle nature and susceptibility to cracking pose significant challenges for long-term performance and structural integrity (Amran, et al. 2022, Chen, et al. 2023, Gagg 2014). Cracks in concrete can compromise structural durability by providing pathways for water, chlorides, and other aggressive agents, which lead to deterioration (Zeng, et al. 2023). Traditional repair methods, including grouting, epoxy injection, and patching, often address surface cracks but fail to repair internal damage effectively (Keshmiry, et al. 2024). These methods are also labour-intensive, costly, and sometimes unsuitable for repairing inaccessible areas, highlighting the need for alternative approaches. The advent of self-healing concrete has gained considerable attention as a sustainable and efficient solution for improving concrete durability. Among various self-healing mechanisms, bacteria-based healing has emerged as a promising approach, utilising microbial activity to precipitate calcium carbonate and seal cracks (Osta and Mukhtar 2024). This process not only restores structural integrity but also enhances resistance to chemical attacks and water ingress (Khaled, et al. 2024). This chapter provides a comprehensive review of concrete deterioration mechanisms and explores the advancements in autogenous and autonomic healing systems, with an emphasis on bacteria-based self-healing concrete.

2.2 Deterioration Mechanisms of Concrete

Concrete structures are subjected to various forms of deterioration due to environmental, chemical, and physical stressors, which affect their durability and lifespan (Adesina and Zhang 2024). The degradation process often begins with microcracks that expand over time, allowing moisture, oxygen, and harmful substances to penetrate the material (Golewski 2023). These agents accelerate the deterioration process, leading to reduced mechanical properties and structural failure (Huang, et al. 2025). Chemical attacks, such as acid and sulphate reactions, cause dissolution of cementitious compounds, resulting in volume expansion and cracking. Similarly, chloride ions penetrate concrete and dispel reinforcement steel, initiating corrosion that leads to further cracking and spalling (Zhang, et al. 2024, Sun, et al. 2022). Physical factors, such as freeze-thaw cycles and thermal expansion, also induce stresses that contribute to crack formation. Overloading and impact forces further exacerbate damage by creating microcracks that propagate under cyclic loading conditions (Yan, et al. 2021). These mechanisms emphasise the need for advanced materials capable of resisting deterioration and autonomously repairing damage (Almutairi, et al. 2020, Tian, et al. 2024). This section details the primary causes of concrete deterioration, providing a foundation for understanding the importance of self-healing technologies in modern construction.

2.2.1 Chemical Attack

Chemical attack is a primary deterioration mechanism in concrete, involving the reaction of external aggressive agents with the hydration products of cement paste (Danish, et al. 2020). In a well-hydrated cement matrix, the key hydration products include calcium hydroxide ($Ca(OH)_2$), calcium silicate hydrate (C–S–H), and calcium aluminate phases such as

monosulfoaluminate (Yang, et al. 2018). These compounds contribute significantly to the mechanical integrity and durability of concrete. However, they are vulnerable to a variety of chemically aggressive substances, including sulphates, chlorides, acids, and carbon dioxide (Zhang, et al. 2024). The interaction between these substances and cementitious compounds can lead to expansive reactions, dissolution, and loss of structural cohesion.

One of the most aggressive chemical attacks is sulphate attack. Sulphate ions penetrate the concrete matrix and react with calcium hydroxide to form gypsum ($CaSO_4 \cdot 2H_2O$) and with calcium aluminate hydrates to form ettringite ($3CaO \cdot Al_2O_3 \cdot 3CaSO_4 \cdot 32H_2O$). These products occupy a larger volume than the original compounds, leading to internal stress, cracking, and disintegration of the matrix (da Rocha Gomes, et al. 2023). The formation of magnesium hydroxide (brucite) and magnesium silicate hydrate from reactions with magnesium sulphate also contributes to strength loss and increased porosity (Ammar, et al. 2024, Liang and Wang 2024).

$$MgSO_4 + Ca(OH)_2 \rightarrow Mg(OH)_2 + CaSO_4 2H_2O \quad (2.1)$$

$$MgSO_4 + Ca(OH)_2 + CaO.Al_2O_3.CaSO_4.18H_2O \rightarrow Mg(OH)_2 + 3CaO.Al_2O_3.3CaSO_4.32H_2O \quad (2.2)$$

In addition to sulphate attack, carbonation is another chemical process that compromises concrete durability. Carbon dioxide from the atmosphere reacts with calcium hydroxide to form calcium carbonate ($CaCO_3$) (Alshaeer, et al. 2022). In high CO_2 concentrations, this can further convert to calcium bicarbonate, especially in moist environments, leading to pH reduction and depassivation of reinforcement (Rodriguez-Navarro, et al. 2023).

$$CO_2 + Ca(OH)_2 \rightarrow CaCO_3 + H_2O \quad (2.3)$$

$$CaCO_3 + H_2O + CO_2 \rightarrow Ca(HCO_3)_2 \quad (2.4)$$

Chloride ions also pose a significant risk by reacting with the aluminium oxide phase in the cement to form Friedel's salts or by diffusing through cracks and pores to the steel reinforcement and causing corrosion (Teymouri and Shakouri 2023). These chemical attacks are often synergistic and may occur simultaneously, thus accelerating degradation. For example, simultaneous intrusion of carbonation and chlorides can exacerbate corrosion of reinforcing steel more than intrusion alone (Dousti and Khaksar 2023). The consequences include reduced mechanical strength, surface spalling, increased permeability, and ultimately structural failure (Hoseini, et al. 2009). Traditional mitigation strategies include the use of supplementary cementitious materials, low permeability mixtures and surface coatings (Pramanik, et al. 2024). However, these methods have limitations in sealing internal micro-cracks or coping with dynamic damage. Emerging self-healing technologies - particularly those utilising microbial-induced calcium carbonate precipitation (MICP) - offer a proactive approach to resist chemical attack by autonomously sealing cracks and blocking ion transport pathways.

2.2.2 Corrosion of Embedded Metal

In reinforced concrete, loss of steel passivity by carbonation or chloride ingress commonly leads to distributed microcracks and narrow longitudinal cracks along the reinforcement. Corrosion of pre-embedded steel reinforcement is a major cause of deterioration of reinforced concrete structures. Under alkaline conditions resulting from cement hydration, a passive oxide film forms on the surface of the steel, providing natural protection (Vu, et al. 2022). However,

external factors such as carbonation and chloride intrusion can damage this protective film. Carbonation converts calcium hydroxide to calcium carbonate, which lowers the pH of the concrete and reduces the stability of the passive film (Mahi and Ridoy 2025). Chloride ions - usually from de-icing salts or environmental exposure - can directly damage this layer, triggering localised corrosion even when alkalinity is maintained (Mahi and Ridoy 2025). In the presence of Cl^-, the steel passive film locally breaks down and soluble Fe–Cl complexes form, sustaining anodic dissolution (Vu, et al. 2022):

$$Fe \rightarrow Fe^{2+} + 2e^- \tag{2.5}$$

$$Fe^{2+} + 2Cl^- \rightleftharpoons FeCl_2(aq) \tag{2.6}$$

Cathodic oxygen reduction balances the reaction:

$$O_2 + 2H_2O + 4e^- \rightarrow 4OH^- \tag{2.7}$$

Hydrolysis of $FeCl_2$ lowers local pH and further destabilises passivity, producing porous rust that cracks the cover (Vu, et al. 2022). Once the passive layer is ruptured, electrochemical reactions begin to occur on the steel surface. The anodic region loses electrons through iron oxidation, while the cathodic region promotes oxygen reduction (Li, et al. 2007). These reactions produce rust, which expands in volume and creates tensile stresses that cause the surrounding concrete to crack and spall. Moisture and oxygen accelerate this process, especially under alternating wet and dry conditions (Shwetha, et al. 2024). The sequence of passivity breakdown, rust expansion and cover tensile stress typically produces microcrack

networks and longitudinal splitting cracks, which may progress to delamination and spalling under wet–dry cycling.

2.2.3 Fire and Heat

Thermal exposure and subsequent cooling generate dense microcracking in the cement matrix and can induce longitudinal cracking parallel to reinforcement or along heated surfaces due to differential expansion and shrinkage. Exposure to high temperatures during a fire can severely damage the structural integrity of concrete (Amran, et al. 2022). At temperatures above 300 °C, chemically bound water in hydration products is released, leading to shrinkage and internal micro-cracking. Continued heating breaks down key compounds such as calcium hydroxide and calcium silicate hydrate, which are essential for strength and cohesion (Fares, et al. 2010). At the same time, the difference in thermal expansion between the aggregate and the cement paste creates internal stresses that typically lead to surface spalling and deeper cracking. These heat-induced damages are usually irreversible and can significantly reduce the load-bearing capacity of structural members.

While fire-resistant coatings can delay thermal penetration, they do not address damage already incurred, nor can they restore mechanical performance (Golewski 2023). In contrast, self-healing concrete systems, particularly those activated by moisture or biological processes, show potential for post-fire crack repair (Albert and Liew 2024). By sealing microcracks formed during thermal cycles, self-healing materials contribute to structural resilience and enhance recovery after fire exposure(Amran, et al. 2022). Consequently, high-temperature damage is characterised by irreversible microcracks and narrow longitudinal cracks that increase transport connectivity in the damaged concrete.

2.2.4 Wet and Dry Cycles

Concrete exposed to alternating wet and dry conditions undergoes repeated expansion and contraction, leading to microcrack formation and surface scaling. These cycles accelerate the ingress of water, chlorides, and other harmful agents, compounding the deterioration process (Wang, et al. 2024). In coastal and humid environments, wet and dry cycles pose significant challenges for concrete durability, particularly in areas with poor drainage (Dai, et al. 2024). Sealants and coatings can mitigate these effects to some extent, but their performance deteriorates over time (Offei, et al. 2023). Self-healing concrete addresses this issue by autonomously repairing microcracks and maintaining low permeability, thus reducing vulnerability to cyclic moisture exposure (Cappellesso, et al. 2024).

2.2.5 Overload and Impact

Structural overloading and impact forces can cause sudden failure or initiate microcracks that propagate under repeated loading. Bridges, pavements, and industrial floors are particularly susceptible to such damage, which affects their load-bearing capacity and safety (Klym, et al. 2025). While reinforcement techniques can improve resistance, they do not address crack propagation once damage occurs. Self-healing concrete, through microbial-induced calcium carbonate precipitation, provides an effective solution by sealing cracks and restoring mechanical properties, ensuring structural reliability under dynamic loading conditions (Amran, et al. 2022).

2.3 Autogenous Healing

Autogenous healing is the natural ability of concrete to seal microcracks without external intervention (Qiao, et al. 2025). This process is the result of the continued hydration and carbonation of unreacted cement particles in contact with water. Autogenous healing first appeared in the 19th century and is considered to be a self-healing mechanism driven by chemical processes inherent in the cement matrix (Lahmann, et al. 2023, Hanna 2024). The main effects of this healing mechanism include the formation of additional hydrated calcium silicate gels (C-S-H) and precipitated calcium carbonate ($CaCO_3$), which plugs cracks and reduces permeability (Liu, et al. 2022).

Autogenous healing is usually effective for cracks smaller than 0.2 mm. In such fine cracks, the infiltration of water reactivates the hydration of the unhydrated cement particles, forming an additional C-S-H gel that fills and seals the micro-voids (Roig-Flores and Serna 2020). At the same time, atmospheric carbon dioxide dissolves in the water within the cracks to form carbonate and bicarbonate ions, which then react with calcium ions released from the cement matrix to produce calcium carbonate deposits (Rajadesingu, et al. 2024). This multi-step process is reflected in the following reactions (Qiao, et al. 2025):

$$CO_2 + H_2O \rightleftharpoons H^+ + HCO_3^- \rightleftharpoons 2H^+ + CO_3^{2-} \tag{2.8}$$

$$Ca^{2+} + CO_3^{2-} \rightleftharpoons C_aCO_3 \tag{2.9}$$

$$Ca^{2+} + HCO_3^- \rightleftharpoons C_aCO_3 + H^+ \tag{2.10}$$

The efficiency of autogenous healing is highly dependent on the availability of water and unhydrated cement, as well as environmental conditions such as temperature, humidity and crack geometry (Mohamed, et al. 2023). Studies have shown that healing is usually confined to the outer surface of the specimen, where water and CO_2 are more readily available (De Souza and Sanchez 2023). X-ray and other imaging techniques have confirmed that calcium carbonate deposition is concentrated near the surface of the crack, with limited penetration into the deeper portion.

To enhance self-healing, mineral admixtures and supplementary cementitious materials (e.g., fly ash, slag and silica fume) have been incorporated into mix designs (Amran, et al. 2022, De Souza, et al. 2024). These materials improve internal curing and ion utilisation, thereby increasing the potential for self-healing under favourable conditions. However, the self-healing capability remains limited when addressing cracks.

2.4 Autonomic Healing

Autonomic healing mechanisms employ embedded healing agents that are activated when cracks form, enabling the concrete to autonomously repair itself (Dallaev 2024). Unlike autogenous healing, which relies on the natural properties of cement hydration, autonomic systems are engineered to address larger cracks and more severe damage. These systems generally incorporate healing agents encapsulated in capsules, vascular networks, or bacterial carriers, releasing active compounds upon cracking (Van Tittelboom and De Belie 2013, Huang, et al. 2016). The agents react with water and carbonates to form precipitates, sealing the cracks. Among the various methods, bacterial-based self-healing has shown great promise due to its

sustainable and durable approach (Wong, et al. 2024). This section explores the mechanisms of autonomic healing, emphasising vascular systems and bacteria-based methods.

2.4.1 Vascular Method

The vascular method mimics the biological circulatory system, embedding hollow channels or tubes within concrete (Minnebo, et al. 2017). These networks carry healing agents, such as epoxy or polymer resins, which flow into cracks upon damage (JE, et al. 2020). When cracks breach the channels, capillary action releases the agents, which solidify to fill the gaps. Vascular systems offer the advantage of repeated healing cycles, as channels can be replenished with fresh agents (Selvarajoo, et al. 2020). However, challenges such as clogging, channel alignment, and manufacturing complexity limit their widespread application. Recent advances in 3D printing and smart materials have improved vascular designs, enabling better integration with concrete matrices (Yu 2021). Research continues to focus on optimizing channel durability and flow dynamics to enhance the effectiveness of vascular systems in self-healing concrete.

2.4.2 Bacteria-Based MICP

Bacteria-based systems utilise microbial activity to induce calcium carbonate precipitation, providing a bio-mineralisation process for sealing cracks. This approach incorporates urease-producing bacteria, nutrients, and carriers into the concrete mix (Choi, et al. 2017). Upon crack formation, water infiltrates the concrete, activating dormant bacterial spores (Wong, et al. 2024). The bacteria hydrolyse urea, producing carbonate ions that react with calcium to precipitate calcium carbonate, effectively sealing the cracks. This method not only restores structural integrity but also reduces permeability, enhancing resistance to water ingress and corrosion

(Elgendy, et al. 2025). Studies have demonstrated that bacterial self-healing systems can repair cracks up to 1.4 mm wide, making them suitable for practical applications (Adibinia, et al. 2025). Further research aims to improve bacterial viability, optimise nutrient delivery, and develop eco-friendly carriers to enhance performance and scalability.

2.5 Bacteria-Based Self-Healing Concrete

Bacteria-based self-healing concrete is a promising innovation for developing autonomous repair systems for civil infrastructure. It operates through a process known as Microbial Induced Calcium Carbonate Precipitation (MICP), in which specific bacterial strains promote the formation of $CaCO_3$, which seals cracks (Lee, et al. 2025). This process kicks in when cracks form, allowing moisture and oxygen to seep into the concrete, triggering bacterial activity. In the presence of nutrients and a calcium source, the bacteria initiate a cascade of biochemical reactions that culminate in the formation of calcite, restoring the integrity of the material (Elgendy, et al. 2025, Alshaeer, et al. 2022).

Two main MICP pathways have been extensively studied. The first involves the oxidation of organic calcium compounds such as calcium lactate. In this pathway, aerobic bacteria consume calcium lactate and produce calcium carbonate, carbon dioxide and water (Wong, et al. 2024). The carbon dioxide produced can further react with calcium hydroxide in the cement matrix to produce additional $CaCO_3$, which promotes crack sealing (Choi, et al. 2017):

$$CaC_6H_{10}O_6 + 6O_2 \rightarrow CaCO_3 + 5CO_2 + 5H_2O \quad (2.11)$$

$$CO_2 + Ca(OH)_2 \rightarrow CaCO_3 + H_2O \quad (2.12)$$

The second mechanism is based on urea hydrolysis, whereby urease-producing bacteria catalyse the breakdown of urea into ammonium and carbonate ions (De Souza, et al. 2024). These carbonate ions combine with calcium ions in the system to precipitate calcium carbonate. The reaction proceeds through a series of steps (De Souza, et al. 2024):

$$CO(NH_2)_2 + H_2O \rightarrow NH_2COOH + NH_3 \quad (2.13)$$

$$NH_2COOH + H_2O \rightarrow NH_3 + H_2CO_3 \quad (2.14)$$

$$H_2CO_3 \rightarrow HCO_{3-} + H^+ \quad (2.15)$$

$$2NH_3 + 2H_2O \rightarrow 2NH_4{}^+ + 2OH^- \quad (2.16)$$

$$HCO_3^- + H^+ + 2NH_4^+ + 2OH^- \rightarrow CO_3^{2-} + 2NH_4^+ + 2H_2O \quad (2.17)$$

The efficiency of these systems is highly dependent on factors such as bacterial strain, nutrient type, protective carrier type and the width of the crack region. In addition, the use of carriers such as expanded perlite, natural fibres and hydrogels enhances the viability of the bacteria and ensures targeted healing (Yan, et al. 2023). One of the main advantages of bacteria-based systems is that they can remain dormant in the form of spores and are not activated until moisture enters, making them suitable for long-term application (Jonkers and Schlangen 2008, Aytekin, et al. 2023). In summary, MICP-based self-healing technology offers a sustainable, environmentally friendly and durable solution for reducing crack propagation, permeability and corrosion of reinforcement in concrete structures (Zhang, et al. 2021).

2.5.1 Bacteria

The bacterial strains used in self-healing concrete must possess high survivability in harsh alkaline environments and the ability to produce urease enzymes for calcium carbonate precipitation (Ivaškė, et al. 2023). *Sporosarcina pasteurii*, a urease-producing bacterium, is widely utilised due to its resilience and effectiveness in inducing mineralisation (Li, et al. 2022). These bacteria can withstand high pH levels typical of concrete environments, enabling prolonged viability. Urease catalyses the hydrolysis of urea into ammonium and carbonate ions, which subsequently react with calcium ions to form calcium carbonate (Krajewska 2018). This mineral deposition seals cracks and restores mechanical strength. The bacterial spores remain dormant in the absence of water but become active upon crack formation, making them highly adaptable to dynamic conditions (Javeed, et al. 2024). Genetic modification and optimisation of bacterial strains have further improved their efficiency, ensuring faster and more uniform healing responses. Future research continues to explore the integration of bioengineered bacteria to enhance healing performance under diverse environmental conditions.

2.5.2 Nutrient and Organic Precursor

The availability of nutrients is essential for sustaining bacterial activity and facilitating calcium carbonate precipitation (Javeed, et al. 2024). Nutrient sources such as calcium lactate, urea, and yeast extract are commonly incorporated to supply carbon and nitrogen for microbial metabolism. Calcium lactate is particularly effective, as it reacts with carbonate ions to produce calcium carbonate while minimising pH fluctuations (Wong, et al. 2024). The controlled release of nutrients ensures prolonged bacterial viability and consistent healing performance. Encapsulation techniques are often employed to protect nutrients from premature degradation

and optimise their release during crack formation. Research into alternative organic precursors, including bio-based polymers and gel-like matrices, has shown promise in extending nutrient availability and enhancing crack-sealing efficiency (Lotfi, et al. 2021). Future studies aim to develop eco-friendly and cost-effective nutrient systems to promote large-scale adoption of bacteria-based self-healing concrete.

2.5.3 Carrier Compound

Carriers play a crucial role in maintaining bacterial viability and enabling activation during self-healing concrete crack formation. The harsh environment in the cement matrix, which is characterised by high alkalinity, high heat of hydration and limited pore space, tends to affect bacterial survival when added directly (Wong, et al. 2024). To overcome this problem, various carrier materials have been used to immobilise bacterial spores and protect them during mixing and maintenance. The most studied of these are expanded clay particles, lightweight aggregates (LWA), expanded perlite aggregates (EPA), zeolites, hydrogels and natural fibres (Alazhari, et al. 2018, Roulia and Vassiliadis 2008, Wang, et al. 2021). Expanded perlite, due to its porous and lightweight properties, provides ample internal space for nutrient and bacterial storage and facilitates water entry; however, its smooth surface can limit bacterial attachment, thus reducing healing efficiency. In contrast, natural fibres such as jute and flax have a rough, absorbent and biodegradable surface that enhances bacterial colonisation and promotes calcium carbonate precipitation. These fibres also act as mechanical bridges in cracks, improving healing and structural integrity.

Recent studies have validated the performance of different carriers under varied conditions. Ehsan et al. (Khan, et al. 2021) used *Halobacillus halophilus* embedded in EPA with calcium

lactate to enhance self-healing efficiency under freshwater, tidal, and marine exposure. Their findings showed a 16% improvement in healing in submerged marine conditions compared to control specimens, attributing the increased performance to aragonite formation facilitated by water and oxygen in cracks. Similarly, Stuckrath et al. (Stuckrath, et al. 2014) applied *Bacillus pseudofirmus* with LWA as a healing system, achieving complete closure of cracks up to 0.46 mm after 100 days of water immersion. In another approach, researchers encapsulated bacteria in silica gel and polyurethane glass tubes, successfully sealing cracks between 0.15 mm and 0.17 mm (Hu, et al. 2018). These examples illustrate that both carrier selection and protection strategy significantly affect the healing process.

Natural fibres such as jute and flax are attractive reinforcements for cementitious matrices used in bacteria-based self-healing. Their elongated geometry bridges cracks and increases post-cracking ductility, while their high capillary absorption and water retention keep cracks moist and deliver nutrients to immobilised bacteria (Wang, et al. 2019). The cellulose/hemicellulose-rich, micro fibrillated surfaces are hydrophilic and provide numerous attachment sites for cells and extracellular polymeric substances, promoting nucleation and growth of $CaCO_3$ directly on the crack faces (Wong, et al. 2024). These advantages are balanced by limitations that must be managed. Natural fibres can be susceptible to alkaline degradation and biological decay; at higher dosages they may reduce workability and increase entrained air, which tends to depress compressive strength (Choi, et al. 2017). The fibre–matrix interfacial transition zone is heterogeneous and often favours debonding and pull-out rather than rupture, making mechanical response sensitive to dispersion quality, embedment length, and fibre geometry.

2.6 Effect of Crack Width on Healing

Crack width has a strong influence on the effectiveness of microbial-induced calcium carbonate precipitation as a self-healing mechanism for concrete. Existing studies have shown that the ability of concrete to self-repair through autogenous mechanisms such as sustained hydration or carbonation is usually effective for cracks less than 0.3 mm in width (Amran, et al. 2022). For cracks, especially those exceeding 0.8 mm, the effectiveness of MICP-based repair is significantly reduced due to challenges in nutrient diffusion, bacterial colonisation and calcite precipitation efficiency. Larger cracks typically have limited bacterial activity and incomplete sealing, which is usually limited to surface deposition rather than full-depth healing (Huang, et al. 2013). In practice large cracks are usually exacerbated by sustained mechanical loading, etc. The rate of crack exacerbation is usually greater than the repair effect of MICP, resulting in wide cracks (>1mm).

To overcome these limitations, recent research has focused on the strategic use of carrier materials to enhance bacterial viability, nutrient delivery and localised calcium carbonate precipitation within larger cracks. A variety of carrier materials have been investigated, including expanded perlite aggregates (EPAs), lightweight polymers, silica gel, polyurethane, hydrogels and natural fibres (Matalkah and Soroushian 2018, Hamada, et al. 2023, McKay, et al. 2024).Expanded perlite has good porosity and water retention, but due to its smooth surface texture, bacterial attachment is limited (Alazhari, et al. 2018). In contrast, natural fibres such as jute and flax exhibit superior properties due to their inherent surface roughness, water absorption capacity and biodegradability, all of which favour bacterial blooms and improve calcite deposition.

2.7 Self-Healing Effectiveness

The effectiveness of self-healing concrete is evaluated based on its ability to seal cracks, restore mechanical properties, and improve durability (Osta and Mukhtar 2024). Bacteria-based systems demonstrate promising results in enhancing concrete performance under various environmental conditions (Guo, et al. 2023). This section examines key performance metrics, including crack-sealing efficiency, mechanical strength recovery, and durability against permeability and corrosion (De Souza and Sanchez 2023). These metrics provide insights into the practical applicability and long-term performance of bacteria-based self-healing concrete systems.

Microcracks are the dominant ingress pathways for moisture, CO_2 and chlorides; they raise permeability, accelerate steel depassivation and corrosion initiation, and act as initiation sites for fatigue-driven crack coalescence. Because microcracks are numerous and distributed, sealing them yields disproportionate gains in transport resistance and durability relative to repairing a few larger cracks. In MICP systems, nutrient transport and bacterial colonisation are also most efficient in this width regime, which is why microcracks are prime targets for autonomous healing.

2.7.1 Crack Sealing After Healing

Crack sealing is a fundamental indicator of self-healing performance. The sealing process relies on microbial-induced calcium carbonate precipitation (MICP), which deposits minerals within cracks and bonds the surrounding matrix (Shu, et al. 2024). Environmental factors such as moisture availability, temperature, and crack orientation significantly influence sealing

efficiency (Khan, et al. 2021). Laboratory experiments have demonstrated that healing can occur within 28 to 56 days under optimal conditions, with visible reductions in crack width and surface continuity. Advanced imaging techniques, including scanning electron microscopy (SEM) and X-ray micro-computed tomography, validate the formation of calcite deposits within cracks, confirming the sealing process. While smaller cracks tend to heal faster and more completely, ongoing research explores methods to enhance healing performance in larger cracks through optimised bacterial carriers and nutrient delivery systems (Wang, et al. 2022).

2.7.2 Durability After Healing

Evaluating durability is crucial for understanding the long-term performance of self-healing concrete, particularly when subjected to harsh environmental conditions. Durability assessments generally focus on how effectively the healed concrete prevents water and aggressive substances from entering through cracks, thereby reducing corrosion risk and structural degradation (Rajadesingu, et al. 2024, Blagojevic 2016). In bacterial self-healing systems, durability is closely linked to how well microbial-induced calcium carbonate fills cracks and blocks water ingress.

Water permeability tests are commonly employed to measure the effectiveness of crack sealing in self-healing concrete. Reduced water permeability indicates effective healing and enhanced durability. Several studies have highlighted significant improvements in water permeability through bacterial self-healing. For instance, Wang et al. (Wang, et al. 2019) reported up to an 85% reduction in water permeability in mortar specimens using bacterial self-healing, compared to control samples without bacteria. Similarly, Luo et al. (Wong, et al. 2024) showed that concrete containing biochar as a bacterial carrier significantly reduced water ingress,

achieving approximately 70–80% improvement over untreated specimens. The porous structure and high surface area of biochar facilitated bacterial colonisation and calcium carbonate deposition, creating a dense barrier against water flow (Roulia and Vassiliadis 2008).

2.7.3 Comparative overview of self-healing mechanisms

Having reviewed self-healing approaches and the specific features of bacteria-based MICP and carrier materials, it is helpful to compare the principal mechanisms side-by-side. Accordingly, Table 2.1 summarises the effective crack-size, repeatability, integration, and main strengths and limitations for the main strategies in the literature.

Table 2.1 Comparative overview of self-healing mechanisms

Mechanism	Activation trigger	Typical crack-size	Repeatability	Integration complexity	Key strengths	Main limitations
Autogenous (continued hydration / carbonation)	Moisture /CO_2 ingress	≤ 0.2–0.3 mm	Limited	Very Low	No added system; inherently available	Narrow envelope; environment-dependent
Crystalline admixtures	Water ingress	≤ 0.3–0.5 mm	Moderate	Low	Simple dosing; durable crystals	Mix-chemistry sensitive; moisture required
Microcapsules (polymers/minerals)	Crack ruptures capsule	≤ 0.5–0.7 mm	One-shot	Medium	Targeted release; tailored agents	Irreversible; potential premature rupture/clogging
Vascular networks (tubes/channels)	Crack intercepts network; refill	≤ 1.0 mm+ (design-dependent)	**High** (refillable)	**High**	Multiple healing cycles; controllable	Fabrication complexity; durability of network
Bacteria-based MICP (granular carriers, e.g., EPA)	Moisture activates spores; nutrients present	≈ 0.6–1.0 mm (context-dependent)	Multi-cycle	Medium	Good permeability reduction; scalable materials	Precipitation often edge-biased; carrier surface less scaffold-forming
Bacteria-based MICP (natural fibres, e.g., jute/flax)	Moisture activates spores; nutrients present	**≈ 0.8–1.3 mm** with effective fibres	Multi-cycle	Medium	Strong sealing of microcrack networks	Performance sensitive to fibre geometry/dosage and curing moisture

Taken together with Table 2.1 indicates that MICP with natural-fibre carriers uniquely combines multi-cycle healing with low relative cost and embodied carbon, while offering a wider crack-width envelope than autogenous or crystalline routes. Nevertheless, performance remains sensitive to carrier geometry, dispersion, and moisture/nutrient logistics.

2.8 Discussion

Based on the literature review following research gaps have been identified:

- Limited understanding of carrier property influence: The geometric characteristics of bacterial carriers, including shape, size and surface texture, play a crucial role in the efficiency of the self-repair process. However, systematic studies comparing the effects of different carrier geometries on MICP efficiency, cleavage bridging ability, and overall mechanical properties are lacking. Research focused on optimising carrier morphology could significantly improve self-healing concrete technology.
- Unexplored biochemical mechanisms in bacteria-carrier interactions Current studies typically measure the effectiveness of bacterial carriers in terms of practical outcomes like crack sealing or durability improvement. However, the fundamental biochemical interactions between bacteria and carrier materials, such as how carrier chemistry influences bacterial attachment, growth, and genetic expression, are largely unexplored. Investigating these mechanisms at the molecular and cellular levels would provide deeper insights, enabling the development of better carriers tailored specifically to bacterial activity.
- Lack of Comparative Studies on Carrier Performance. Most existing research evaluates bacterial self-healing using individual carrier types in isolation, which makes it difficult

to directly compare their effectiveness. There is a clear lack of systematic studies that directly contrast multiple carriers under identical conditions, limiting our ability to determine which materials offer the best overall healing performance. More comparative studies would help establish guidelines for selecting carriers based on performance criteria and practical considerations.

- Limitations in Healing Capacity Beyond the Microcrack Scale. While bacterial self-healing concrete performs effectively for narrow cracks, significant limitations remain when the damage extends beyond the range typically addressed by microbial activity. These include reduced bacterial retention, restricted nutrient transport, and inconsistent calcium carbonate precipitation. The mechanisms that govern bacterial colonisation, survival, and mineral formation under such conditions are not yet fully understood. Addressing these challenges is essential to improve the applicability and reliability of microbial-based self-healing systems for more demanding structural conditions.

2.9 Aim of Research

This research aims to develop a bacteria-based mortar with improved crack healing properties. Bacteria-based material has higher self-healing potential as compared to autogenous healing. However, the lack of research on its use with ecological friendly material, and the impact of sustaining load on its performance restricts the application of bacteria-based cementitious composites in the field. Within this context the research objectives are summarised as:

- To investigate the interaction mechanisms between bacteria and carrier materials by analysing microstructural characteristics and mineralisation patterns.

- To examine the formation and colonisation behaviour on jute, flax, and expanded perlite aggregate (EPA), and evaluate their role in facilitating the MICP process.

- To evaluate and compare the crack-healing performance of mortar specimens incorporating different bacterial carriers by measuring crack closure efficiency.

- To evaluate the capacity of different bacterial carriers to promote effective healing in cracks (>1 mm), with a focus on improving bacterial retention and calcium carbonate deposition within large crack volumes.

References:

[1] Adesina, A., J. Zhang, Impact of concrete structures durability on its sustainability and climate resiliency, Next Sustainability 3 (2024) 100025.

[2] Adibinia, A., H. Dehghan Khalili, M.M. Mohebbi, M. Momeni, P. Moradi, S. Ghouhestani, A. Poorkarimi, Biomaterial-Assisted Self-Healing for Crack Reduction in High-Performance Centrifugal Concrete Piles, Buildings 15(7) (2025) 1064.

[3] Alazhari, M., T. Sharma, A. Heath, R. Cooper, K. Paine, Application of expanded perlite encapsulated bacteria and growth media for self-healing concrete, Construction and Building Materials 160 (2018) 610-619.

[4] Albert, C.M., K.C. Liew, Recent development and challenges in enhancing fire performance on wood and wood-based composites: A 10-year review from 2012 to 2021, Journal of Bioresources and Bioproducts 9(1) (2024) 27-42.

[5] Almutairi, M.D., A.I. Aria, V.K. Thakur, M.A. Khan, Self-healing mechanisms for 3D-printed polymeric structures: From lab to reality, Polymers 12(7) (2020) 1534.

[6] Alshaeer, H.A.Y., J. Irwan, A.F. Alshalif, A. Al-Fakih, D.Y.Z. Ewais, A. Salmi, A.A. Alhokabi, Review on carbonation study of reinforcement concrete incorporating with bacteria as self-healing approach, Materials 15(16) (2022) 5543.

[7] Ammar, M.A., A. Chegenizadeh, M.A. Budihardjo, H. Nikraz, The Effects of Crystalline Admixtures on Concrete Permeability and Compressive Strength: A Review, Buildings 14(9) (2024) 3000.

[8] Amran, M., S.-S. Huang, A.M. Onaizi, G. Murali, H.S. Abdelgader, Fire spalling behavior of high-strength concrete: A critical review, Construction and Building Materials 341 (2022) 127902.

[9] Amran, M., A.M. Onaizi, R. Fediuk, N.I. Vatin, R.S. Muhammad Rashid, H. Abdelgader, T. Ozbakkaloglu, Self-healing concrete as a prospective construction material: a review, Materials 15(9) (2022) 3214.

[10] Aytekin, B., A. Mardani, Ş. Yazıcı, State-of-art review of bacteria-based self-healing concrete: Biomineralization process, crack healing, and mechanical properties, Construction and Building Materials 378 (2023) 131198.

[11] Blagojevic, A., The influence of cracks on the durability and service life of reinforced concrete structures in relation to chloride-induced corrosion: A look from a different perspective, Ph.D. Thesis, Delft University of Technology (2016).

[12] Cappellesso, V., L. Ferrara, E. Gruyaert, K. Van Tittelboom, N. De Belie, Resilient crystalline admixture in ultra-high performance self-healing concrete under cyclic freeze-thaw with de-icing salts, Cement and Concrete Research 181 (2024) 107524.

[13] Chen, L., Z. Chen, Z. Xie, L. Wei, J. Hua, L. Huang, P.-S. Yap, Recent developments on natural fiber concrete: A review of properties, sustainability, applications, barriers, and opportunities, Developments in the Built Environment 16 (2023) 100255.

[14] Choi, S.-G., K. Wang, Z. Wen, J. Chu, Mortar crack repair using microbial induced calcite precipitation method, Cement and Concrete Composites 83 (2017) 209-221.

[15] da Rocha Gomes, S., L. Ferrara, L. Sánchez, M.S. Moreno, A comprehensive review of cementitious grouts: Composition, properties, requirements and advanced performance, Construction and building materials 375 (2023) 130991.

[16] Dai, Z., S. He, A. Chen, L. Xiao, G. Mei, Experimental investigation on chloride transport in semi-buried concrete exposed to seawater wet-dry cycles in coastal soil environment, Case Studies in Construction Materials 20 (2024) e03360.

[17] Dallaev, R., Advances in materials with self-healing properties: a brief review, Materials 17(10) (2024) 2464.

[18] Danish, A., M.A. Mosaberpanah, M.U. Salim, Past and present techniques of self-healing in cementitious materials: A critical review on efficiency of implemented treatments, Journal of Materials Research and Technology 9(3) (2020) 6883-6899.

[19] De Souza, D.J., L.F. Sanchez, Understanding the efficiency of autogenous and autonomous self-healing of conventional concrete mixtures through mechanical and microscopical analysis, Cement and Concrete Research 172 (2023) 107219.

[20] De Souza, D.J., L.F. Sanchez, A. Biparva, Influence of engineered self-healing systems on ASR damage development in concrete, Cement and Concrete Composites 147 (2024) 105440.

[21] Dousti, A., H. Khaksar, Impact of Simultaneous Carbonation and Chloride Attack on Chloride Diffusion in Portland Cement Concrete Mixtures Blended with Natural Zeolite and Silica Fume, Journal of Materials in Civil Engineering 35(12) (2023) 04023478.

[22] Elgendy, I.M., N.E. Elkaliny, H.M. Saleh, G.O. Darwish, M.M. Almostafa, K. Metwally, G. Yahya, Y.A.-G. Mahmoud, Bacteria-powered self-healing concrete: Breakthroughs, challenges, and future prospects, Journal of Industrial Microbiology and Biotechnology 52 (2025) 51.

[23] Fares, H., S. Remond, A. Noumowe, A. Cousture, High temperature behaviour of self-consolidating concrete: microstructure and physicochemical properties, Cement and Concrete Research 40(3) (2010) 488-496.

[24] Gagg, C.R., Cement and concrete as an engineering material: An historic appraisal and case study analysis, Engineering Failure Analysis 40 (2014) 114-140.

[25] Golewski, G.L., The phenomenon of cracking in cement concretes and reinforced concrete structures: the mechanism of cracks formation, causes of their initiation, types and places of occurrence, and methods of detection—a review, Buildings 13(3) (2023) 765.

[26] Guo, Y., K. Xiang, H. Wang, X. Liu, Q. Ye, X. Wang, Experimental study on self-healing and mechanical properties of sisal fiber-loaded microbial concrete, Materials Research Express 10(4) (2023) 045701.

[27] Hamada, H.M., J. Shi, M.S. Al Jawahery, A. Majdi, S.T. Yousif, G. Kaplan, Application of natural fibres in cement concrete: A critical review, Materials Today Communications 35 (2023) 105833.

[28] Hanna, J., Self-Healing Concrete Techniques and Technologies and Applications, Recent Progress in Materials 6(1) (2024) 1-20.

[29] Hoseini, M., V. Bindiganavile, N. Banthia, The effect of mechanical stress on permeability of concrete: A review, Cement and Concrete Composites 31(4) (2009) 213-220.

[30] Hu, Z.-X., X.-M. Hu, W.-M. Cheng, Y.-Y. Zhao, M.-Y. Wu, Performance optimization of one-component polyurethane healing agent for self-healing concrete, Construction and Building Materials 179 (2018) 151-159.

[31] Huang, D., X. Wang, X. Li, L. Su, J. Tian, Y. Li, Y. Liu, Research on the mechanical properties and pore structure deterioration of Basalt-polyvinyl alcohol hybrid fiber concrete under the coupling effects of sulfate attack and freeze-thaw cycles, Construction and Building Materials 473 (2025) 140949.

[32] Huang, H., G. Ye, D. Damidot, Characterization and quantification of self-healing behaviors of microcracks due to further hydration in cement paste, Cement and Concrete Research 52 (2013) 71-81.

[33] Huang, H., G. Ye, C. Qian, E. Schlangen, Self-healing in cementitious materials: Materials, methods and service conditions, Materials & Design 92 (2016) 499-511.

[34] Ivaškė, A., V. Gribniak, R. Jakubovskis, J. Urbonavičius, Bacterial viability in self-healing concrete: A case study of non-ureolytic Bacillus species, Microorganisms 11(10) (2023) 2402.

[35] Javeed, Y., Y. Goh, K.H. Mo, S.P. Yap, B.F. Leo, Microbial self-healing in concrete: A comprehensive exploration of bacterial viability, implementation techniques, and mechanical properties, Journal of Materials Research and Technology 29 (2024) 2376-2395.

[36] JE, P.C., M.T. Sultan, C.P. Selvan, S. Irulappasamy, F. Mustapha, A.A. Basri, S.N. Safri, Manufacturing challenges in self-healing technology for polymer composites—a review, Journal of Materials Research and Technology 9(4) (2020) 7370-7379.

[37] Jonkers, H.M., E. Schlangen, Development of a bacteria-based self healing concrete, Tailor made concrete structures 1 (2008) 425-430.

[38] Keshmiry, A., S. Hassani, U. Dackermann, J. Li, Assessment, repair, and retrofitting of masonry structures: A comprehensive review, Construction and Building Materials 442 (2024) 137380.

[39] Khaled, A., A. el Mahdi Safhi, A.M. Soliman, Post-fire curing and autogenous self-healing in alkali-activated slag: Microstructures and healing mechanisms, Construction and Building Materials 428 (2024) 136334.

[40] Khan, M.B.E., L. Shen, D. Dias-da-Costa, Crack healing performance of bacteria-based mortar under sustained tensile loading in marine environment, Cement and Concrete Composites 120 (2021) 104055.

[41] Khan, M.B.E., L. Shen, D. Dias-da-Costa, Self-healing behaviour of bio-concrete in submerged and tidal marine environments, Construction and Building Materials 277 (2021) 122332.

[42] Klym, A., Y. Blikharskyy, V. Gunka, O. Poliak, J. Selejdak, Z. Blikharskyy, An Overview of the Main Types of Damage and the Retrofitting of Reinforced Concrete Bridges, Sustainability(2071-1050) 17(6) (2025) 2506.

[43] Krajewska, B., Urease-aided calcium carbonate mineralization for engineering applications: A review, Journal of advanced research 13 (2018) 59-67.

[44] Lahmann, D., C. Edvardsen, S. Kessler, Autogenous self-healing of concrete: Experimental design and test methods□ A review, Engineering Reports 5(1) (2023) e12565.

[45] Lee, H.W., S.A. Rahmaninezhad, L. Meng, W.V. Srubar Iii, C.M. Sales, Y.A. Farnam, M.H. Hubler, A.R. Najafi, Prediction of microbial-induced calcium carbonate precipitation for self-healing cementitious material, Cement and Concrete Composites 158 (2025) 105945.

[46] Li, C.-Q., J. Zheng, W. Lawanwisut, R.E. Melchers, Concrete delamination caused by steel reinforcement corrosion, Journal of Materials in Civil Engineering 19(7) (2007) 591-600.

[47] Li, L., T. Liu, G. Jiang, C. Fang, B. Qu, S. Zheng, G. Yang, C. Tang, Insight into the temperature stimulation on the self-healing properties of cement-based materials, Construction and Building Materials 361 (2022) 129704.

[48] Liang, N., Z. Wang, Permeability Effect and Nonlinear Coupling Characteristics of Rock–Soil Interaction with Water, Processes 12(4) (2024) 828.

[49] Liu, X., P. Feng, Y. Cai, X. Yu, C. Yu, Q. Ran, Carbonation behavior of calcium silicate hydrate (CSH): Its potential for CO2 capture, Chemical Engineering Journal 431 (2022) 134243.

[50] Lotfi, A., H. Li, D.V. Dao, G. Prusty, Natural fiber–reinforced composites: A review on material, manufacturing, and machinability, Journal of Thermoplastic Composite Materials 34(2) (2021) 238-284.

[51] Mahi, M.S.H., T.A. Ridoy, Corrosion Mechanisms in Reinforced Concrete: Causes, Effects, and Sustainable Mitigation Strategies, Current Problems in Research 1(1) (2025) 52-66.

[52] Matalkah, F., P. Soroushian, Freeze thaw and deicer salt scaling resistance of concrete prepared with alkali aluminosilicate cement, Construction and Building Materials 163 (2018) 200-213.

[53] McKay, I., J. Vargas, L. Yang, R.M. Felfel, A review of natural fibres and biopolymer composites: progress, limitations, and enhancement strategies, Materials 17(19) (2024) 4878.

[54] Minnebo, P., G. Thierens, G. De Valck, K. Van Tittelboom, N. De Belie, D. Van Hemelrijck, E. Tsangouri, A novel design of autonomously healed concrete: Towards a vascular healing network, Materials 10(1) (2017) 49.

[55] Mohamed, A., Y. Zhou, E. Bertolesi, M. Liu, F. Liao, M. Fan, Factors influencing self-healing mechanisms of cementitious materials: A review, Construction and Building Materials 393 (2023) 131550.

[56] Offei, I., A. Guo, Z. Sun, C. Qi, N. Sathitsuksanoh, Preventing ASR-induced deteriorations with hydrophobic aggregates-a feasibility study, Construction and Building Materials 394 (2023) 132277.

[57] Osta, M.O., F. Mukhtar, Effect of bacteria on uncracked concrete mechanical properties correlated with damage self-healing efficiency–A critical review, Developments in the Built Environment 17 (2024) 100301.

[58] Pramanik, S.K., M. Bhuiyan, D. Robert, R. Roychand, L. Gao, I. Cole, B.K. Pramanik, Bio-corrosion in concrete sewer systems: Mechanisms and mitigation strategies, Science of The Total Environment 921 (2024) 171231.

[59] Qiao, Y., S. Chen, C. Wang, Y. Zhuge, J. Ma, New classification, historical developments, technology readiness level and application conditions of self-healing concrete technologies, Journal of Building Engineering 108 (2025) 112869.

[60] Rajadesingu, S., K.C. Mendonce, N. Palani, P. Monisha, P. Vijayakumar, S. Ayyadurai, Exploring the potential of bacterial concrete: A sustainable solution for remediation of crack and durability enhancement–A critical review, Construction and Building Materials 439 (2024) 137238.

[61] Rodriguez-Navarro, C., T. Ilić, E. Ruiz-Agudo, K. Elert, Carbonation mechanisms and kinetics of lime-based binders: An overview, Cement and Concrete Research 173 (2023) 107301.

[62] Roig-Flores, M., P. Serna, Concrete early-age crack closing by autogenous healing, Sustainability 12(11) (2020) 4476.

[63] Roulia, M., A.A. Vassiliadis, Sorption characterization of a cationic dye retained by clays and perlite, Microporous and Mesoporous Materials 116(1-3) (2008) 732-740.

[64] Selvarajoo, T., R. Davies, D. Gardner, B. Freeman, A. Jefferson, Characterisation of a vascular self-healing cementitious material system: flow and curing properties, Construction and Building Materials 245 (2020) 118332.

[65] Shu, Y., Y. Song, H. Fang, D. Wang, W. Lu, C. Zhao, L. Chen, X. Song, Enhancing microbial-induced carbonate precipitation (MICP) sand consolidation with alkali-treated jute fibers, Powder Technology 441 (2024) 119845.

[66] Shwetha, K., B. Praveen, B.K. Devendra, A review on corrosion inhibitors: types, mechanisms, electrochemical analysis, corrosion rate and efficiency of corrosion inhibitors on mild steel in an acidic environment, Results in Surfaces and Interfaces 16 (2024) 100258.

[67] Stuckrath, C., R. Serpell, L.M. Valenzuela, M. Lopez, Quantification of chemical and biological calcium carbonate precipitation: performance of self-healing in reinforced mortar containing chemical admixtures, Cement and Concrete Composites 50 (2014) 10-15.

[68] Sun, H., H. Zou, X. Li, S.A. Memon, B. Yuan, F. Xing, X. Zhang, J. Ren, Combined effects of sulfate and chloride attack on steel reinforced mortar under drying–immersion cycles, Buildings 12(8) (2022) 1252.

[69] Teymouri, M., M. Shakouri, Chloride desorption mechanisms of cement pastes containing fly ash, Construction and Building Materials 370 (2023) 130667.

[70] Tian, Q., J. Zhou, J. Hou, Z. Zhou, Z. Liang, M. Sun, J. Hu, J. Huang, Building the future: Smart concrete as a key element in next-generation construction, Construction and Building Materials 429 (2024) 136364.

[71] Van Tittelboom, K., N. De Belie, Self-healing in cementitious materials—A review, Materials 6(6) (2013) 2182-2217.

[72] Vu, T.H., L.C. Dang, G. Kang, V. Sirivivatnanon, Chloride induced corrosion of steel reinforcement in alkali activated slag concretes: A critical review, Case Studies in Construction Materials 16 (2022) e01112.

[73] Wang, L., C. Chen, R. Liu, P. Zhu, H. Liu, H. Jiang, J. Yu, Chloride Corrosion Process of Concrete with Different Water–Binder Ratios under Variable Temperature Drying–Wetting Cycles, Materials 17(10) (2024) 2263.

[74] Wang, X., L. Chang, X. Shi, L. Wang, Effect of hot-alkali treatment on the structure composition of jute fabrics and mechanical properties of laminated composites, Materials 12(9) (2019) 1386.

[75] Wang, X., S. Chen, Z. Yang, J. Ren, X. Zhang, F. Xing, Self-healing concrete incorporating mineral additives and encapsulated lightweight aggregates: Preparation and application, Construction and Building Materials 301 (2021) 124119.

[76] Wang, X., J. Xu, Z. Wang, W. Yao, Use of recycled concrete aggregates as carriers for self-healing of concrete cracks by bacteria with high urease activity, Construction and Building Materials 337 (2022) 127581.

[77] Wong, P.Y., J. Mal, A. Sandak, L. Luo, J. Jian, N. Pradhan, Advances in microbial self-healing concrete: A critical review of mechanisms, developments, and future directions, Science of The Total Environment 947 (2024) 174553.

[78] Yan, C., H. Song, J. Pfister, T.L. Andersen, S.J. Warden, R. Bhargava, M.E. Kersh, Effect of fatigue loading and rest on impact strength of rat ulna, Journal of Biomechanics 123 (2021) 110449.

[79] Yan, Y., G. Jia, Y. Zhang, Y. Gao, Z. Li, The influence of expanded perlite as a bio-carrier on the freeze–thaw properties of self-healing concrete, Construction and Building Materials 409 (2023) 133891.

[80] Yang, H., Y. Che, F. Leng, Calcium leaching behavior of cementitious materials in hydrochloric acid solution, Scientific reports 8(1) (2018) 8806.

[81] Yu, X., The fundamental elements of strategy: Concepts, Theories and Cases, Springer Nature (2021) 1007.

[82] Zeng, C., Z.-s. Zheng, Y.-j. Huang, H. Zhang, Chloride-induced 3D non-uniform corrosion of steel in reinforced concrete considering mesoscale heterogeneities and early-age cracks, Construction and Building Materials 409 (2023) 133778.

[83] Zhang, C., J. Li, M. Yu, Y. Lu, S. Liu, Mechanism and Performance Control Methods of Sulfate Attack on Concrete: A Review, Materials 17(19) (2024) 4836.

[84] Zhang, X., Z. Jin, M. Li, C. Qian, Effects of carrier on the performance of bacteria-based self-healing concrete, Construction and Building Materials 305 (2021) 124771.

Chapter 3 Experimental Program

It is essential to comprehensively understand the experimental methods and materials used to develop bacteria-based self-healing cementitious materials. Although several studies have previously focused on individual bacterial carriers, a systematic experimental approach considering multiple aspects, such as compatibility between bacteria and carriers, material preparation, and methods for assessing healing performance, is lacking in existing literature. Therefore, this chapter provides a detailed description of experimental procedures developed to evaluate natural fibres (jute and flax) and expanded perlite aggregate (EPA) as bacterial carriers. The experimental methods described here include material characterisation, bacterial immobilisation, carrier compatibility assessments (water absorption, SEM, FTIR), and mortar specimen preparation protocols. The outcomes of this systematic program facilitate accurate evaluation and comparison of carrier effectiveness in enhancing self-healing capabilities. In this chapter, the author of this thesis was the primary contributor and was responsible for experimental design, conducting laboratory tests, data analysis, and interpretation of the results.

3.1 Introduction

This chapter provides a detailed overview of the experimental methods and materials used to investigate the performance of natural fibres and expanded perlite aggregate (EPA) as bacterial carriers for self-healing cementitious materials. Firstly, the properties, selection criteria and preparation methods of the selected carriers (jute fibre, flax fibre and EPA) are described in detail, including their sources, physical treatments and properties.

The second part of this chapter describes the immobilisation of bacterial spores on the carrier surface. It was used to study the synergy and compatibility between bacteria ((*Sporosarcina pasteurii*) and various carrier materials (natural fibres-flax, jute and expanded perlite aggregate- EPA). Optimisation of bacterial colonisation and biopolymer formation. These biopolymers are important intermediates for promoting microbial-induced calcium carbonate precipitation (MICP), thus directly affecting the efficiency of the self-repair mechanism. And the compatibility and interaction of these carriers with bacteria were specifically evaluated by controlled laboratory assessments including bacterial growth measurements (OD600), scanning electron microscopy (SEM) and Fourier transform infrared spectroscopy (FTIR).

The final sections outline the preparation and testing protocols for mortar specimens embedded with the bacterial carriers, assessing mechanical properties, crack healing capability, and durability performance. Additionally, microstructural analyses using SEM provide insights into the internal healing processes, further illustrating the synergy between bacterial activity and carrier functionality. This integrated experimental approach systematically explores how the compatibility between bacteria and carrier materials influences the effectiveness of self-healing and overall performance in cementitious systems.

3.2 Materials

This section details the materials employed to systematically evaluate the compatibility and synergistic interactions between bacteria and carrier materials for enhancing self-healing in cementitious mortar. The primary materials discussed include the bacterial strain (*Sporosarcina pasteurii*), selected carrier materials (jute fibres, flax fibres, and expanded perlite aggregate), chemical reagents.

3.2.1 Self-healing agent preparation

Sporosarcina pasteurii is a urease-producing bacterium commonly used in bio-cementation and self-healing mortar applications due to its ability to precipitate $CaCO_3$ (Ghosh, et al. 2019). In this study, *Sporosarcina pasteurii* bacteria (ATCC 11859) was adopted and obtained from ATCC Australia (Gibson 1934).

Bacteria were grown in ATCC Medium 1376: *Bacillus pasteurii* NH4-YE Medium (Yeast extract (20g/L), Tris buffer (15.75g/L), (NH4)2 SO4 (10g/L)) at 30°C (Bhaduri, et al. 2016). Sporulation was induced by adding 10ml of $MnCl_2$/L of bacteria broth solution (Khan, et al. 2021). The concentration of bacteria at the time of sporulation was 7×10^8 cell/ml measured by Thermofisher Countess II automated cell counter. Spores were harvested by centrifuging the spore solution in 1800 rpm for 3mins (Khan, et al. 2021). The bacterial spore sludge was suspended by distilled water for further use.

3.2.2 Carrier Materials

Three distinct carrier materials were evaluated in this research:

Jute Fibre: A natural fibre obtained commercially from Australian suppliers. The fibres had an initial density of approximately 1.3 g/cm³ and were chosen due to their high surface roughness, hydrophilicity, and excellent liquid retention properties, facilitating bacterial adhesion and colonisation. The jute fibres exhibited a length-to-diameter ratio of around 100:1.

Flax Fibre: A biodegradable natural fibre sourced locally, with a density of 1.2 g/cm³. Compared to jute, flax fibres exhibit a smoother surface texture, allowing the study of the effect

of different fibre textures on bacterial interactions. The flax fibres exhibited a length-to-diameter ratio of around 90:1.

Expanded Perlite Aggregate (EPA): A commercially available mineral carrier provided by Ausperl Pty Limited (Waitakere, Auckland, New Zealand). EPA featured a density of approximately 0.1 g/cm³, with particle sizes ranging from 0.075 mm to 4 mm. EPA was selected as a conventional bacterial carrier commonly reported in previous literature, thus serving as a reference control.

In this study three carriers were chosen to represent distinct but complementary archetypes. Jute and flax are renewable plant fibres with similar length and density but contrasting surface textures: jute has a rough, highly fibrillated surface and very high-water absorption, whereas flax is comparatively smoother and slightly less absorbent. This pair allows the influence of fibre roughness and surface chemistry on microbial colonisation and bio-cement formation to be examined while keeping geometry comparable. Both fibres also act as crack-bridging elements, so that any healing is concentrated along mechanically relevant paths. Expanded perlite aggregate (EPA) was selected as a widely used porous mineral carrier in bio-concrete studies and serves as a benchmark for granular, non-bridging systems. Its highly porous interior provides storage for spores and nutrients, but its external surface is relatively smooth and inorganic. Together, jute, flax and EPA therefore bracket differences in shape/aspect ratio (fibres vs. particles), surface roughness/chemistry and water-management behaviour (capillary wicking vs. internal reservoir) under identical microbiological and mix conditions. Other sustainable carriers such as biochar and alternative fibres are acknowledged as promising options but are beyond the scope of the present comparative programme and are identified as targets for future studies building on these mechanistic insights.

Flax was intentionally included as the smoother-surface, lower-roughness natural fibre to isolate the role of surface texture and chemistry from geometry when comparing bio-carriers. Although flax is reported to be susceptible to alkaline degradation over long durations, in this study it is used at a moderate dosage (≈1 vol %) and subjected to a mild alkali cleaning to remove surface waxes and loosely bound hemicellulose, improving wetting and bacterial attachment without severe fibre etching. The evaluation window is limited to early-age healing periods, during which MICP produces a mineral layer at the fibre–crack interface that can partially encapsulate fibres (Feng, et al. 2022). Within these conditions flax serves as a necessary 'smooth-surface' bound against jute's rougher surface, allowing a controlled comparison of carrier surface effects on microbial colonisation and $CaCO_3$ deposition (Ghosh, et al. 2019).

Prior to testing, the fibres were cut to 8-10 mm lengths to simulate typical dimensions used in fibre-reinforced concrete, where short fibres allow for even dispersion without clumping (Chen, et al. 2023). The fibres underwent an alkaline treatment with a 6% sodium hydroxide (NaOH) solution for 3 hours (Wang, et al. 2019). This treatment was applied to remove surface impurities, hemicellulose and lignin, increasing the effective surface area and improving the mechanical properties (Zhong, et al. 2022). EPA also undergoes the same alkali treatment, in order to make the same comparison with fibres. But this one doesn't affect its properties. After alkali pretreatment, all carriers were rinsed with distilled water and dried at 40°C to a constant weight. Then sterilised via autoclaving at 121°C for 20 minutes to eliminate any microbial contamination and ensure consistent initial conditions. Though autoclaving can reduce fibre tensile strength slightly, literature indicates it does not compromise surface roughness or microbial adhesion, which are more critical for colonisation and healing efficacy (Chen, et al. 2023).

3.2.3 Chemical Reagents

The main chemical reagents employed is cementation solution. The cementation solution consisted of 55.5g/L calcium chloride, 30.2g/L urea and 0.5g/L yeast extract (Dubey, et al. 2022). The pH of Medium E was measured at 8-9, ideal for calcium carbonate crystallisation via urease hydrolysis.

3.3 Compatibility and Synergy Between Bacteria and Carriers

This section describes experimental methods designed to systematically investigate the compatibility and symbiotic interactions between *Sporosarcina pasteurii* bacteria and selected carrier materials (jute fibres, flax fibres, and EPA). The compatibility between bacteria and carriers significantly affects microbial colonisation, biopolymer formation, and subsequent calcium carbonate precipitation—critical processes in achieving effective self-healing within cementitious materials.

3.3.1 Water Absorption Test

The first step in evaluating compatibility involved assessing the water absorption capacity of each carrier, as this property significantly affects bacterial colonisation by controlling nutrient availability and bacterial solution retention (Feng, et al. 2022).

Three replicate samples of each carrier type (jute fibres, flax fibres, and EPA) were weighed in a dry condition and then fully immersed in distilled water at room temperature (approximately 25°C). At regular intervals (every 1 hour, until 24 hours), samples were removed, carefully

surface-dried using absorbent paper, and weighed again (Dubey, et al. 2023). The water absorption for each material was calculated as a percentage increase in weight relative to their initial dry weight (Rauf, et al. 2020, Khan, et al. 2023). The absorption rate in this study was defined based on weight and is expressed as a percentage calculated using the following formula:

$$\text{Absorption Rate}(\%) = \left(\frac{\text{Wet weight} - \text{Dry weight}}{\text{Dry weight}}\right) \times 100\% \qquad (3.1)$$

3.3.2 Experimental Media Preparation

Medium A (Figure 3.1A) was a ATCC Medium 1376: *Bacillus pasteurii* NH4-YE Medium and served as a control. The pH of Medium was maintained at 9, optimised for bacterial growth and metabolic activity. Medium B (Figure 3.1B) had one carrier —flax, jute, or EPA— and the nutrient solution. This medium provided another control to observe the behaviour of the carriers alone without bacteria. Medium D (Figure 3.1D) was composed of the nutrient solution and 1 mL of *Sporosarcina pasteurii* bacterial solution without carriers. This was used as a control to compare bacterial growth in the presence of carriers (Medium C). Finally, medium C (Figure 3.1C) contained one type of carrier (flax, jute, or EPA) having absorbed Medium D. This medium was tested to assess bacterial colonisation and calcium carbonate precipitation. OD600 was used to assess the bacterial growth potential in Mediums C and D, and the surface characteristics of carriers in Mediums B and C were investigated by scanning electron microscopy (SEM) where applicable. OD600 measurements were carried out by using a UV-visible spectrophotometer at a wavelength of 600 nm (Haase, et al. 2017). The carrier with bacteria and nutrition medium (Medium C) was compared with the control medium of bacteria and nutrition medium (Medium D) for growth assessment using OD600. By comparing OD600

measurements from Mediums A and B, it was observed that the fibres did not directly affect the clarity of the liquid. Calibration was performed using the nutrition medium, which served as the negative control group without bacteria and carrier.

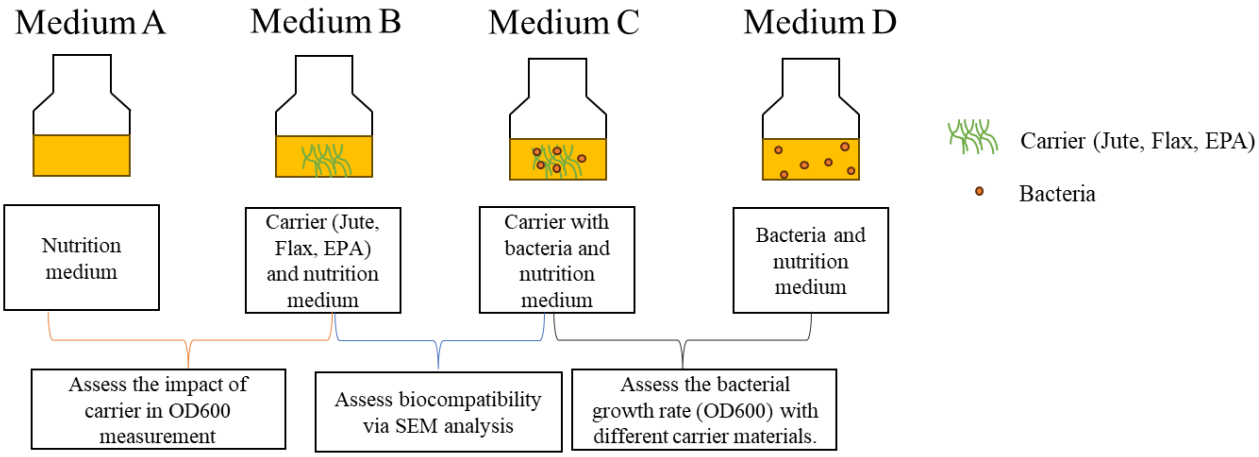

Figure 3.1: Mediums and tests: OD600 measurement, biocompatibility, and bacterial growth.

3.3.3 Bacterial Immobilisation and Incubation

The sterilised carriers were separately placed into 500 mL conical flasks containing 200 mL of nutrient medium. For Medium C, 1 mL of Sporosarcina pasteurii bacterial spores seed solution was added to each carrier to simulate in-situ immobilisation, as occurs in concrete when bacteria are first embedded within carriers prior to casting. This approach ensures that bacterial interaction with the carrier precedes any environmental exposure, mimicking the self-healing design process. For Medium D, the bacteria spore solution was directly added into the nutrition medium. All the flasks were subsequently incubated at 30°C for 20 hours with continuous shaking at 120 rpm to facilitate bacterial colonisation (Ghosh, et al. 2019). These conditions

facilitated optimal bacterial growth, ensuring uniform colonisation and enabling consistent monitoring of bacterial activity and interactions.

3.3.4 Bacterial Growth Monitoring

Optical Density (OD600) measurements were recorded hourly using a UV-visible spectrophotometer (600 nm wavelength) (Stuckrath, et al. 2014). These measurements provided a quantitative assessment of bacterial growth and proliferation on each carrier, as well as baseline growth in the control media (Mediums A and D). The spectrophotometer was calibrated using sterile nutrient medium (Medium A) to ensure accurate and reliable bacterial concentration data.

3.3.5 Morphology Characterisation of Carriers

To investigate the surface morphology of flax, jute, and EPA following bacterial symbiosis, samples of Mediums A and C were placed in the same flasks used for the bacterial growth test after OD600 measurements. All medium samples were incubated for one week at 30°C and shaking at 120 rpm. After incubation, the carriers were carefully removed from the medium, and the surface of each carrier was gently wiped with a dry tissue until no droplets remained. The carriers were then dried at 40 °C temperature and prepared for scanning electron microscopy analysis. SEM was used to examine the surface characteristics and observe the bacterial colonisation and biopolymer matrix formation on each carrier.

3.3.6 FTIR Analysis

Fourier transform infrared spectroscopy (FTIR) is used to assess the interaction between natural fibres and bacterial activity during scaffold formation. The carriers for bacterial colonisation in Section 3.3.2 (Medium B and Medium C) were selected. Two samples were prepared for each category to have enough quantity to cover the plate during FTIR analysis. To ensure safety and eliminate bioactivity, all samples were autoclaved in the laboratory at 121°C for 20 minutes to effectively kill the bacteria (Khan, et al. 2021). The samples were then dried completely to remove residual moisture prior to analysis.

FTIR analysis can identify the functional groups and chemical bonds present in the sample, thus confirming the formation of biopolymers. Spectra in the range of 400 to 4000 cm^{-1} were recorded using a FTIR spectrometer (Wang, et al. 2022). Characteristic absorption bands corresponding to biopolymer functional groups (e.g. carbon-oxygen, methyl, methylene groups) were analysed to validate changes in chemical composition due to bacterial activity (Andersen, et al. 1991).

3.3.7 Bio-cementation Test

The analysis of bio-cementation formation was carried out, focusing on calcium carbonate precipitation. SEM allowed to identify patterns of bacterial colonisation and mineralisation to highlight the effectiveness of the different carriers in supporting bacterial activity and enhancing the self-healing properties of the concrete through bacterial induced mineralisation. Specific details of the carrier preparation and testing are provided next.

The weight of the carriers in each set was determined according to the water absorption capacity to ensure that each absorbed an equal volume of liquid. This prevented variations in

liquid absorption from impacting the subsequent results in the cementation solution. The experiments included medium groups C. Each type of Medium C included three sets of samples. Specifically, three flax fibre samples (4 grams each), three jute fibre samples (3.6 grams each), and three EPA samples (5.5 grams each) were prepared. Each sample was combined with the corresponding *Sporosarcina pasteurii* bacterial solution and nutrient medium. This preparation accounted for differences in material weights. These specific weights were selected to ensure same amount of bacteria and nutrition solution across all carriers for direct comparison (Wang, et al. 2012). The details of each carrier preparation and experimental procedure are given next.

As shown in Figure 3.2, the bio-cementation experiments were conducted using an especially modified cementation solution. The pH of Medium E was measured at 8-9, ideal for calcium carbonate crystallisation via urease hydrolysis. All carriers and bacteria were incubated at 30°C for one week, shaken at 120 rpm. After incubation, the surface of all carrier was wiped with a paper tissue to ensure that the surface was clear of any liquid before immersion in the cementation solution (Medium E) (Begum, et al. 2021). Subsequently, carriers were incubated at a controlled temperature of 30 °C for 1 day (Dubey, et al. 2022). After this all the carriers were removed from cementation solution and oven dried at a constant temperature of 40 °C to a constant weight. A vacuum drying step was applied to remove residual moisture before coating. To enhance surface conductivity, samples were sputter-coated with a thin gold layer (~5 nm) at 20 mA for 1–2 minutes. SEM imaging was conducted using a Zeiss Sigma HD field emission scanning electron microscope (Oberkochen, Germany) operated at 5 kV to examine bacterial attachment, biopolymer formation, and surface morphology (Khan, et al. 2021).

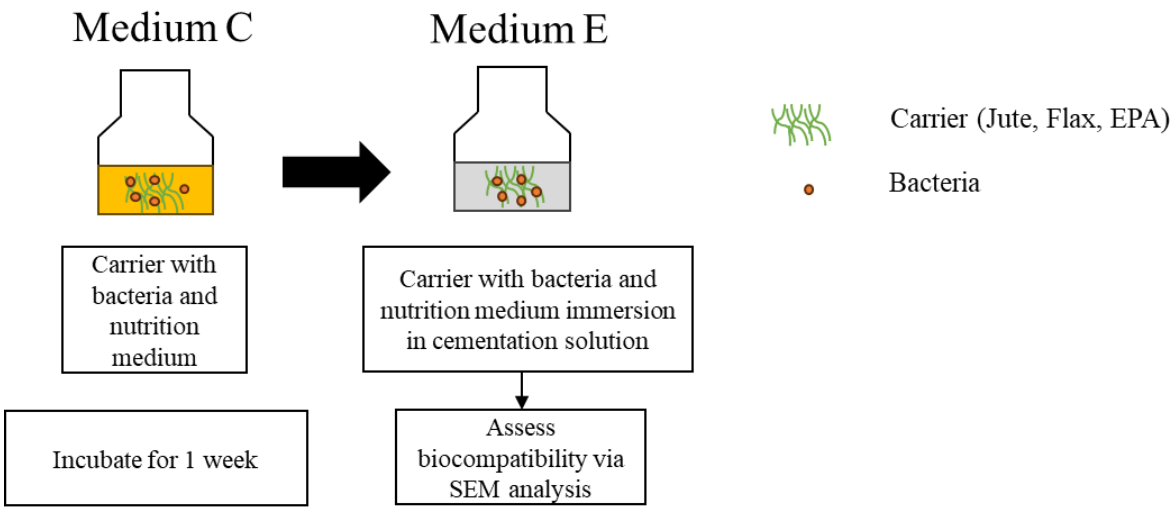

Figure 3.2: Mediums and tests: bio-cementation test.

3.4 Evaluation of Fibre and EPA as Bacterial Carriers in Mortars

To investigate the impact of different bacterial carriers on self-healing performance, a systematic experimental program was designed involving the preparation of carrier materials, mortar mixing, mechanical testing, and healing evaluation. Three carrier types—natural jute fibre, flax fibre, and expanded perlite aggregate (EPA)—were tested at two volumetric dosages (1% and 1.5%) in combination with Sporosarcina pasteurii bacteria. The carrier materials were biologically activated through immersion in bacterial suspensions and nutrient solutions, followed by incorporation into mortar specimens with consistent mix proportions. Reinforced mortar prisms were cracked under controlled loading conditions and subsequently cured under high-humidity environments to evaluate healing. The full test program included mechanical strength testing, image-based crack width monitoring, water permeability assessment, and microstructural analysis via SEM to assess the healing efficiency of each carrier type.

3.4.1 Bacterial Immobilisation

As shown in Figure 3.3, the diluted bacterial suspension was adsorbed in the pores of natural fibres and EPA for 180 minutes. After adsorption, the nature fibre and EPA were dried at 40°C until reaching constant weight. The jute, flax and EPA were divided into two parts each. The first portion was sprayed with *Bacillus pasteurii* NH4-YE Medium nutrient solution on the carrier surface using a spray bottle. The spray volume was 200 ml per carrier. In the second portion, cementation solution was sprayed onto the surface of the carriers using a spray bottle, again in an amount of 200 g per carrier (Dubey, et al. 2022). After spraying, the natural fibres and EPA are dried at 40°C for 24 hours to reach a constant weight (Guo, et al. 2023). To further examine bacterial attachment and surface morphology, selected carriers from each group were subjected to scanning electron microscopy (SEM) analysis, as detailed in Section 3.4.8.

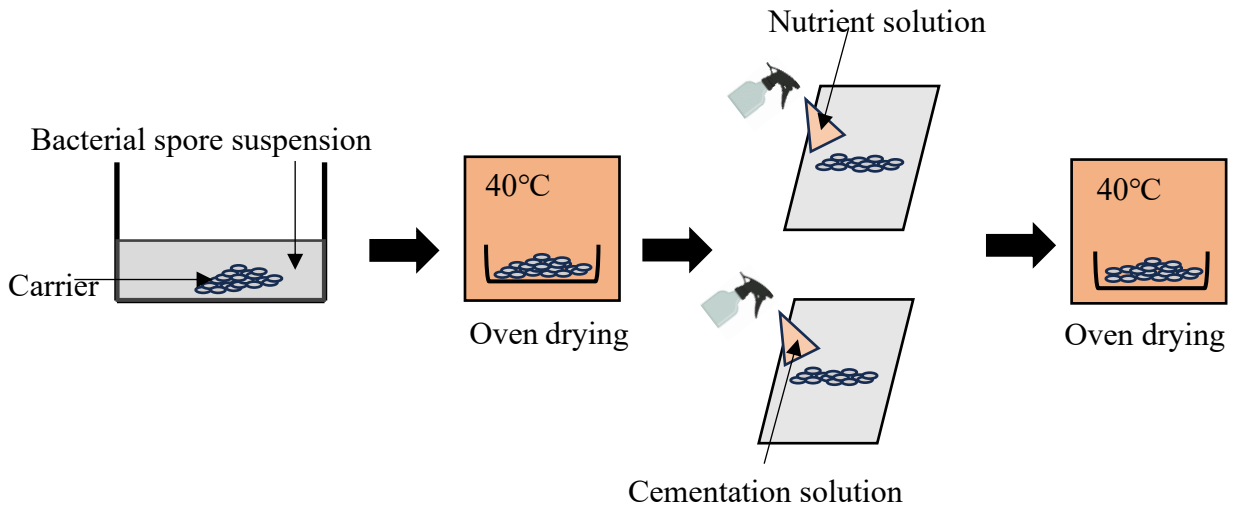

Figure 3.3: Flow chart of carrier preparation

3.4.2 Mortar Mix Design

To evaluate the MICP performance of the different carriers, six types of mortar specimens were prepared to characterise their repair capacity, identifying the healing taking place as indicated by white material developing in the cracks. Mortar mixtures were prepared using Ordinary Portland Cement conforming to ASTM C150 (Rauf, et al. 2020). Seven different types of mortar specimens were prepared using river sand, cement, water and carrier. The water-cement ratio was fixed at 0.5. Adding carriers that have fully absorbed bacterial spores and nutrients to the mortar mixture. Each carrier was incorporated into mortar based on its volume fraction relative to the total specimen volume, with two dosage levels: 1% and 1.5%. The specimens were accordingly named to reflect carrier type and content, in this case Jute-1, Jute-1.5, Flax-1, Flax-1.5, EPA-1, and EPA-1.5. The specimens without bacterial spores and carriers were named as 'control'. The fibres were carefully added to the mortar to avoid agglomeration effects to achieve a uniform distribution of fibres in the mortar (Rauf, et al. 2020).

3.4.3 Mechanical Properties

The mechanical properties of the mortar specimens were evaluated by measuring both compressive and flexural strength to assess the structural effect of different bacterial carriers. All specimens were cured under identical conditions in freshwater for consistency.

Flexural strength tests were conducted using prism specimens with dimensions of $40 \times 40 \times 160\ \text{mm}^3$. The tests followed the three-point bending method in accordance with ASTM C348 (Park, et al. 2021). After 28 days of curing, three specimens from each group were tested for flexural strength using a universal testing machine (Khaneghahi, et al. 2023). The flexural strength was calculated using the relation

$$f_t = \frac{3FL}{2bd^2} \tag{3.2}$$

where F is the maximum load at fracture (N), L is the span length between supports (mm), B is the width of specimen(mm), and d is the depth of specimen(mm). The flexural strain energy (U) absorbed by the mortar under flexural loading was calculated as the area under the stress-strain curve, given by the integral (Park, et al. 2021):

$$U = \int_0^L \int_A f_t \, d\varepsilon dA \, dx \tag{3.3}$$

where L is total length of prism (mm), f_t is the flexural strength in mortar (MPa), ε is the corresponding strain, and A is the cross-section area of the prism.

The compressive strength tests were performed on $50 \times 50 \times 50$ mm^3 cubes using a Sintech 65/G testing machine in accordance with ASTM C109 (Harish, et al. 2016). Three replicate specimens from each carrier group were tested at the same 28 days. Compressive strength was determined using

$$f_c = \frac{P}{A} \tag{3.4}$$

where f_c is the compressive strength (MPa), P is the maximum load (N), A is the cross-sectional area of the specimen (mm^2).

To reflect the consistency and repeatability of the measured results, the coefficient of variation (Co.V, expressed as a percentage) was also calculated for all mechanical property results, which including flexural strength, compressive strength and strain energy.

3.4.4 Crack Formation

The specimens were reinforced with 12 mm diameter rebars placed longitudinally in the centre of the samples and extending 80 mm from the ends of the prisms to act as clamping devices (Khan, et al. 2021). After the first 28 days of curing, all reinforced specimens were subjected to axial tensile loads under direct tensile testing, using a Sintech 65/G, to produce cracks of at least 1 mm in width (Alazhari, et al. 2018, Wang, et al. 2021, Hu, et al. 2018, Vafaei and Ghahremaninezhad 2024). After removing the samples from the machine, the initial crack width was measured, and the samples were placed in an environmental chamber PHC Europe B.V. MLR-352H with a temperature setting of 30°C and 90% humidity (Khaustov, et al. 2022). The crack width was measured again after 28 and 56 days of exposure. A schematic of the sample crack healing measurement scheme is shown in Figure 3.4.

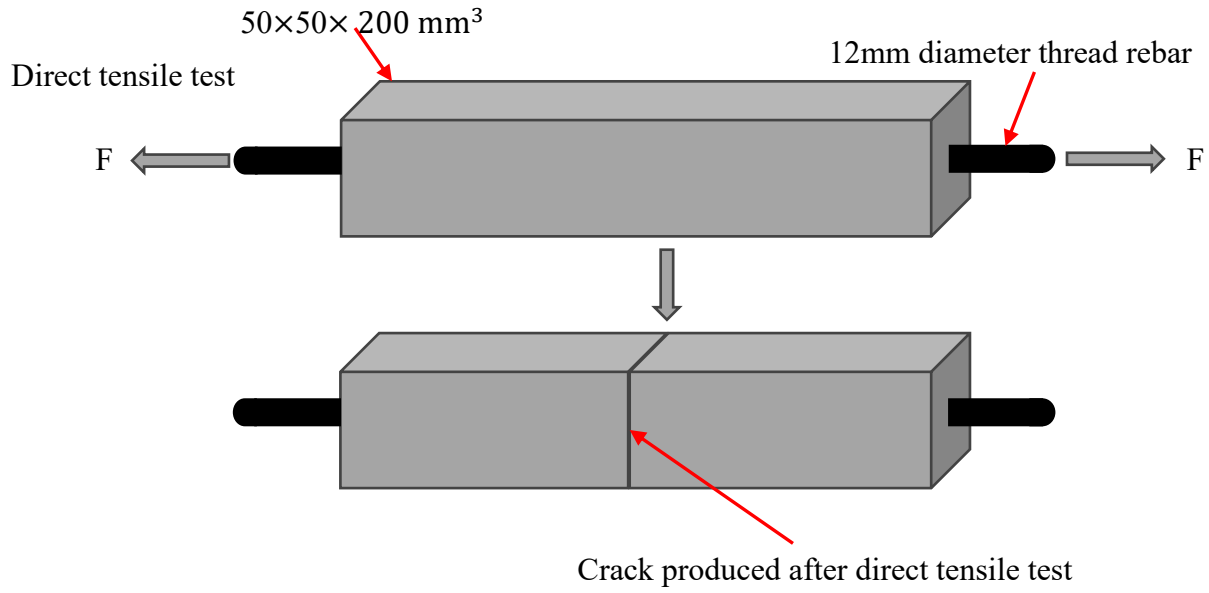

Figure 3.4: Schematic diagram representing the crack healing measurement.

3.4.5 Crack-healing Width Distribution

Images of the prism faces were acquired using a Nikon D810 camera with AF-S NIKKOR 28–300 mm lenses (resolution: 7360 × 4912 pixels). The camera was positioned at a fixed distance of 300 mm from the surface of the specimen to ensure consistent imaging conditions. The first set of images was taken immediately after cracking the sample. Images of the cracks were taken again after 28 and 56 days of exposure to curing. Crack widths were analysed using image processing (Chen, et al. 2024, Chen, et al. 2024). The central area of each face of the prism (crack length of 40 mm) was examined, with the exception of a 5 mm portion of each corner where the healing could not be reliably performed (Khan, et al. 2021). While analysing the crack profile, each row of pixels across the crack width was considered a crack segment measurement.

Pixel values were monitored at each observation interval, and reduction in crack width was interpreted as evidence of healing. Each sample had at least one crack across all 4 faces. Each pixel size around 0.025 mm. The crack width was calculated by the line pixel number times each pixel size.

Both the crack closure percentage and the frequency of fully healed cracks were analysed in relation to the same defined crack width intervals. This approach illustrates the relationship between crack width (mm) and the corresponding healing performance (%) for various self-healing mortar specimens incorporating different bacterial carriers.

To evaluate the crack healing ability of each mortar specimen. Percentage crack closure was calculated by subtracting the number of crack pixels at the time of healing from the number of initial crack pixels, dividing the result by the number of initial crack pixels. This reflects the extent to which the original cracks have closed over time due to self-healing.

To determine the frequency of fully healed cracks, each crack segment was monitored during the healing period. A segment was considered ‘fully healed’ if its pixel value reduced to zero in the observations. The frequency of fully healed cracks within each crack width range was determined by dividing the number of fully healed cracks segments by the total number of segments within that range.

3.4.6 Effect of Crack Depth on Healing

The crack faces were examined to assess the extent of healing depth. To do this, the healed specimens were cut along the bluelines to a depth of 20 mm, half the depth of the specimen, as shown in Figure 3.5. The exposed faces were first inspected using a high-resolution digital camera under consistent lighting conditions to capture visible healing evidenced as white calcium carbonate deposits. For selected areas, further observation was carried out using SEM to examine mineral formation and bacterial activity at a finer scale. The SEM analysis procedure is detailed in Section 3.4.8, where cracked prism specimens were sampled and prepared for microstructural analysis after the healing period. These observations provided visual confirmation of $CaCO_3$ precipitation and microbial colonisation along the crack surfaces. A schematic of the crack-enhancing prisms is shown in Figure 3.5.

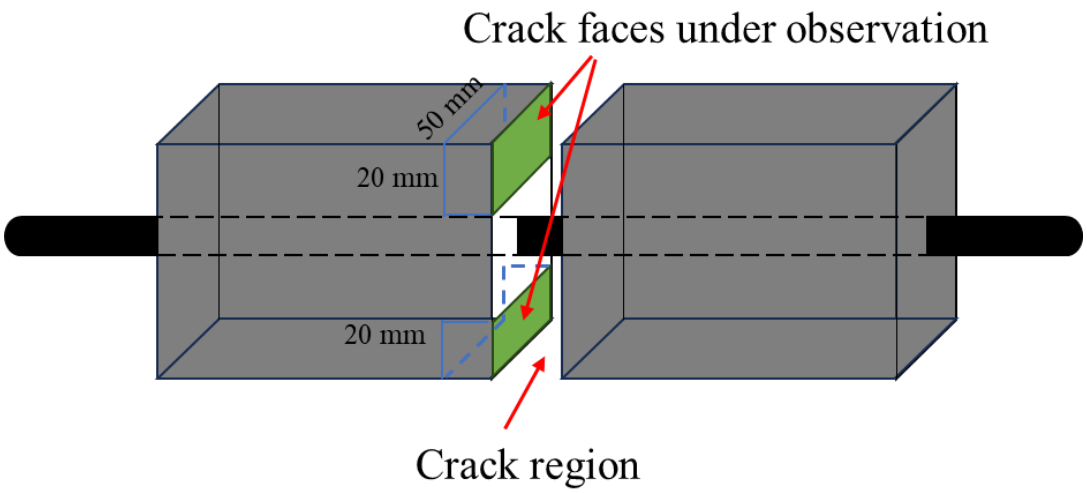

Figure 3.5: Cracked prisms at 56 days of exposure with green section showing to observe crack faces.

3.4.7 Water Permeability Experiments

Water permeability tests were conducted at 0 days and after 56 days of crack healing. Permeability tests ran until a steady volumetric flow was reached, typically 20–40 min. Specimens were pre-saturated and de-aired. Lave is the total visible crack length on the two long faces measured along a centreline; Wave is the mean width from calibrated images.

To avoid the influence of water seepage during the test on the subsequent healing performance, tested specimens did not undergo further healing process after the water permeability test (Lee, et al. 2024). To ensure the consistency among the water permeability tests, comparisons were performed between specimens of the same batch and with similar crack widths. The water permeability set-up is shown in Figure 3.6.

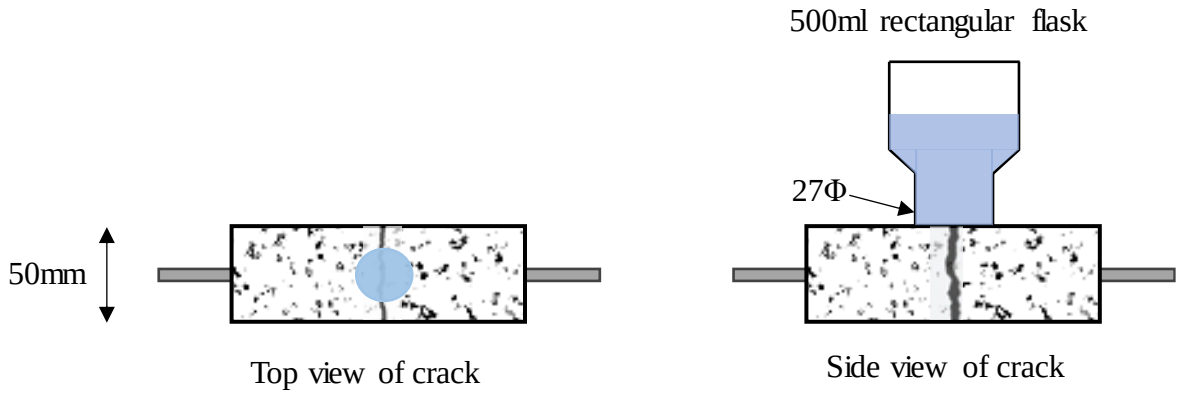

Figure 3.6: Water permeability set-up.

The average flow velocity (cm/s) for each specimen at different healing times was calculated as follows.

$$Flow\ velocity\ = \frac{500}{L_{ave} \times W_{ave} \times t} \tag{3.5}$$

Where L_{ave} is the average length (cm) of cracks on both sides of the specimen; W_{ave} is the average width (cm) of cracks (found by measuring the width once per cm along the crack length direction and then taken the average value); t is the time spent on 500mL water consumption in the permeability test. The smaller the flow velocity of the specimen, the better the self-healing effect of the crack.

3.4.8 Morphology Characterisation

Scanning electron microscopy (SEM) was employed to characterise both the colonisation of bacteria on carrier surfaces and the formation of healing compounds within the cracks. A Phenom XL scanning electron microscope was used for all imaging procedures.

To assess bacterial colonisation, samples of jute, flax, and EPA were extracted after undergoing one week of bacterial symbiosis. These carriers were first dried at 40 °C to a constant weight, then mounted and gold-coated using a sputter coater to enhance surface conductivity (Khan, et al. 2021). SEM imaging at 5 kV was performed to examine bacterial attachment, biopolymer formation, and surface morphology (Carter, et al. 2023).

For crack healing analysis, specimens were taken from the cracked prism surfaces after 56 days of exposure under healing conditions. The green-highlighted regions in Figure 3.5 indicate the areas that were cut and exposed to observe internal crack faces. These samples were air-dried for seven days, then coated with gold before SEM examination (Ratzka, et al. 2023). The imaging focused on identifying $CaCO_3$ precipitates, assessing their morphology, distribution, and correlation with microbial activity on the crack surfaces.

3.5 Summary

This chapter presented a detailed description of the materials and experimental methods employed in this thesis. The properties and preparation of the bacterial strain (*Sporosarcina pasteurii*) and carrier materials (jute fibre, flax fibre, and expanded perlite aggregate—EPA) were introduced. The compatibility and symbiotic relationship between bacteria and carriers

were investigated through water absorption tests, optical density (OD600) measurements, scanning electron microscopy (SEM), Fourier-transform infrared spectroscopy (FTIR), and bio-cementation experiments. Following this, the preparation of mortar specimens containing bacterial carriers was described, and methods for evaluating their mechanical performance and self-healing capabilities were explained.

References:

[1] Alazhari, M., T. Sharma, A. Heath, R. Cooper, K. Paine, Application of expanded perlite encapsulated bacteria and growth media for self-healing concrete, Construction and Building Materials 160 (2018) 610-619.

[2] Andersen, F.A., L. Brecevic, G. Beuter, D.B. Dell'Amico, F. Calderazzo, N.J. Bjerrum, A.E. Underhill, Infrared spectra of amorphous and crystalline calcium carbonate, Acta Chem. Scand 45(10) (1991) 1018-1024.

[3] Begum, H.A., T.R. Tanni, M.A. Shahid, Analysis of water absorption of different natural fibers, Journal of Textile Science and Technology 7(4) (2021) 152-160.

[4] Bhaduri, S., N. Debnath, S. Mitra, Y. Liu, A. Kumar, Microbiologically induced calcite precipitation mediated by Sporosarcina pasteurii, JoVE (Journal of Visualized Experiments) (110) (2016) e53253.

[5] Carter, M.S., M.J. Tuttle, J.A. Mancini, R. Martineau, C.-S. Hung, M.K. Gupta, Microbially induced calcium carbonate precipitation by sporosarcina pasteurii: a case study in optimizing biological CaCO3 precipitation, Applied and Environmental Microbiology 89(8) (2023) e01794-22.

[6] Chen, L., Z. Chen, Z. Xie, L. Wei, J. Hua, L. Huang, P.-S. Yap, Recent developments on natural fiber concrete: A review of properties, sustainability, applications, barriers, and opportunities, Developments in the Built Environment 16 (2023) 100255.

[7] Chen, Z., E.A. Shamsabadi, S. Jiang, L. Shen, D. Dias-da-Costa, An average pooling designed Transformer for robust crack segmentation, Automation in Construction 162 (2024) 105367.

[8] Chen, Z., E.A. Shamsabadi, S. Jiang, L. Shen, D. Dias-da-Costa, Vision Mamba-based autonomous crack segmentation on concrete, asphalt, and masonry surfaces, arXiv:2406.16518 (2024).

[9] Dubey, A.A., N.K. Dhami, K. Ravi, A. Mukherjee, Erosion mitigation with biocementation: a review on applications, challenges, & future perspectives, Reviews in Environmental Science and Bio/Technology 22(4) (2023) 1059-1091.

[10] Dubey, A.A., J. Hooper-Lewis, K. Ravi, N.K. Dhami, A. Mukherjee, Biopolymer-biocement composite treatment for stabilisation of soil against both current and wave erosion, Acta Geotechnica 17(12) (2022) 5391-5410.

[11] Dubey, A.A., R. Murugan, K. Ravi, A. Mukherjee, N.K. Dhami, Investigation on the impact of cementation media concentration on properties of biocement under stimulation and augmentation approaches, Journal of Hazardous, Toxic, and Radioactive Waste 26(1) (2022) 04021050.

[12] Feng, C., X. Zong, B. Cui, H. Guo, W. Zhang, J. Zhu, Application of carrier materials in self-healing cement-based materials based on microbial-induced mineralization, Crystals 12(6) (2022) 797.

[13] Ghosh, T., S. Bhaduri, C. Montemagno, A. Kumar, Sporosarcina pasteurii can form nanoscale calcium carbonate crystals on cell surface, PloS one 14(1) (2019) e0210339.

[14] Gibson, T., An investigation of the Bacillus Pasteuri Group: II. Special physiology of the organisms, Journal of bacteriology 28(3) (1934) 313-322.

[15] Guo, Y., K. Xiang, H. Wang, X. Liu, Q. Ye, X. Wang, Experimental study on self-healing and mechanical properties of sisal fiber-loaded microbial concrete, Materials Research Express 10(4) (2023) 045701.

[16] Haase, H., L. Jordan, L. Keitel, C. Keil, B. Mahltig, Comparison of methods for determining the effectiveness of antibacterial functionalized textiles, PLoS One 12(11) (2017) e0188304.

[17] Harish, B., B. Hanumesh, T. Siddesh, B. Siddhalingesh, An experimental investigation on partial replacement of cement by glass powder in concrete, International Research Journal of Engineering and Technology 3(10) (2016) 1218–1224.

[18] Hu, Z.-X., X.-M. Hu, W.-M. Cheng, Y.-Y. Zhao, M.-Y. Wu, Performance optimization of one-component polyurethane healing agent for self-healing concrete, Construction and Building Materials 179 (2018) 151-159.

[19] Khan, M.B.E., D. Dias-da-Costa, L. Shen, Factors affecting the self-healing performance of bacteria-based cementitious composites: a review, Construction and Building Materials 384 (2023) 131271.

[20] Khan, M.B.E., L. Shen, D. Dias-da-Costa, Crack healing performance of bacteria-based mortar under sustained tensile loading in marine environment, Cement and Concrete Composites 120 (2021) 104055.

[21] Khan, M.B.E., L. Shen, D. Dias-da-Costa, Self-healing behaviour of bio-concrete in submerged and tidal marine environments, Construction and Building Materials 277 (2021) 122332.

[22] Khaneghahi, M.H., D. Kamireddi, S.A. Rahmaninezhad, A. Sadighi, C.L. Schauer, C.M. Sales, A.R. Najafi, A. Cotton, R. Street, Y.A. Farnam, Development of a nature-inspired polymeric fiber (BioFiber) for advanced delivery of self-healing agents into concrete, Construction and Building Materials 408 (2023) 133765.

[23] Khaustov, V.A., I. Döker, O. Joharchi, D.V. Kazakov, A.A. Khaustov, M. Moradi, X.-D. Fang, P. Klimov, A new, broadly distributed species of predacious mites, Neoseiulus neoagrestis sp. nov.,(Acari: Phytoseiidae) discovered through GenBank data mining and extensive morphological analyses, Systematic and Applied Acarology 27(10) (2022) 2038-2061.

[24] Lee, D.K., K.J. Shin, K.M. Lee, Evaluation of crack width and self-healing performance of concrete based on fluid flow characteristics: Comparison between water permeability test and gas diffusion test, Construction and Building Materials 411 (2024) 134118.

[25] Park, J., Q.T. Bui, J. Lee, C. Joh, I.-H. Yang, Interlayer Strength of 3D-Printed Mortar Reinforced by Postinstalled Reinforcement, Materials 14(21) (2021) 6630.

[26] Ratzka, P., P. Zaslansky, P.G. Jost-Brinkmann, Scanning electron microscopy evaluation of enamel surfaces using different air-polishing powders in the orthodontic setting: An in vitro study, Journal of Orofacial Orthopedics/Fortschritte der Kieferorthopädie 85 (2023) 1-10.

[27] Rauf, M., W. Khaliq, R.A. Khushnood, I. Ahmed, Comparative performance of different bacteria immobilized in natural fibers for self-healing in concrete, Construction and Building Materials 258 (2020) 119578.

[28] Stuckrath, C., R. Serpell, L.M. Valenzuela, M. Lopez, Quantification of chemical and biological calcium carbonate precipitation: performance of self-healing in reinforced mortar containing chemical admixtures, Cement and Concrete Composites 50 (2014) 10-15.

[29] Vafaei, B., A. Ghahremaninezhad, Self-healing effect of hydrogels in cement slag and fly ash pastes, Construction and Building Materials 438 (2024) 137036.

[30] Wang, J.-Y., N. De Belie, W. Verstraete, Diatomaceous earth as a protective vehicle for bacteria applied for self-healing concrete, Journal of industrial microbiology and biotechnology 39(4) (2012) 567-577.

[31] Wang, X., L. Chang, X. Shi, L. Wang, Effect of hot-alkali treatment on the structure composition of jute fabrics and mechanical properties of laminated composites, Materials 12(9) (2019) 1386.

[32] Wang, X., S. Chen, Z. Yang, J. Ren, X. Zhang, F. Xing, Self-healing concrete incorporating mineral additives and encapsulated lightweight aggregates: Preparation and application, Construction and Building Materials 301 (2021) 124119.

[33] Wang, Y.-S., H.-S. Lee, R.-S. Lin, X.-Y. Wang, Effect of silicate-modified calcium oxide-based expansive agent on engineering properties and self-healing of ultra-high-strength concrete, Journal of Building Engineering 50 (2022) 104230.

[34] Zhong, J., X. Li, Y. Yao, J. Zhou, S. Cao, X. Zhang, Y. Jian, K. Zhao, Effect of acid-alkali treatment on serum protein adsorption and bacterial adhesion to porous titanium, Journal of Materials Science: Materials in Medicine 33(2) (2022) 20.

Chapter 4 Compatibility and Synergy between Bacteria and Carriers

4.1 Introduction

Several critical factors must be considered to assess effective bacteria-based self-healing for mortar, particularly the compatibility between the bacteria and the chosen carrier materials. In conventional microbial self-healing concrete studies, selecting a suitable carrier is often based on trial and error, changing one parameter at a time (Guo, et al. 2023) (Korniejenko, et al. 2020). However, this traditional approach can lead to extensive experimental workloads and does not fully capture the interaction complexities between the bacteria and various carrier characteristics (Alazhari, et al. 2018, Wang, et al. 2021, Hu, et al. 2018, Vafaei and Ghahremaninezhad 2024). Furthermore, multiple carrier properties, such as water absorption, surface morphology, chemical compatibility, and biopolymer support capacity, significantly influence the microbial-induced calcium carbonate precipitation (MICP) process. Therefore, establishing an effective and systematic approach to evaluating the compatibility and synergistic effects between bacteria and carrier materials is critical.

To improve experimental efficiency and reliability, this study employed a systematic approach involving comparative assessments across multiple parameters. Specifically, natural fibres (jute and flax) and a conventional porous aggregate (expanded perlite aggregate—EPA) were comparatively evaluated in terms of their ability to support bacterial colonisation, biopolymer formation, and calcium carbonate precipitation. Instead of relying on a single-factor approach, this multi-parametric assessment provided a comprehensive understanding of how carrier properties influence bacterial activity and subsequent self-healing performance.

The bacterial growth potential and colonisation patterns on different carriers will be first examined using water absorption rate (Section 4.2), OD600 measurements (Section 4.3) and SEM (Section 4.4). The FTIR analysis (Section 4.5) will identify chemical composition changes in each carrier after bacterial symbiosis, providing further insights into biopolymer formation. The effectiveness of these carriers in promoting mineralisation through MICP will then be assessed in Section 4.6. The bio-cementation test will evaluate the collaborative role of bacteria and the different carriers to determine their impact on enhancing the self-healing properties of concrete.

4.2 Water Absorption Rate

Water absorption is a key characteristic influencing the performance of bacterial carriers in self-healing systems, as it governs the total amount of the available nutrients essential for bacterial viability and activity. Figure 4.7 presents the time-dependent water absorption rate of the three carrier materials (jute, flax, and EPA) over a 24-hour period.

All carriers exhibited rapid initial absorption, with significant increases occurring within the first 2 hours. Jute fibres showed the highest overall water absorption capacity, reaching a stable value of approximately 522%, followed by flax of 471%. In contrast, EPA's absorption reached only about 341%, displaying a relatively lower absorption profile. The superior absorption capacity of jute and flax stems from their cellulose microstructure and capillary porosity, which enables them to retain more liquid. The higher liquid retention enhances their potential as reservoirs of nutrients and bacteria, maintaining bacterial activities for a longer period of time.

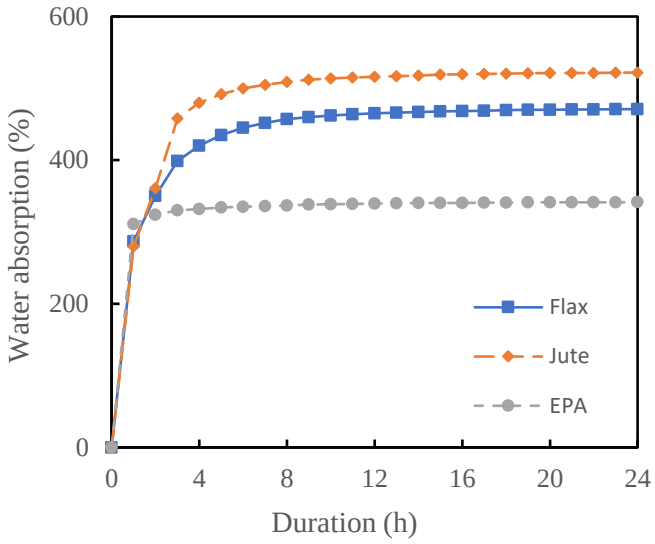

Figure 4.7: Water absorption rate of flax, jute and EPA

4.3 OD600 Measurement

Figure 4.8 shows the OD600 growth curves for the Medium C and Medium D. During the first 4 hours, the OD600 readings remain low due to the sparse bacterial population. From 4 to 12 hours, the readings steadily increase due to an exponential bacterial growth. Compared to the control medium (Medium D), the slopes of the jute and flax based mediums are steeper, suggesting a more rapid bacterial growth. After 16 hours, the growth curves level off due to the stabilisation phase where the rate of bacteria division equals the rate of bacteria death.

It should be denoted that jute and flax mediums showed comparable growth rates, exceeding those cultured in bacteria and nutrition medium. The bacteria have a higher tendency to grow on the surface of natural fibres compared to bacteria alone in the medium. This is attributed to the hydrophilic and rough surface of natural fibres, which can provide an ideal substrate to support growth (Pommet, et al. 2008).

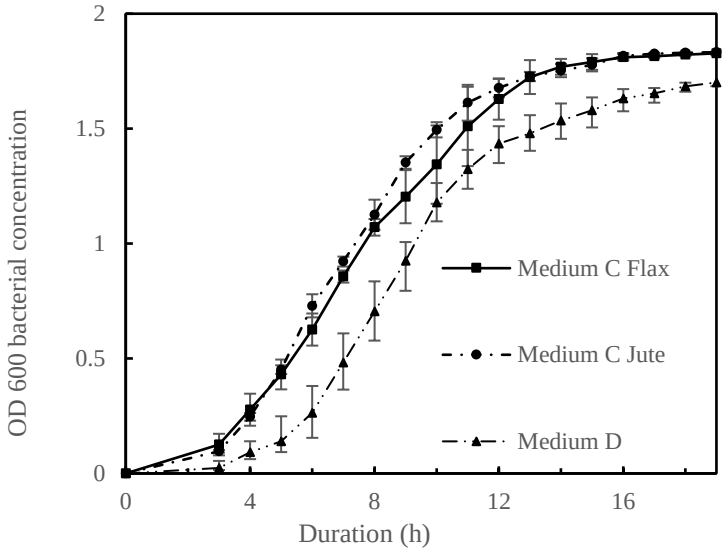

Figure 4.8: OD600 measurements showing the effect of natural fibres on bacterial growth.

4.4 Carrier Surface Morphology

Flax fibres exhibited a 5% weight increase following one week of symbiosis with bacteria, while jute fibres showed a 3% increase after the same process. To ensure accuracy, the dry weight of fibres was compared to the weight after bacterial symbiosis. This weight gain is due to the attachment of biopolymers to the fibre surface. As shown in Figure 4.9, biopolymers are visibly present on the surface of jute fibres, forming a coating that can be observed under magnification. In contrast, no visible biopolymer layer is apparent on flax fibres, despite the increase in weight. This suggests that while both flax and jute fibres retain biopolymers to some extent, the distribution and visibility differ, with jute showing a more substantial surface coating. The attachment of the biopolymers to the surface can support bacteria growth by enabling nucleation sites. The biopolymers are extracellular products of the bacteria growing on the fibre surface and their surfaces are modified by the bacteria at the nanoscale (Pommet,

et al. 2008). The biopolymer was not found in any bacteria and nutrition medium and EPA medium.

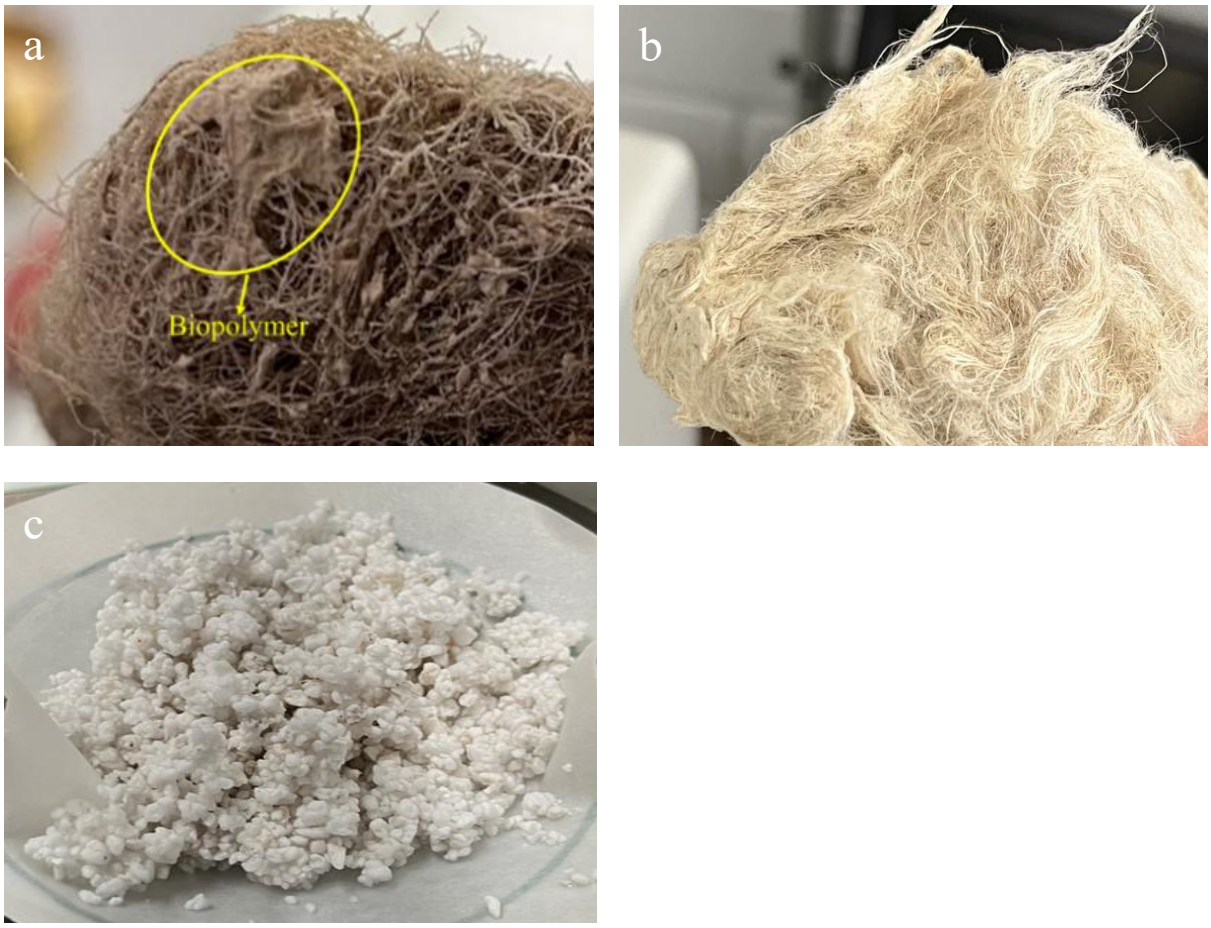

Figure 4.9: Photos of (a) jute fibre, (b) flax fibre and (c) EPA after bacterial symbiosis.

Beyond topography, natural fibres present cellulose/hemicellulose-rich, hydrophilic surfaces that can facilitate bacterial attachment and extracellular polymer formation. The ureolytic strain used here is alkali-tolerant, operating in alkaline conditions characteristic of cementitious matrices; thus, improved colonisation on fibres need not stem from local acidification (Lee, et al. 2024). Nevertheless, limited dissolution of low-molecular-weight organics and acid–base buffering at fibre interfaces may produce subtle near-surface pH differences compared with

silicate EPA (Ghosh, et al. 2019). These chemistry-driven effects were not measured in this study; we therefore interpret them as plausible contributors to the more continuous biofilm/mineral layers observed on fibres, to be examined directly in future work.

The SEM images in Figure 4.10 show the various stages of bacteria growth with jute fibre. The surface of the fibre is initially smooth – see Figure 4.10a. After 4 days, the bacterial cells and the biopolymers produced are noticeable over the surface of the fibre – see Figure 4.10b. After 7 days – see Figure 4.10c – the biopolymer completely covers the surface of the jute fibre, and many bacterial cells are also present on the surface. The biopolymer forms a scaffolding structure that can facilitate the growth of the bacteria over the surface. The scaffolding has a multilayered structure in which the bacteria nucleates and divides.

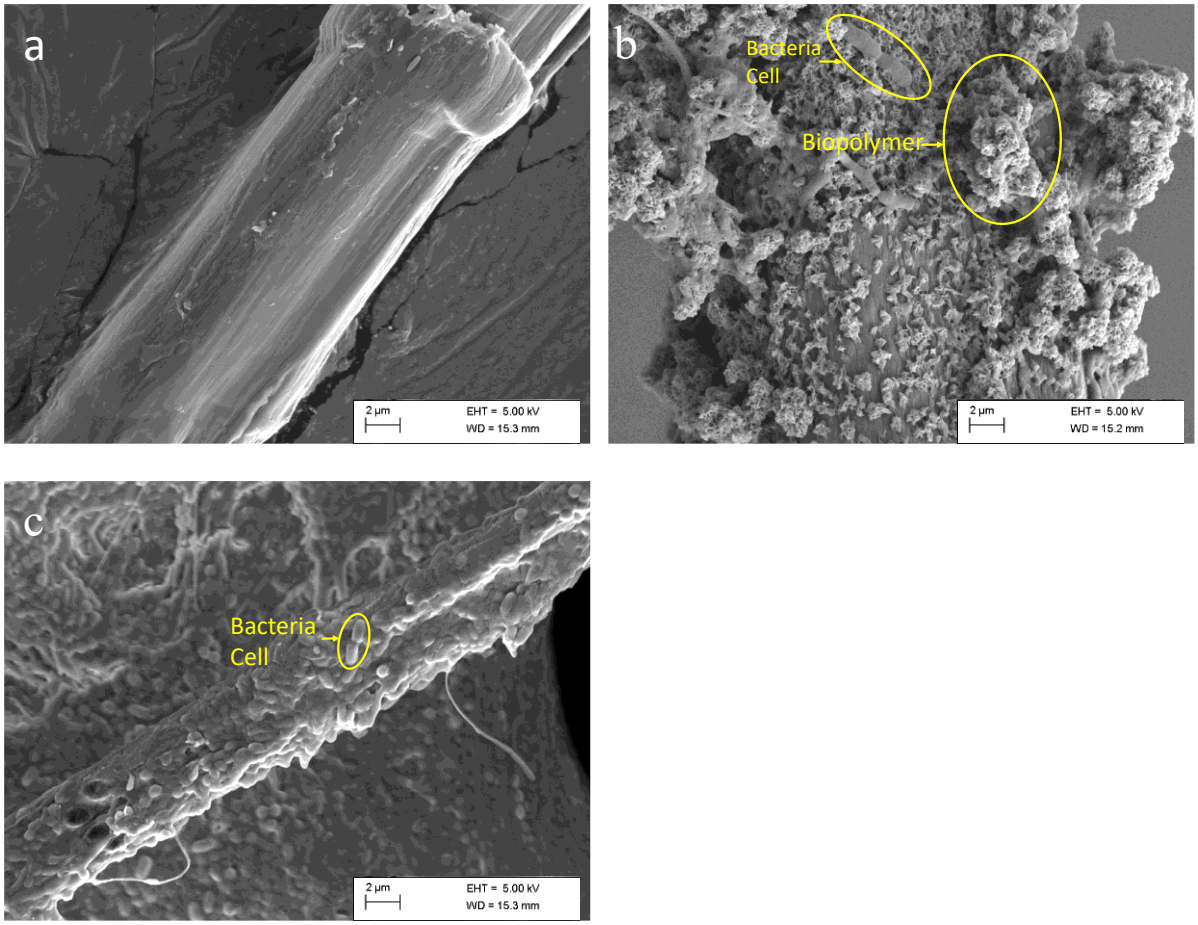

Figure 4.10: SEM images of bacterial growth on jute fibres: (a) initial stage; and after symbiosis with bacteria for (b) 4 days and (c) 7 days.

Figure 4.11 presents the different stages of bacterial growth with flax fibres. The fibre surface is initially flat and smooth – see Figure 4.11a. However, bacterial cells and some biopolymers are already attached to the fibre surface after 4 days (Figure 4.11b). In contrast with the jute fibres, the biopolymers have only one layer at the surface and are not enough to form the scaffolding structure. The rough surface regions formed are in marked contrast to the otherwise smooth surface of the fibre. After 7 days, the single layered biopolymer almost extends over the complete surface (Figure 4.11c).

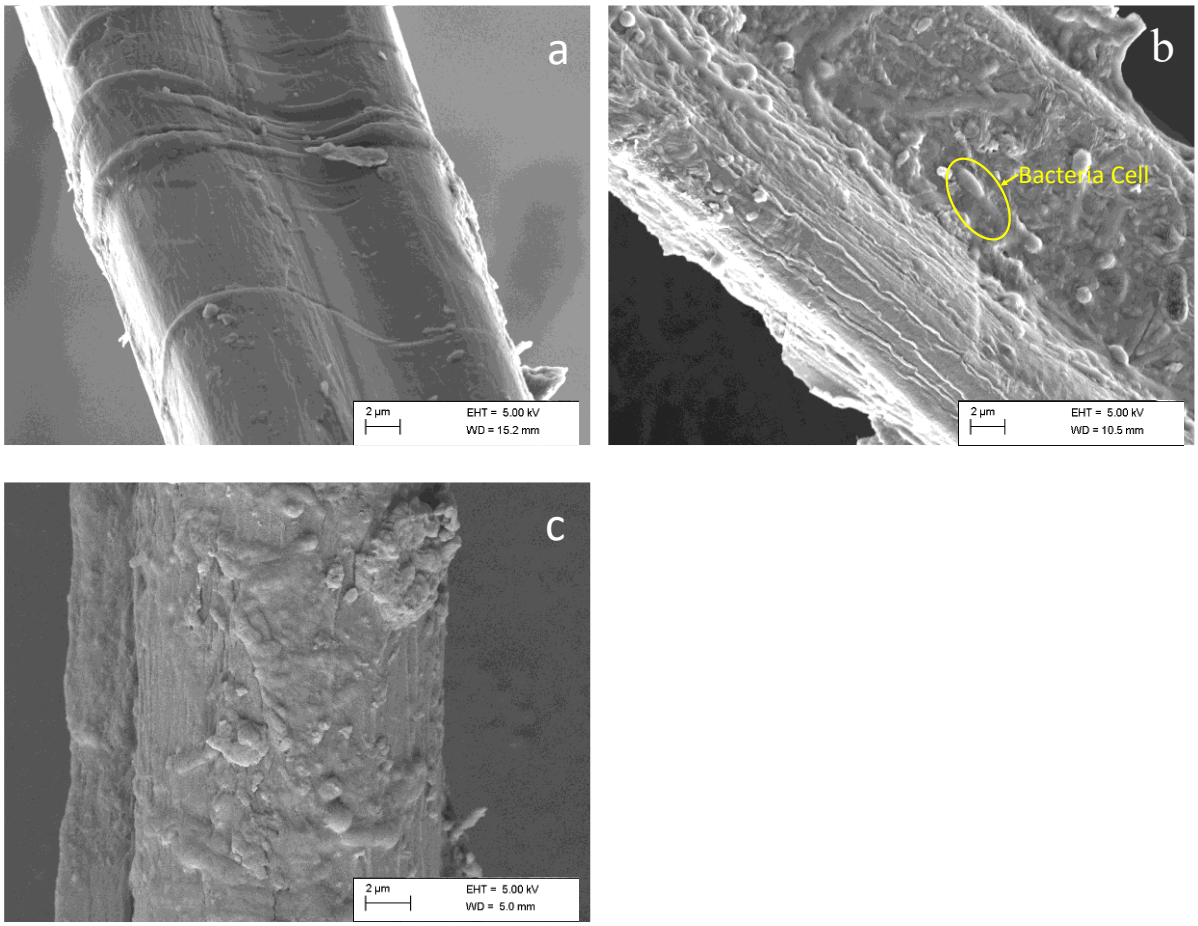

Figure 4.11: SEM images of bacterial growth on flax fibres: (a) initial stage; and after symbiosis with bacteria for (b) 4 days and (c) 7days.

The symbiosis process found with the EPA – see Figure 4.12– is different from that with the fibres. After 7 days the surface (Figure 4.12a) shows no signs of biopolymer layers, despite the presence of the bacterial cells on the surface – see Figure 4.12b. The EPA is a commonly used carrier in bio-concrete due to its good water absorption, and the significant presence of bacterial cells on the surface further confirms its suitability as a carrier. This effectiveness as a bacterial carrier was previously confirmed by the SEM images of Jiang et al (Jiang, et al. 2020).

As compared with EPAs, natural fibres show an enhanced ability to develop biopolymer structure on their surfaces. This can be associated to the presence of cellulose, hemicellulose, and lignin (Imran, et al. 2020), which are similar to biopolymers and can increase bacterial affinity for natural fibre materials. In addition to folds, crevices and micropores on the fibre surface provide more sites for bacteria to nucleate (Zhong, et al. 2022). These structural can enhance bacterial colonisation.

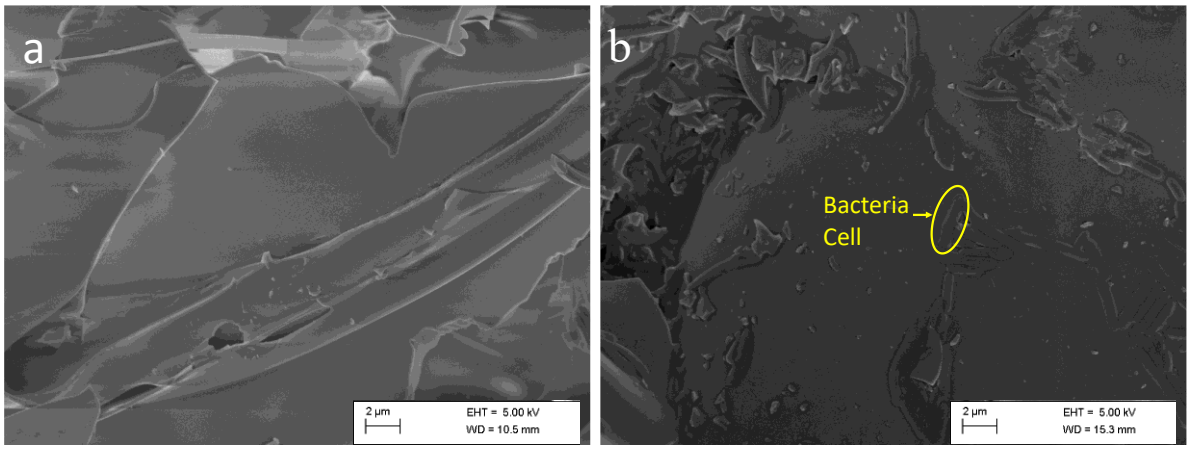

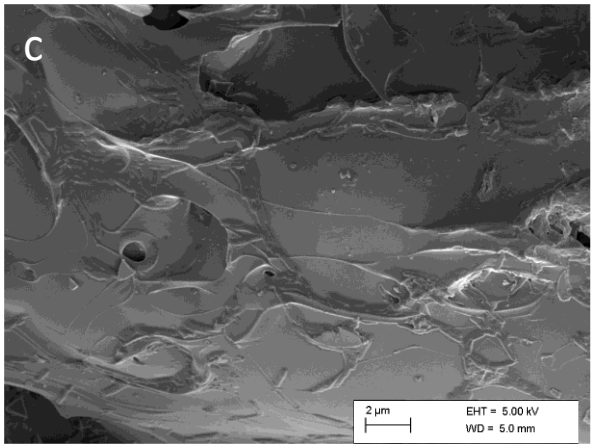

Figure 4.12: SEM images of bacterial growth on EPA: (a) initial stage; and after symbiosis with bacteria for (b) 4 days and (c) 7 days.

The SEM micrographs in Figure. 4.10–4.12 were obtained under identical instrument settings and are used to describe morphology. Because greyscale contrast cannot uniquely distinguish EPS, $CaCO_3$ and substrate, no SEM-based surface-coverage values are reported here, and mineral identification is presented as evidence consistent with carbonate formation. EDS analysis and X-ray elemental mapping were not performed in this thesis.

4.5 FTIR Results

FTIR analysis was conducted to assess the chemical modifications in jute, flax and EPA after the treatment of nutrition solution (Medium B) and bacterial symbiosis (Medium C). The spectra differences in Figure 4.13 provide insights into the changes in methyl and methylene (C-H), carbon-oxygen (C-O) and silicon-oxygen (Si-O) functional groups (Huang, et al. 2013, Reddy and Ravitheja 2019, Ravitheja, et al. 2022). These functional groups can indicate the relevant biopolymer formation on the carriers.

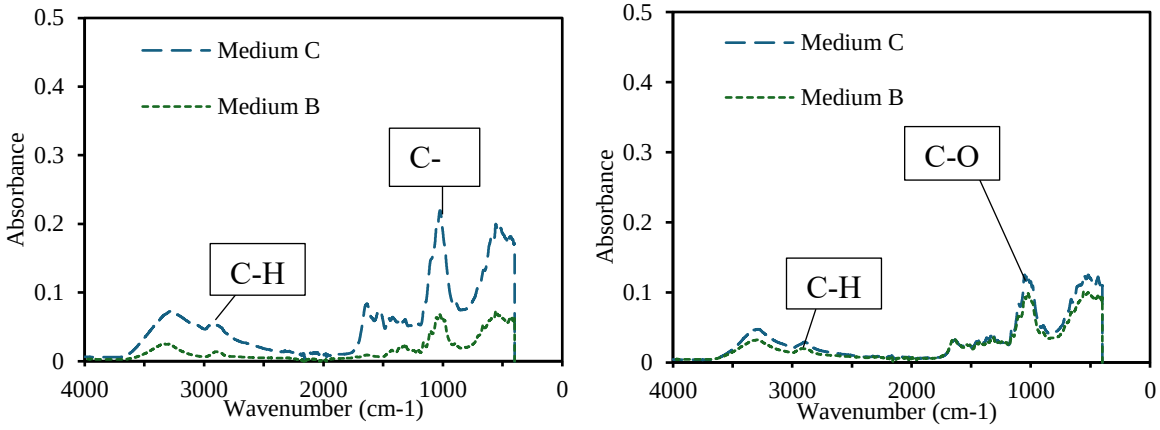

(a) jute

(b) flax

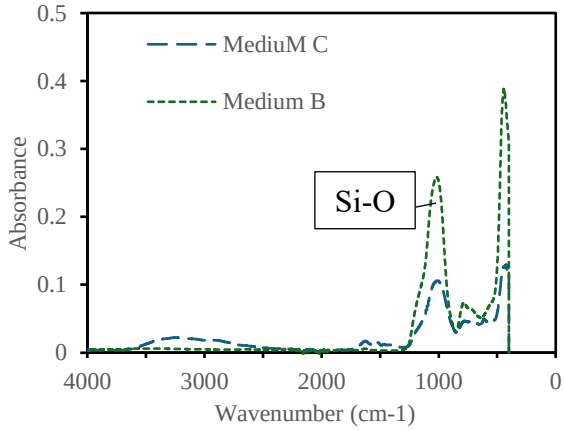

(c) EPA

Figure 4.13: FTIR results for:(a) jute fibre, (b)flax fibre and (c) EPA treated in different solutions.

As shown in Figure 4.13a and 7b, the C-H (2900 cm^{-1}) and C-O (1042 cm^{-1}) stretching peaks are more prominent in Medium C than in Medium B, suggesting bacterial symbiosis promotes biopolymer formation without degrading the cellulose backbone (Horikawa, et al. 2019, Patel, et al. 2016). These observations imply that bacterial activity modifies the jute and flax surface by introducing biopolymers. However, the smaller increase in the C-O peak intensity for flax relative to jute suggests that flax provide less biopolymer support, potentially due to differences in fibre composition or bacterial interaction. In Figure 4.13c, the mineralogical nature of the

EPA is further emphasised by the predominant Si-O oscillations (1000-1200 cm-^{1}) (Borrajo, et al. 2004). The lack of significant C-O or C-H peaks in EPA compared to jute and flax confirms its inorganic composition and the absence of effective biopolymer formation.

FTIR analysis showed that bacterial symbiosis and different responses for different carriers. Jute and flax showed stronger biopolymer formation (C-H/C-O peaks) after bacterial symbiosis (Medium C), indicating enhanced biopolymer formation on their surfaces (Liu 2021, Sun 2009). While these peaks are not unique to bacterial biopolymers, their consistent and pronounced increase after incubation suggests surface-level biochemical changes associated with biopolymer production. And in combination with previous SEM results, flax had weaker biopolymer support than jute, suggesting synergistic limitations. In contrast, EPA lacked organic peaks. Natural fibres are involved in biopolymer production through bacterial adhesion, whereas EPA is not compatible with biopolymers and relies mainly on adherent bacteria.

In this work FTIR is applied as a qualitative, comparative method. Spectra acquired under identical settings allow within-specimen comparison of peak intensities/areas before and after bacterial exposure. Increases in the C–O (~1040 cm^{-1}) and C–H (≈2850–2950 cm^{-1}) regions are interpreted as qualitative confirmation of biopolymer formation on fibre surfaces; however, because these vibrations are also present in the native fibres, FTIR does not provide a quantitative measure of polymer amount nor an unambiguous chemical fingerprint.

4.6 Comparative Analysis of MICP on Natural and Traditional Carrier

The MICP process was compared across the three different carriers. Figure 4.14 presents the SEM images concerning the $CaCO_3$ formation on the carriers in the bio-cementation

experiments. $CaCO_3$ forms a cohesive continuous surface on the jute fibre surface in Medium E, completely covering the fibre — see Figure 4.14a. This is due to the biopolymer scaffolds constructed by the bacteria, which act as the basic structure for the MICP, resulting in a uniquely shaped calcium carbonate layer. In the case of the Medium E with flax, the calcium carbonate crystals do not completely cover the fibre surface – see Figure 4.14b. These crystals nucleate on the surface but do not aggregate into a continuous layer. In the case of Medium E with EPA, calcium carbonate is only present on the outer surface, with no crystals forming on the inner side. This occurs because the bacteria do not nucleate or produce a biopolymer matrix inside the EPA; rather the EPA serves as a storage medium, gradually releasing the bacteria into the cementation solution. This process leads to the production of calcium carbonate, which precipitates and settles to the bottom of the cementation solution and adheres to the surface of the EPA.

From Figure 4.14, it can be observed that the same bacteria can generate calcium carbonate with different shapes depending on the type of carrier, and this difference can be attributed to the unique structure of biopolymers. In Figure 4.14a, the bacteria on the surface of jute fibre constructed a biopolymer in the shape of a scaffold, which promotes the growth of interconnected calcium carbonate crystals to form a calcium carbonate layer covering the surface. In Figure 4.14b the surface of the flax exhibited only a single layer of biopolymers, which did not help to achieve the complete connection of the calcium carbonate crystals. Figure 4.15 shows the structural differences between the internal and external layers of the EPA sample. The external layer appears some calcium carbonate deposits along the edges, in contrast the internal layers exhibit a smoother structure. The contrast between these layers suggests that mineralization primarily occurs on the external surface.

On flax, the coating observed after symbiosis appears as a single, continuous layer. Along the fibre spans the film has an almost uniform thickness, its edges are generally smooth and straight without the step-like terraces that would indicate successive growth fronts, and no overlapping lamellae are visible even at higher magnification. In contrast, jute fibres exhibit a distinctly different morphology: the surface shows stacked, ridge-like laminae with overlapping fronts, giving a terraced appearance consistent with a multilayer biopolymer scaffold. These qualitative morphological differences support the interpretation that the flax coating is predominantly single-layered, whereas jute develops a thicker, multilayer structure.

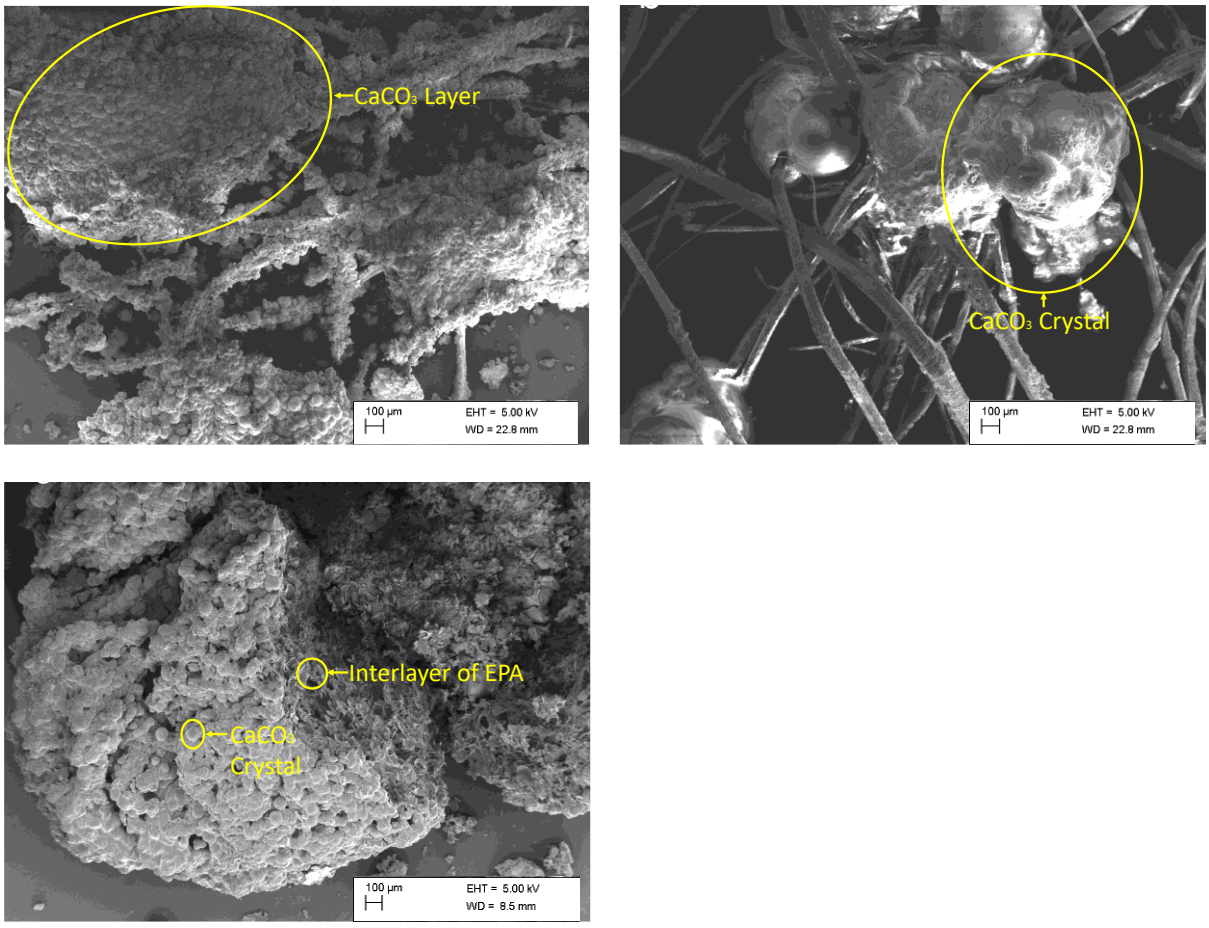

Figure 4.14: SEM images of the (a) jute fibre, (b) flax fibre and (c) EPA surface at the end of MICP process. (Note that CaCO3 crystals stack on the surface of EPA in Fig. 6c).

Spencer et al. (Spencer, et al. 2020) also used jute fibre as a carrier in their MICP process. In their study, they observed that jute fibres were covered with discrete clusters of calcium carbonate, rather than continuous layers of calcium carbonate, and that the fibres did not support the formation of interconnected calcium carbonate structures (Spencer, et al. 2020). This contrasts with our findings, where the presence of biopolymer scaffolds on the fibres played a crucial role in promoting interconnected calcium carbonate formation. In the study by Spencer et al. (Spencer, et al. 2020) calcium carbonate deposition on jute fibres appeared as discrete clusters rather than a continuous layer, with no explicit mentioning of biopolymer presence or formation on the fibre surfaces. This difference in morphology may suggest that, without biopolymer scaffolding, calcium carbonate is less likely to form interconnected structures. Our findings support the hypothesis that biopolymer structures are essential for facilitating an effective MICP process and achieving more uniform and continuous calcium carbonate deposition.

The comparative results for EPA are quite different from those for natural fibres. The SEM image of the internal structure of EPA after the MICP process shows smooth, unaltered surfaces, indicating that no $CaCO_3$ crystals have formed internally — see Figure 4.15. This is consistent with the behaviour of the EPA in bacterial solutions, where the smooth surface demonstrates the ability to store bacteria but not to form biopolymers. These findings confirm that EPA is primarily a passive storage medium, with bacterial activity limited to pore interiors. In contrast, natural fibres allow bacterial colonisation and scaffold formation on external surfaces. We frame this as a functional contrast—external biopolymer formation on fibres vs. internal encapsulation by EPA. No depth-resolved analysis of EPA was undertaken in this study. Qualitative SEM suggests that precipitation is concentrated near the particle surface, with minimal deposits on interior pore walls, but we did not map elemental distributions or viability

as a function of depth; therefore, any micro-environment gradient within EPA remains unquantified.

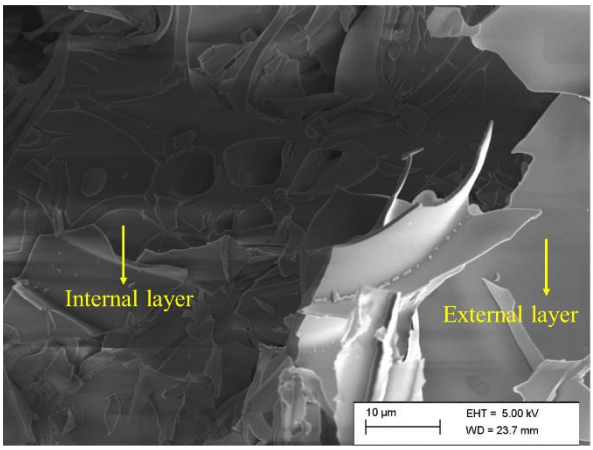

Figure 4.15: SEM images of the EPA internal layer at the end of MICP process.

In summary, SEM images demonstrate that the variations in MICP behaviour across jute, flax, and EPA are directly influenced by the ability of the bacteria to colonise the carriers and the formation of biopolymer matrices. The presence of a well-developed biopolymer scaffold enhances calcium carbonate precipitation, while its absence limits mineralisation efficiency and structural integration. Bacteria play a crucial role in coordinating calcium carbonate production, while the substrate-specific interactions involving biopolymer scaffolds significantly influence the locations and extent of calcium carbonate nucleation and precipitation.

4.7 Conclusions

The synergistic interactions between natural fibres and *Sporosarcina pasteurii* bacteria was investigated with a focus on their ability to potentially promote healing in concrete. The results

demonstrated that natural fibres, when combined with bacteria, exhibit better compatibility and generate bacterial biopolymers as compared to EPAs. After being symbiotic with the bacterial culture treatment, flax and jute fibres showed a weight increase of 5% and 3%, respectively, after one week. This modification of the carrier surface increases the number of nucleation sites for bacterial growth and enhances the microbial-induced calcium carbonate precipitation process. In contrast with EPA, natural fibres enable bacteria to generate a biopolymer over the surface that can support efficient self-healing in concrete. The biopolymer, however, is different for flax and jute fibres. In the case of flax, only one layer develops to produce a rough surface, whereas in the case of jute several layers leading to a scaffolding multi-layered structure develop. In both cases, the biopolymer can promote bacterial growth and generates nucleation sites. The role of natural fibres (jute and flax) as bacterial scaffolds in bio-cement formation was also investigated. FTIR analyses provided important insights into bacterial interactions confirmed the formation of biopolymers on natural fibers (especially jute), as indicated by characteristic absorption peaks in the range of 3000-3500 cm^{-1} and 1500-2000 cm^{-1}. Furthermore, confirming that EPA does not contribute to biopolymer formation, but simply functions as a physical carrier for bacteria in synthesis of calcium carbonate.

In summary, the observed differences in MICP behaviour across flax, jute, and EPA carriers are primarily driven by the interactions between bacteria and the presence or absence of biopolymer matrices. Natural fibres provide a more favourable environment for bacterial colonisation and biopolymer formation, which directly influences the extent and morphology of calcium carbonate precipitation. The comparative analysis suggests that natural fibres, particularly jute and flax, have significant potential to enhance the self-healing performance of bacteria-based bio-concrete, while EPA, though effective at storing and releasing bacteria, lacks the biopolymer support required for internal calcium carbonate formation.

It is anticipated that the compatibility between fibres and bacteria can be beneficial to enhance the local healing of cracks in concrete structures. Future investigations will target the optimisation of these natural fibre to maximise their self-healing capabilities and further assess their practical applications in construction.

References

[1] Alazhari, M., T. Sharma, A. Heath, R. Cooper, K. Paine, Application of expanded perlite encapsulated bacteria and growth media for self-healing concrete, Construction and Building Materials 160 (2018) 610-619.

[2] Borrajo, J.P., S. Liste, J. Serra, P. González, S. Chiussi, B. León, M. Pérez Amor, H.O. Ylänen, M. Hupa, Influence of the network modifier content on the bioactivity of silicate glasses, Key Engineering Materials 254 (2004) 23-26.

[3] Guo, Y., K. Xiang, H. Wang, X. Liu, Q. Ye, X. Wang, Experimental study on self-healing and mechanical properties of sisal fiber-loaded microbial concrete, Materials Research Express 10(4) (2023) 045701.

[4] Horikawa, Y., S. Hirano, A. Mihashi, Y. Kobayashi, S. Zhai, J. Sugiyama, Prediction of lignin contents from infrared spectroscopy: chemical digestion and lignin/biomass ratios of Cryptomeria japonica, Applied biochemistry and biotechnology 188 (2019) 1066-1076.

[5] Hu, Z.-X., X.-M. Hu, W.-M. Cheng, Y.-Y. Zhao, M.-Y. Wu, Performance optimization of one-component polyurethane healing agent for self-healing concrete, Construction and Building Materials 179 (2018) 151-159.

[6] Huang, H., G. Ye, D. Damidot, Characterization and quantification of self-healing behaviors of microcracks due to further hydration in cement paste, Cement and Concrete Research 52 (2013) 71-81.

[7] Imran, M.A., S. Gowthaman, K. Nakashima, S. Kawasaki, The influence of the addition of plant-based natural fibers (Jute) on biocemented sand using MICP method, Materials 13(18) (2020) 4198.

[8] Jiang, L., G. Jia, C. Jiang, Z. Li, Sugar-coated expanded perlite as a bacterial carrier for crack-healing concrete applications, Construction and Building Materials 232 (2020) 117222.

[9] Korniejenko, K., B. Figiela, H. Šimonová, B. Kucharczyková, M.D. Guigou, M. Łach, The influence of fibre pre-treatment on the mechanical properties of the geopolymer composites, MATEC Web of Conferences, EDP Sciences 322 (2020) 01012.

[10] Liu, X., IR spectrum and characteristic absorption bands, Organic chemistry I, LibreTexts (2024),1-3.

[11] Patel, C.M., A.A. Barot, V. Kumar Sinha, Sequential liquefaction of Nicotiana tabacum stems biomass by crude polyhydric alcohols for the production of polyols and rigid polyurethane foams, Journal of Applied Polymer Science 133(38) (2016) 43974.

[12] Pommet, M., J. Juntaro, J.Y. Heng, A. Mantalaris, A.F. Lee, K. Wilson, G. Kalinka, M.S. Shaffer, A. Bismarck, Surface modification of natural fibers using bacteria: depositing bacterial cellulose onto natural fibers to create hierarchical fiber reinforced nanocomposites, Biomacromolecules 9(6) (2008) 1643-1651.

[13] Ravitheja, A., T.C.S. Reddy, C. Sashidhar, Improvising the Self-Healing Capabilities of Concrete Using Different Pozzolanic Materials and Crystalline Admixtures, Journal of Wuhan University of Technology-Mater. Sci. Ed. 37(3) (2022) 429-439.

[14] Reddy, T.C.S., A. Ravitheja, Macro mechanical properties of self healing concrete with crystalline admixture under different environments, Ain Shams Engineering Journal 10(1) (2019) 23-32.

[15] Spencer, C.A., L. van Paassen, H. Sass, Effect of jute fibres on the process of MICP and properties of biocemented sand, Materials 13(23) (2020) 5429.

[16] Sun, Q., The Raman OH stretching bands of liquid water, Vibrational Spectroscopy 51(2) (2009) 213-217.

[17] Vafaei, B., A. Ghahremaninezhad, Self-healing effect of hydrogels in cement slag and fly ash pastes, Construction and Building Materials 438 (2024) 137036.

[18] Wang, X., S. Chen, Z. Yang, J. Ren, X. Zhang, F. Xing, Self-healing concrete incorporating mineral additives and encapsulated lightweight aggregates: Preparation and application, Construction and Building Materials 301 (2021) 124119.

[19] Zhong, J., X. Li, Y. Yao, J. Zhou, S. Cao, X. Zhang, Y. Jian, K. Zhao, Effect of acid-alkali treatment on serum protein adsorption and bacterial adhesion to porous titanium, Journal of Materials Science: Materials in Medicine 33(2) (2022) 20.

Chapter 5: Evaluation of Fibre and EPA as Bacterial Carriers in Mortars

5.1 Introduction

Several critical factors must be considered to successfully select bacterial carriers for effective self-healing mortar, particularly their influence on mechanical performance, crack sealing capability, and durability. Conventionally, evaluating bacterial carrier performance involves varying one parameter at a time, while keeping other factors constant. However, this conventional approach demands extensive experimental efforts and often overlooks interactions between multiple parameters, such as carrier type, dosage, bacterial colonisation efficiency, and healing mechanisms. Given the complexity of microbial-induced calcium carbonate precipitation (MICP) in mortar, adopting an effective comparative approach to simultaneously assess multiple carrier properties is essential.

To enhance experimental efficiency and gain comprehensive insights, this study comparatively evaluated natural fibres (jute and flax) and expanded perlite aggregate (EPA) as bacterial carriers for self-healing mortar applications. Each carrier was systematically tested across multiple parameters, including mechanical strength, crack healing efficiency, and water permeability reduction. Rather than the single-variable method, the comparative evaluation method employed herein provided reliable and detailed results, clearly highlighting how carrier choice impacts the effectiveness of bacteria-based self-healing mortar systems.

5.2 Carrier SEM Image Before Mixing

The SEM images (Figure 5.16) show that all three carrier materials - jute, flax and EPA - absorbed bacterial spores after preparation, which is essential for the MICP process. Both flax and jute fibres have rough, porous surfaces, and show high spore density, making them effective carriers for microbial activity. In contrast, EPA has a smoother surface and showed fewer absorbed spores compared with the fibre carriers. Overall jute and flax are expected to perform better as bacterial carriers due to their better ability to retain spores on their surface.

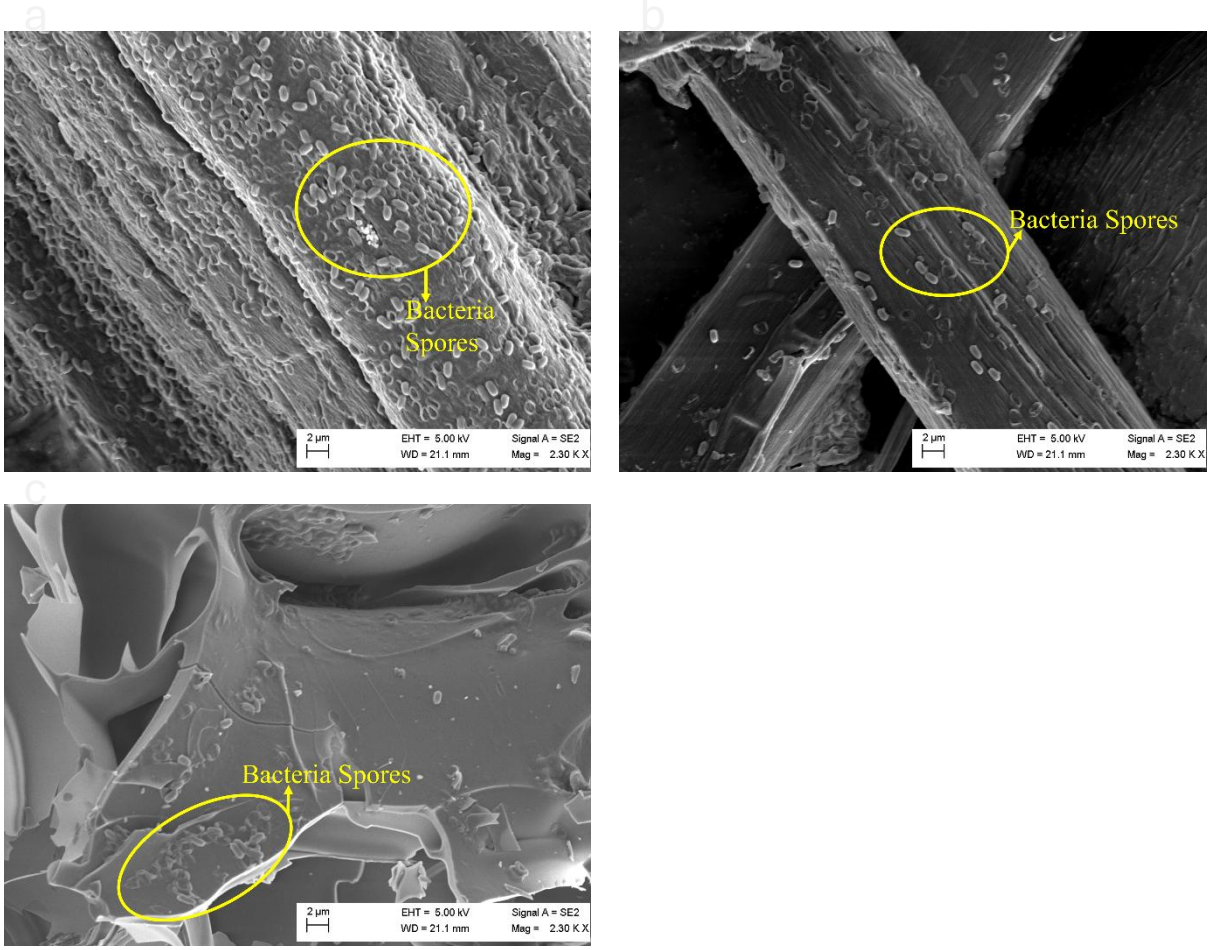

Figure 5.16: SEM image of the carrier after preparation: a) jute, b) flax, c) EPA

5.3 Mechanical Properties of Mortar Specimens

Table 5.2 shows the results of the flexural strength, compressive strength and strain energy of the mortar specimens with the addition of different bacterial carriers. Among all groups, Jute-1 exhibited the highest strain energy, while flax and EPA-based specimens showed lower values. In contrast, the control and EPA specimens had higher compressive strength than the fibre-containing groups.

Table 5.2: Mortar strength test properties

	Compressive strength (f_c)		Flexural strength (f_t)		Flexural strain energy (U)	
	Mean	Co.V	Mean	Co.V	Mean	Co.V
	MPa	%	MPa	%	kN.mm	%
Control	28.4	7	8.6	11	0.152	8
Jute-1	18.6	4	6.7	5	0.458	12
Jute-1.5	15.2	11	6.4	4	0.312	12
Flax-1	9.4	12	4.4	12	0.302	17
Flax-1.5	13.1	1	6.4	9	0.450	15
EPA-1	24.8	8	8.5	6	0.125	1
EPA-1.5	22.1	7	8.1	4	0.166	11

These results suggest that mortar specimens containing jute fibres exhibited a high mechanical performance among the tested carriers. This enhanced performance may be attributed to the fibre's physical characteristics, such as their elongated shape and surface texture. Potentially improved bonding with the mortar and helped effectively bridge cracks. The low strain energy of EPA specimens indicates limited ability to absorb deformation energy, due to their weaker structural role within the crack zone.

The lower compressive and flexural strengths observed in the fibre mixes arise from material effects intrinsic to short plant fibres at the tested dosages: increased occluded-void content and a more compliant fibre–matrix ITZ—even under identical vibration—combined with a pull-out–dominated response that favours post-crack energy absorption rather than peak strength (Horikawa, et al. 2019, Patel, et al. 2016). By contrast, the EPA mix contains granular inclusions that preserve matrix continuity and introduce fewer slip planes; consequently, its compressive strength and first-crack modulus-of-rupture are higher than those of the fibre-reinforced mortars, while its post-crack toughness gain is modest.

5.4 Self-healing Characterisation

Figure 5.17 shows the representative photos of different group of cracked specimens after healing times of 0, 28 and 56 days. As can be seen from the figure, generally the crack width of mortar specimens with self-healing agent decreased gradually with the increase of healing time, and MICP crystals can be observed on their surface.

On Day 0, all specimens exhibit visible cracks ranging from 0.9 mm to 1.5 mm in width. These cracks are significant and continuous across the surface of each specimen. By Day 28, the cracks in most groups show significant progress in healing, with visible white precipitates

forming along the crack lines. Figure 5.17b through 2e (jute and flax specimens) exhibit more substantial healing, with reduced crack visibility. However, cracks in specimens a, f and g (Control and EPA-based specimens) are still noticeable. By Day 56, the jute and flax groups achieved near-complete healing, with the maximum crack sealing of 1.23 mm observed in Group b (Jute-1), showing minimal visible cracks. In particular, the jute specimens (Figure 5.17b and 2c) demonstrate the most extensive crack closure, with minimal visible cracks remaining. The EPA specimens (Figure 5.17f and 2g) show only partial healing. In contrast, the control specimens (Figure 5.17a) showed no healing. While there has been some reduction in crack width, particularly in the EPA-1.5 specimen (Figure 5.17g), the cracks remain more pronounced compared to the jute and flax groups, with some sections of the crack lines still visible. By Day 56, the cracks in the jute and flax specimens were almost entirely healed, with calcium carbonate deposits covering the crack surfaces. However, the cracks in the EPA specimens remained partially visible, with significant gaps in the calcium carbonate deposits.

Based on these visual observations, it is hypothesised that the healing performance of the bacteria-based self-healing mortar is strongly influenced by the type of carrier (Fronczyk, et al. 2023). The jute and flax specimens show a higher healing efficiency compared to the EPA specimens. The natural fibres, jute and flax likely provide a more suitable environment for microbial growth due to their higher water absorption capacities and increased surface roughness (Elfaleh, et al. 2023). This could have allowed for more extensive MICP along the crack surfaces, leading to more efficient healing. The fibre content specimens performed particularly well, possibly due to the higher availability of reactive sites for bacterial activity and crystal formation, which facilitated faster and more complete crack closure (Fahimizadeh, et al. 2022). In contrast, the EPA specimens exhibited less efficient healing, particularly the EPA-1 specimen. The lower water absorption capacity of EPA may have limited the amount

of bacterial growth and nutrient retention within the cracks, reducing the overall extent of healing. The results suggest that jute and flax fibres, particularly jute fibre specimens are more effective carriers for promoting self-healing in mortar due to their superior capacity to support microbial activity and $CaCO_3$ formation.

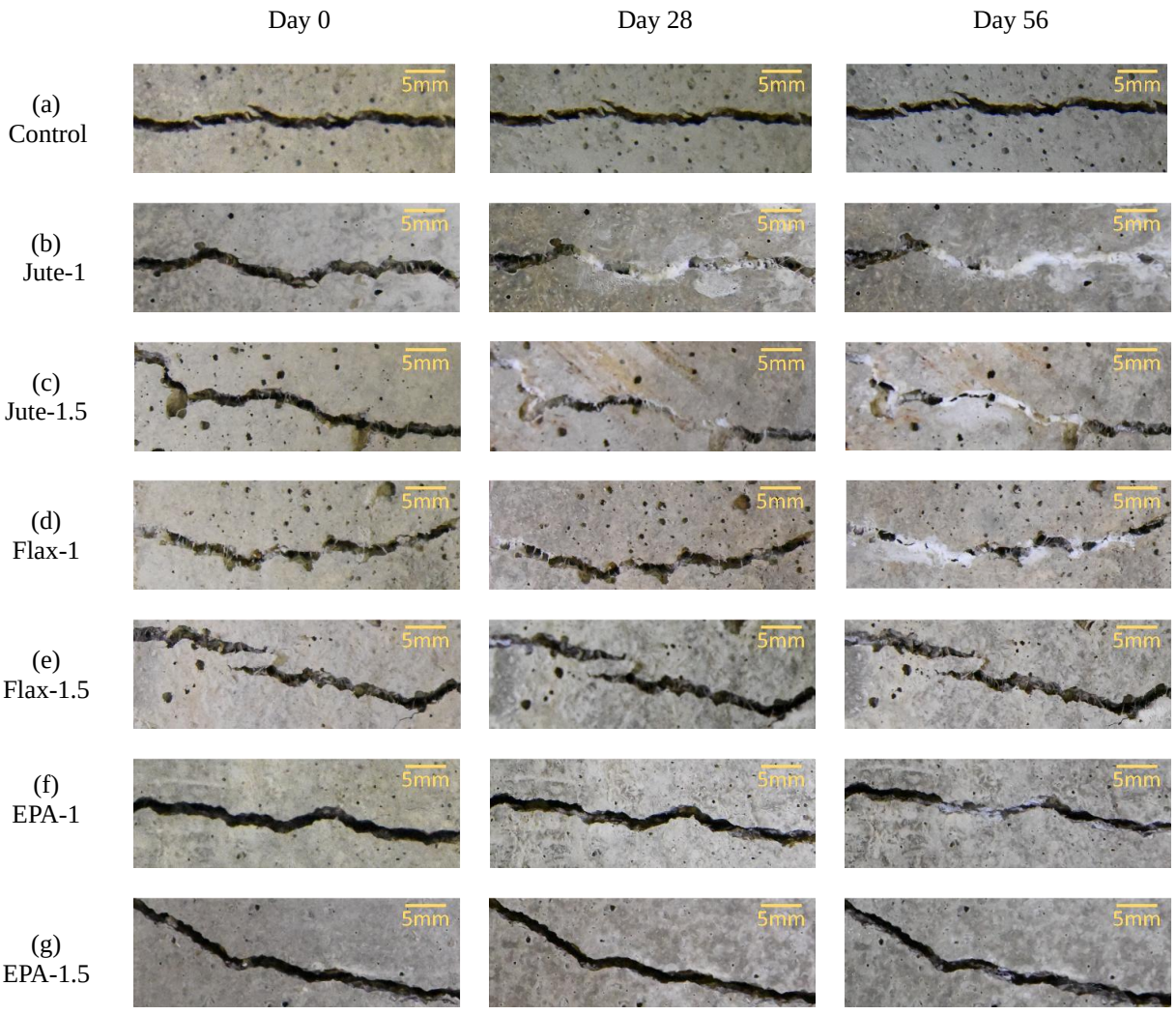

Figure 5.17: Photos of representative crack-healing process in various mortar specimens: a) control, b) Jute-1, c) Jute-1.5, d) Flax-1, e) Flax-1.5, f) EPA-1, g) EPA-1.5.

Figure 5.18 displays a crack mortar surface at 28 days of healing. Red boxes highlight specific regions along the crack lines where visible healing has occurred and magnified insets on the right show close-up views of these regions.

In Figure 5.18a, the jute specimen has dense white mineral deposits at the cracks. The magnified view clearly shows that $CaCO_3$ continuously builds up around the embedded jute fibres. These fibres act as nucleation points and promote local healing. In Figure 5.18b the flax sample also shows clear signs of healing. Although the mineral deposition was thinner compared to jute. Figure 5.18c shows limited healing in the EPA sample. Most of the cracks are still open and the deposits are minimal and discontinuous.

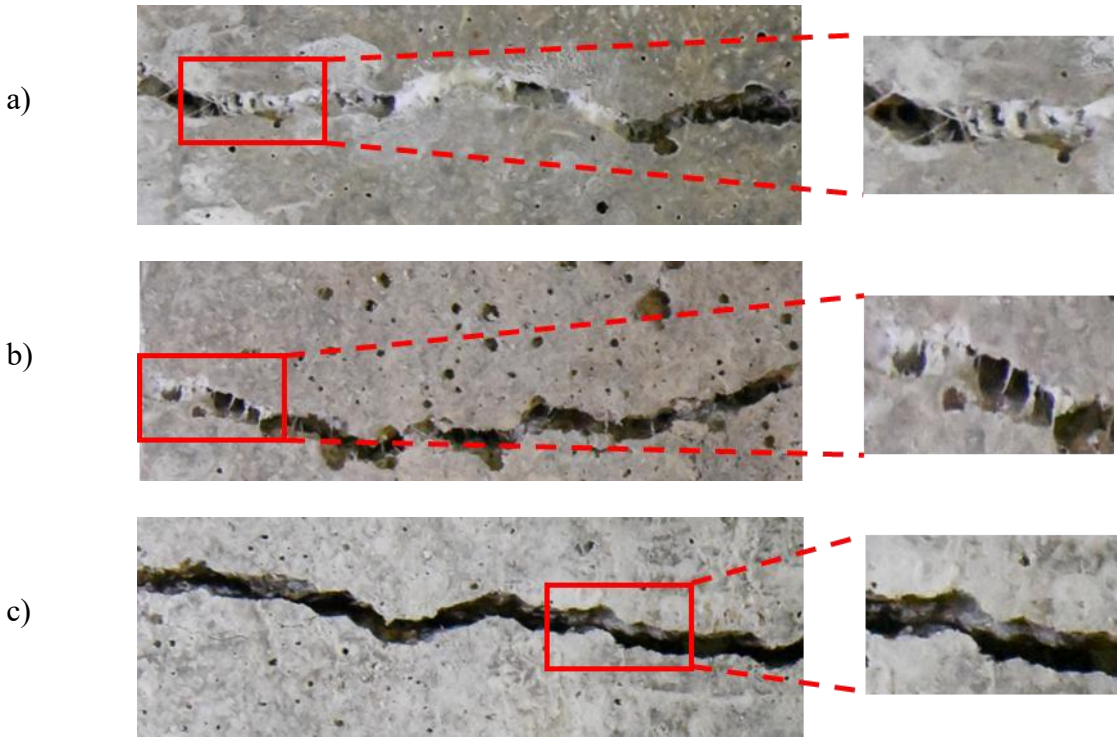

Figure 5.18: crack healing and calcite deposition along crack paths: a) Jute specimen, b) Flax specimen, c) EPA specimen.

It is not necessary for each EPA particle to fracture. We created through-thickness cracks larger than 1 mm under direct tension; these cracks intersect EPA grains and open the EPA–matrix interfaces, establishing hydraulic connectivity so that pore water, nutrients and spores within EPA can exchange with the crack water. Evidence of EPA participation is seen post-healing as deposits appear on/near EPA surfaces within the crack after healing.

5.5 Crack-healing Width Distribution

Figure 5.19a illustrates the relationship between crack width (mm) and the corresponding crack closure percentage (%) for different self-healing mortar specimens incorporating various bacterial carriers.

As expected from Figure 5.19a shows a general decline in healing percentage with increasing crack width, consistent with typical bacterial healing behaviour. That is, narrower cracks are more likely to close due to the limited space for calcite deposition. The control specimens do not perform well across the entire crack width range, which is a side effect of the fact that hydration is not as effective in the case of large cracks. In the smallest crack range (<1.0 mm), the jute-1 group achieves the highest healing percentage at approximately 80%, followed by jute-1.5 at 60%, while both EPA groups are significantly below 50%. As cracks widen to 1.0-1.3 mm, healing percentages decline further, though Jute-1 still maintains superior performance. Beyond 1.3 mm, all groups exhibit a sharp reduction in healing capacity.

Figure 5.19b shows the frequency of fully healed cracks across a range of crack widths. As can be seen from the figure, jute specimens demonstrate the highest frequencies of fully healed cracks, particularly in sub-0.9 mm range where Jute-1 surpasses 50% fully healed frequency, with Jute-1.5 closely trailing. Flax specimens show moderate efficiency (20-40% for small

cracks), but their performance deteriorates beyond 1.0 mm. In contrast, EPA groups consistently underperform, rarely exceeding 25% fully healed frequency even in narrow cracks, and plummeting below 10% for widths over 1.3 mm. The control group, which contains no bacterial carriers, shows negligible healing across all crack widths, with frequencies consistently below 5%. This confirms that the observed healing in fibre and EPA groups is primarily attributed to microbial-induced calcite precipitation rather than autogenous healing. Both subfigures confirm that crack width expansion beyond 1.3 mm universally diminishes healing effectiveness across all material types. Larger cracks are more difficult to heal due to the limited bacterial colonisation and $CaCO_3$ formation within the larger gap (Jiang, et al. 2020). However, even at these larger crack widths, flax-based specimens still demonstrate healing (around 30-40%), similar to the performance of jute in larger cracks.

The analysis shows that the efficacy of self-healing mortar via MICP hinges on carrier material selection and concentration. Jute-1 consistently demonstrates the highest healing performance across all crack widths among the tested specimens. However, increasing the jute content to 1.5% does not lead to further improvement in healing efficiency. This suggests that a 1% jute dosage may be sufficient to achieve optimal healing under the conditions studied, while higher content may not provide additional benefit. Flax-based specimens, though less effective than jute, outperform EPA groups, particularly in cracks under 1 mm. However, the minimal difference between Flax-1 and Flax-1.5 implies limited gains from higher concentrations, likely due to the slightly lower water absorption and nutrient retention of flax compared to jute (Huner 2015). In contrast, EPA groups have the lower healing capacity across all crack sizes, as their poor water absorption and nutrient retention severely restrict microbial viability and $CaCO_3$ deposition. Even at 1.5% concentration, EPA fails to improve healing rates, confirming its unsuitability for MICP applications, especially in wider cracks (>1.3 mm).

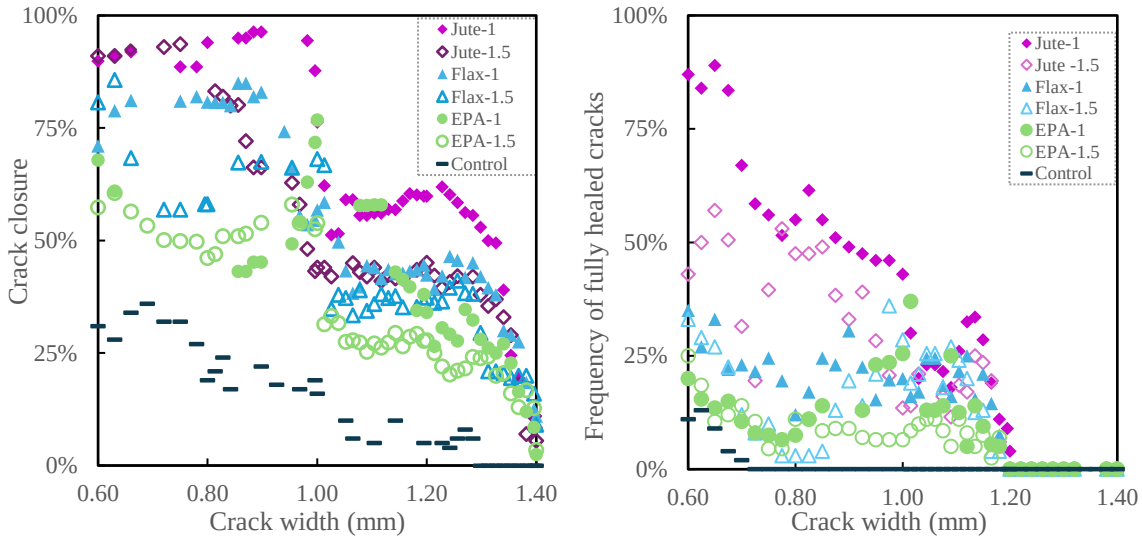

(a) (b)

Figure 5.19: The relationship between the initial crack width and crack-healing percentage at 56 days: a) Detailed crack closure after 56 Days. b) Frequency of Fully Healed Cracks vs. Crack Width

Healing efficiency is governed by the interaction between fibre dosage and initial crack width. An optimum occurs at ≈1 vol% for the fibre mixes, where dispersion is uniform: the resulting network of bridges reduces the effective aperture and aided by capillary wicking along the fibres, sustains moisture and nutrient delivery to the crack faces. Increasing the content to 1.5 vol% does not improve healing; local clustering/shadowing begins to impede transport and reduces the colonisable surface per fibre, so precipitation becomes patchier rather than continuous (see Figure. 5.19). Width effects further reflect both geometry and surface chemistry. With increasing width, the systems become progressively transport-limited; nevertheless, jute at 1% maintains the highest closure up to ~1.2–1.3 mm, consistent with its hierarchical capillarity and rough surface that support a multi-layer bio-scaffold and surface-spanning $CaCO_3$. Flax, with a thinner scaffold, is intermediate, whereas EPA, acting primarily as an internal reservoir with a relatively smooth exterior, tends to form more isolated deposits and is most effective at smaller widths. Thus, the observed dosage × width behaviour reflects a balance between bridging geometry and the carrier's pore structure/connectivity and

scaffoldability, which together control transport, colonisation and the continuity of mineral sealing.

5.6 Effect of Crack Depth on Healing

Figure 5.20 illustrates the cracked surfaces of three different mortar specimens containing different bacterial carriers. These images provide the internal crack morphology and depth of healing after the self-healing process.

Figure 5.20a shows the cracked surface of the jute sample, where a significant amount of white $CaCO_3$ can be clearly observed on the surface of the crack. The presence of $CaCO_3$ on the cracked surface of the jute specimen suggests that MICP is very effective. Compared to the jute specimen, the flax specimen (Figure 5.20b) had a smaller area of $CaCO_3$ generation and did not completely cover the crack section of the specimen. Especially at the edge section, reduced $CaCO_3$ deposition was found. However, $CaCO_3$ was still deposited in the internal region near the rebar, away from the specimen edges. The smoother crack edges and partial healing suggest that although flax is effective, it may not be as good at retaining water and supporting microbial activity as jute. This is consistent with the percent healing observed in Figure 5.19, where the flax specimen, although slightly inferior to the jute specimen, shows good performance. However, the healing rate of the EPA specimen (Figure 5.20c) was low. Few visible $CaCO_3$ deposits were deposited at the margins. However, a small amount of white $CaCO_3$ can still be seen to be generated.

The combined analysis of healing percentages from Figure 5.19 and crack face observations from Figure 5.20 shows natural fibres jute and flax as significantly more effective than EPA in promoting self-healing. The highest healing percentages were observed in the Jute-1 specimen. This, along with the significant calcium carbonate deposition along the crack face, suggests that jute fibres provide an ideal environment for microbial growth and $CaCO_3$ precipitation.

The higher nutrient retention of jute likely enhance microbial activity, resulting in more extensive healing over time (Spencer, et al. 2020). Flax fibres, while effective, appear to provide slightly less support for microbial activity than jute. This is evidenced by the lower healing percentages in Figure 5.19 and the less pronounced $CaCO_3$ deposits on the crack face in Figure 5.20. Nonetheless, flax fibre still shows great healing potential, making it a viable alternative to jute. EPA-based specimens, on the other hand, exhibit poor performance in both healing percentage and crack face analysis. The limited $CaCO_3$ formation indicate that EPA is not suitable for promoting microbial activity necessary for crack healing.

This study did not include a dedicated fracture-micromechanics programme, and the tested prisms are not available for post-hoc fractography; therefore, quantitative discrimination of fibre failure modes was not performed. In line with prior observations on short plant-fibre composites at similar dosages and geometries, the likely governing mechanism is interfacial debonding followed by fibre pull-out, with occasional fibre rupture.

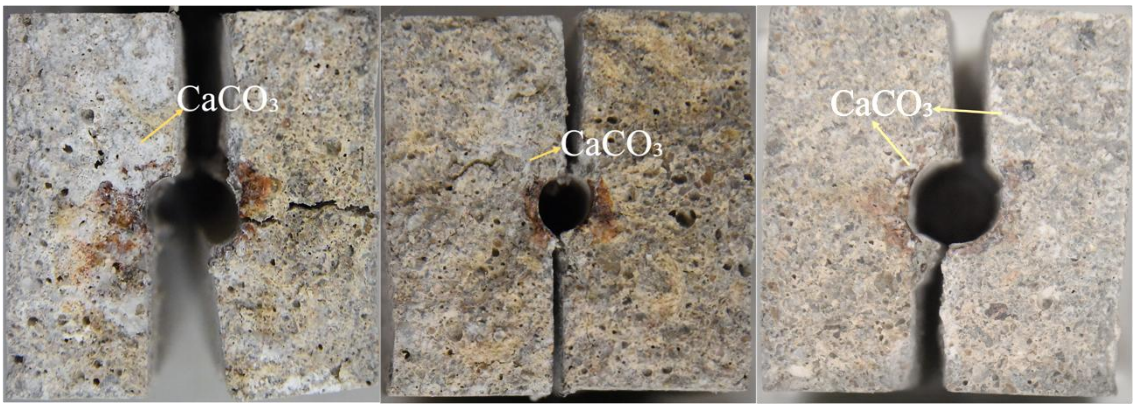

(a) (b) (c)

Figure 5.20: Image of crack faces for (a) Jute specimen, (b) Flax specimen and (c) EPA specimen

Within the fibre geometry used in this study (length 8–10 mm; fixed diameter and dispersion, flax and EPA exhibited a pronounced decline in healing effectiveness as the initial crack width increased and were most reliable for smaller widths ($\lesssim$ 1.0 mm). By contrast, jute at 1 vol% maintained effective sealing up to ~1.2–1.3 mm. Width envelope is geometry-dependent: longer fibres or a higher aspect ratio could increase bridging length and reduce the effective aperture seen by the healing system, potentially extending the treatable width range. Any such adjustment must be balanced against workability and dispersion constraints, which can introduce clustering and diminish transport to the crack faces.

5.7 Water Permeability of Specimens

(a) (b)

Figure 5.21a presents the flow velocity (cm/s) of mortar specimens between control and after the healing period across different carrier groups. In the control state, EPA-1.5 exhibits the highest flow velocity (~30 cm/s), followed by EPA-1. Jute and flax based specimens have significantly lower flow velocities, particularly Jute-1 and Flax-1.5, which record values below 10 cm/s. After healing, a clear reduction in flow velocity is observed across all groups. Jute-1 shows a significant drop. EPA-based specimens also exhibit reduced flow velocity, but the extent of improvement remains less pronounced compared to fibre-based groups. The recovery% values derived from Figure. 5.21b are: 38.1 % for Jute-1 , 36.7 % for Flax-1, 33.0 % for EPA-1.5, 14.3 % for Flax-1.5, 13.3 % for Jute-1.5, and 6.0 % for EPA-1. Thus, the 1 % fibre mixes (especially jute) deliver the largest relative reduction in flow, whereas EPA-1 exhibits limited recovery. Because recovery% can appear high even when the absolute post-healing flow remains large (e.g., EPA-1.5), both metrics are reported for context.

The significantly lower flow velocity after healing indicate that all groups of cracks have been sealed. The jute-based specimens (especially Jute-1) had the best sealing effect. This suggests a superior healing mechanism. The relatively high flow velocity after healing of the EPA specimens implies limited healing efficiency, which may be due to weak microbial interactions or poor crack bridging.

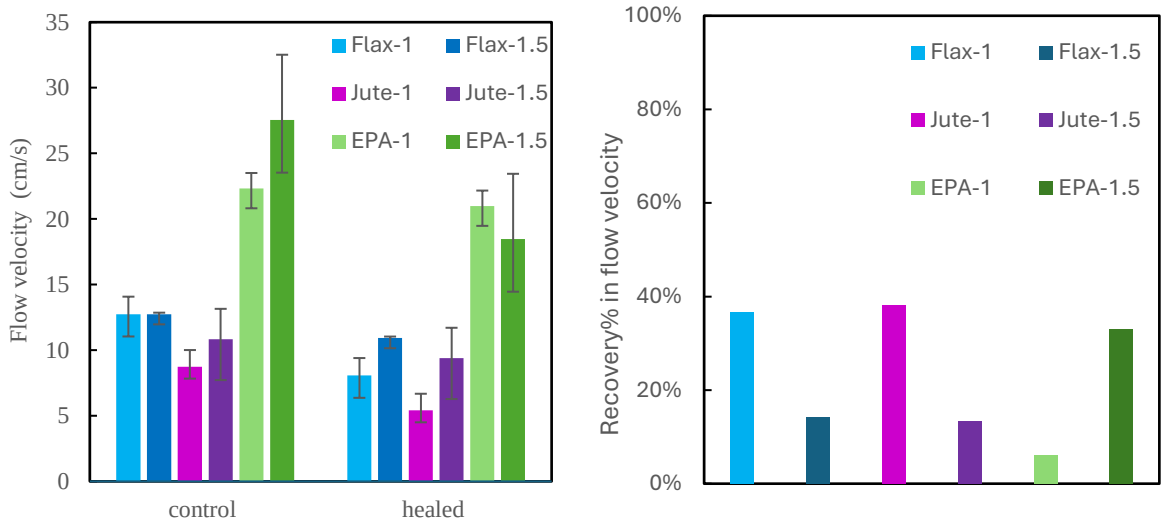

Figure 5.21: a) Flow velocity of mortar specimens before and after healing period. b) Recovery% in flow velocity after healing.

5.8 Microstructure of Self-healing Agent

Figure 5.22 presents a microstructure analysis of healing products within cracked mortar specimens using SEM imaging. The figure compares surface morphologies of jute, flax and EPA-based specimens zero day and after 56 days of healing. The presence of CaCO3 deposits highlighted with yellow annotations, provides visual confirmation of microbial-induced mineral precipitation along the fibre surfaces. (note: SEM appearances for the 1% and 1.5% content of each carrier type, including jute, flax and EPA are visually similar at this stage).

In Figure 5.22a, the jute fibre is clearly visible with a smooth, clean surface, showing no evidence of healing at zero day after specimen cracking. The surface of the jute is relatively clear, with no $CaCO_3$ deposits or signs of microbial activity. In Figure 5.22b, the same jute fibre after 56 days of cracking displays significant $CaCO_3$ precipitation. The fibre surface is now rough and covered indicating substantial microbial activity. The presence of these $CaCO_3$ deposits is crucial for the self-healing process as they aid in closing cracks. The flax fibre in Figure 5.22c similarly shows no visible signs of healing. The surface is smooth and clear, with no $CaCO_3$ or microbial presence. In Figure 5.22d, the flax fibre displays $CaCO_3$ deposits along the fibre surface after 56 days of cracking. Although less dense than in the jute specimens, the $CaCO_3$ has still accumulated around the fibre, indicating that microbial-induced healing has occurred. Figure 5.22e shows the EPA surface, which is smooth, clear, and shows no $CaCO_3$ formation or healing signs. Figure 5.22F shows that $CaCO_3$ precipitation occurred on the EPA surface after healing; however, the deposits appeared more isolated and less integrated with the substrate compared to the denser surface coverage observed in jute and flax specimens.

Jute specimens exhibit the most substantial healing, as shown by the dense $CaCO_3$ deposits around the fibre surface. The rough and porous texture of jute fibres appears to provide an ideal environment for microbial attachment and growth, which is essential for efficient microbial-induced $CaCO_3$ precipitation (MICP) (Spencer, et al. 2020). The uneven, fibrous structure allows $CaCO_3$ to adhere more effectively to the surface, closing cracks and reducing water permeability (Turner, et al. 2023, Zhang, et al. 2024). This supports earlier findings where Jute-1 and Jute-1.5 showed superior healing percentages and permeability reductions compared to other carriers. Although the EPA samples showed some $CaCO_3$ deposition after healing, the degree of healing was much lower than that of jute or flax. The smooth shape of EPA means that its surface area is limited and there are few anchoring sites for bacteria, which reduces the

efficiency of $CaCO_3$ formation. This explains the consistently lower healing percentages and minimal permeability reduction observed in the EPA-based samples. Even if $CaCO_3$ had formed, it was not sufficient to fully repair the cracks or significantly improve the material properties.

	Zero day after cracking	56 days after cracking
Jute specimen	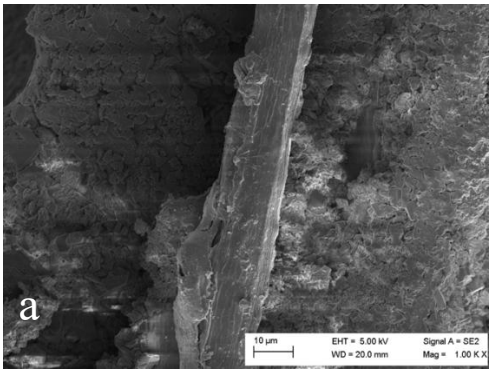	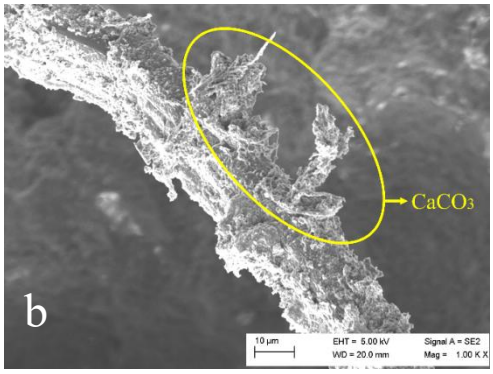
Flax specimen	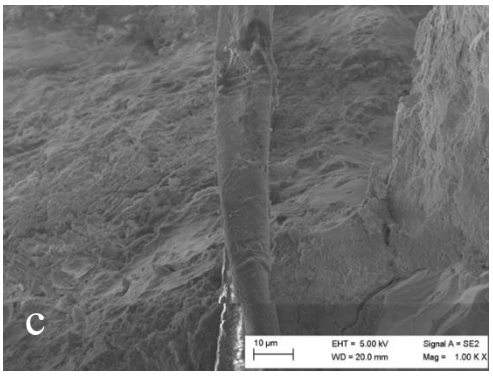	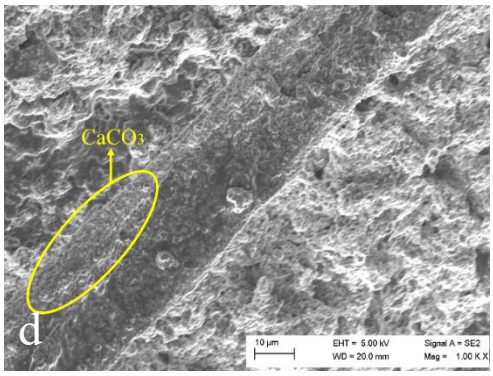
EPA specimen	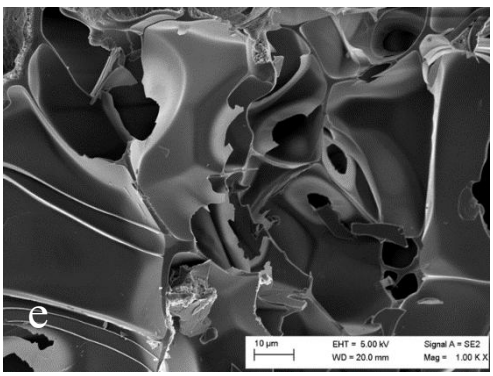	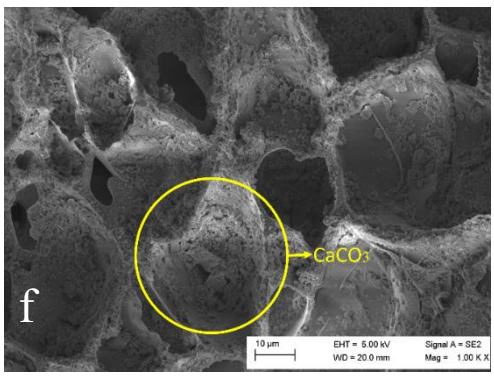

Figure 5.22: Microstructural analysis of healing products in the crack: a) Unhealed Jute specimen, b) Healed Jute specimen, c) Unhealed Flax specimen, d) Healed Flax specimen, e) Unhealed EPA specimen, f) Healed EPA specimen

Although no µCT/MIP/NMR measurements were undertaken, the post-healing drop in flow velocity, together with SEM images showing carbonate along crack faces, indicates that healing primarily reduces the connected fraction of the crack-affected pore network rather than altering bulk matrix porosity. Consistent with the micrographs, the 1 % fibre mixes exhibit the largest qualitative reduction in connectivity (more continuous lining), whereas EPA shows smaller connectivity change with more discontinuous deposits. Because 3-D pore-structure tests were not performed, these statements are reported qualitatively and are identified for quantitative confirmation in future work using micro-CT (connected-porosity/tortuosity metrics) and complementary porosimetry.

5.9 Conclusion

This study provides a comprehensive evaluation of the self-healing abilities of various carrier materials, i.e. jute, flax, and expanded perlite aggregate (EPA), in mortar specimens. The results from multiple tests – crack healing performance, permeability reduction, and SEM analysis – clearly demonstrate that the effectiveness of self-healing in mortar is highly dependent on the type and characteristics of the carrier material used. Among the tested materials, jute consistently proved to be the most effective carrier for microbial-induced calcium carbonate precipitation (MICP). The fibrous and rough surface of jute fibres allowed for enhanced bacterial colonization and $CaCO_3$ formation, which led to superior crack healing,

substantial reductions in water permeability, and the highest flow rate reduction across various crack widths. The Jute-1 specimen achieved the best overall healing performance, indicating that a lower jute content strikes the optimal balance between fibre distribution and microbial activity. These results underscore the importance of selecting a carrier material that not only promotes microbial growth but also provides sufficient surface area for effective $CaCO_3$ deposition. The results also highlight the critical role of crack width in determining healing efficiency. While all carriers showed reduced performance in larger cracks (>1.2 mm), jute was able to maintain relatively high healing effectiveness even in wider cracks, further reinforcing its superiority as a carrier. Conversely, both flax and EPA struggled to maintain effective healing as crack widths increased, indicating that they are more suitable for smaller cracks.

Overall, the comparative results indicate that carrier performance is governed not only by surface roughness but also by a broader set of material attributes. In particular, jute combines an alkali-tolerant organic matrix, connected capillary pores and a cellulose-rich, hydrophilic surface that together provide storage, transport and a scaffold for $CaCO_3$, while flax and EPA are more limited by either weaker scaffold formation or less favourable pore architecture. These observations suggest that, when selecting carriers, chemical composition, pore structure and (for natural fibres) carbon availability should be considered alongside surface morphology, even though a full quantitative characterisation of these factors lies beyond the scope of the present work and is left for future study.

References

[1] Elfaleh, I., F. Abbassi, M. Habibi, F. Ahmad, M. Guedri, M. Nasri, C. Garnier, A comprehensive review of natural fibers and their composites: An eco-friendly alternative to conventional materials, Results in Engineering 19 (2023) 101271.

[2] Fahimizadeh, M., P. Pasbakhsh, L.S. Mae, J.B.L. Tan, R.S. Raman, Multifunctional, sustainable, and biological non-ureolytic self-healing systems for cement-based materials, Engineering 13 (2022) 217-237.

[3] Fronczyk, J., M. Janek, M. Szeląg, A. Pyzik, W. Franus, Immobilization of (bio-) healing agents for self-healing concrete technology: does it really ensure long-term performance?, Composites Part B: Engineering 266 (2023) 110997.

[4] Huner, U., Effect of water absorption on the mechanical properties of flax fiber reinforced epoxy composites, Advances in Science and Technology. Research Journal 9(26) (2015) 1-6.

[5] Jiang, L., G. Jia, C. Jiang, Z. Li, Sugar-coated expanded perlite as a bacterial carrier for crack-healing concrete applications, Construction and Building Materials 232 (2020) 117222.

[6] Spencer, C.A., L. van Paassen, H. Sass, Effect of jute fibres on the process of MICP and properties of biocemented sand, Materials 13(23) (2020) 5429.

[7] Turner, R., G.M. Castro, J. Minto, G. El Mountassir, R.J. Lunn, Treatment of fractured concrete via microbially induced carbonate precipitation: From micro-scale characteristics to macro-scale behaviour, Construction and Building Materials 384 (2023) 131467.

[8] Zhang, Y., Y. Liu, X. Sun, W. Zeng, H. Xing, J. Lin, S. Kang, L. Yu, Application of microbially induced calcium carbonate precipitation (MICP) technique in concrete crack repair: A review, Construction and Building Materials 411 (2024) 134313.

Chapter 6 Conclusions and Recommendations

6.1 Summary and Conclusions

This thesis evaluated the potential of natural fibres (jute and flax) and expanded perlite aggregate (EPA) as bacterial carriers to enhance the self-healing capacity of cementitious composites through microbial-induced calcium carbonate precipitation (MICP). The research focused on fibre-microbe interactions, bacterial colonisation behaviour, crack closure performance, and water permeability recovery. A comprehensive series of laboratory experiments were conducted to understand the synergy between bacterial activity and carrier type, with the aim of identifying a more effective and sustainable alternative to conventional self-healing systems. The key findings of this thesis are summarised below:

Jute fibres facilitated rapid and stable bacterial proliferation, confirmed by optical density (OD600) measurements and microscopy. Flax fibres supported moderate microbial growth, while EPA presented limited bacterial support, resulting in negligible biopolymer presence. This outcome highlighted the crucial role of carrier material choice in sustaining bacterial viability and promoting effective biopolymer formation, essential for subsequent mineralisation.

The microscopic interaction analysis demonstrated that carrier surface characteristics significantly influenced bacterial adhesion and mineral deposition. Among the materials tested, jute fibres exhibited the most effective surface properties due to their roughness and porous structure, enabling extensive bacterial colonisation and multi-layered biopolymer formation. Flax fibres supported moderate biopolymer formation, while EPA, characterised by smoother

surfaces, showed limited bacterial interaction. The robust bacterial attachment on natural fibres enhanced their potential for subsequent calcium carbonate precipitation.

In assessing crack-healing performance, jute fibres emerged as the superior carrier, successfully healing cracks up to 1.23 mm wide. The effectiveness of jute was attributed to its ability to act both as a microbial carrier and a physical bridging material within cracks, significantly enhancing calcium carbonate deposition along crack interfaces. Flax fibres demonstrated moderate healing capabilities, mainly effective in smaller cracks up to approximately 1.0 mm. EPA exhibited significantly lower performance, showing limited healing efficacy, particularly in wider cracks, due to inadequate bacterial colonisation and sparse calcium carbonate formation.

The water permeability reduction tests clearly supported the superiority of natural fibres in enhancing crack sealing. After the healing period, mortar specimens containing jute fibres exhibited the greatest reduction in water permeability, highlighting effective crack sealing and restoration of barrier properties. Flax fibres showed moderate improvements, while EPA specimens displayed minimal change, indicating insufficient sealing performance. This evidence further reinforced the critical importance of the carrier's structural properties and bacterial compatibility in achieving durable and effective crack repair in cementitious composites.

6.2 Recommendations for Future Research

Despite the successful demonstration of the effectiveness of natural fibres in promoting self-healing, several aspects warrant further investigation. Based on the experimental results and identified limitations, the following recommendations are proposed:

(1) Natural fibres were employed here in a single, uniformly conditioned state; longitudinal fibre-level data were not collected. Follow-up work should measure, at multiple ages (e.g., 7, 28, 56, 90 days), (i) single-fibre tensile properties and interfacial bond (pull-out/micro-bond), (ii) pore structure (MIP/BET, dynamic-vapour sorption, micro-CT of lumen/connectivity), and (iii) surface chemistry (SEM–EDS, FTIR, XPS/ToF-SIMS) before and after $CaCO_3$ deposition in alkaline pore solutions. These measurements will link mineral crusting to changes in bridging efficiency, water management, and durability at the composite scale.

(2) To substantiate mineral and polymer identity, future studies will integrate SEM–EDS point spectra with X-ray elemental mapping (EDS maps) on polished cross-sections, verifying Ca–C–O co-location at deposits on fibres and within EPA pores. Where appropriate, XPS/ToF-SIMS and EPS biochemical assays (total carbohydrate/protein; lectin-based confocal staining) will fingerprint extracellular polymers. This package overcomes FTIR's non-uniqueness (C–O/C–H bands in native fibres) and provides phase-resolved, spatially explicit validation.

(3) Although the ureolytic strain used here is alkali-tolerant, cellulose/hemicellulose-rich fibres may moderate near-surface pH and release dissolved organic carbon (DOC) that influences colonisation. Future work will map interfacial pH with micro-electrodes or fluorescent

indicators and quantify DOC/TOC from fibre leachates under controlled bulk alkalinity, then relate these measurements to biofilm continuity and mineral coverage

(4) Resin-impregnated, polished cross-sections of cracked/healed specimens will be analysed by line-scan SEM–EDS and X-ray elemental mapping from the EPA exterior into the interior to quantify any gradients in $CaCO_3$ and associated elements. CLSM live/dead imaging and micro-CT can complement this by resolving viability and pore connectivity with depth.

(5) Beyond the flow-based proxy used here, direct 3-D characterisation is needed. Micro-CT will yield connected-porosity and tortuosity metrics in the crack-adjacent zone before/after healing. MIP and/or NMR relaxometry/gas adsorption will provide pore-size distributions. The hydraulic results will be interpreted together with these structural metrics to isolate how healing narrows hydraulic aperture, adds constrictions, and increases tortuosity.

(6) Longitudinal characterisation that follows the same fibres through service-relevant ages (for example 7, 28, 56 and 90 days) and quantifies how their properties develop with exposure. Single-fibre tensile tests and micro-bond/pull-out experiments will track changes in intrinsic strength, stiffness and interfacial bond as mineral crusts form at the fibre–matrix interface. In parallel, pore-structure measurements—mercury intrusion or gas-adsorption for pore size/volume, dynamic-vapour sorption for moisture retention, and micro-CT for lumen/connectivity—will document how capillary pathways are altered by alkali treatment and $CaCO_3$ deposition.

(7) Future figures will pair high-magnification SEM with annotated EDS maps (Ca, C, O) and scale bars at consistent magnification. Where needed, Raman/XRD will differentiate

calcite/vaterite. This will convert qualitative morphology into quantitative, phase-resolved documentation of healing products.

(8) Quantify pore structure with mercury intrusion porosimetry for macro-pores, and micro-CT for three-dimensional connectivity and tortuosity. These structural data will be coupled with sorptivity/imbibition tests and tracer-release experiments to obtain kinetic descriptors—such as a release half-time and an effective connected-porosity index—under the same microbiology and mix conditions used here. Comparing these indices for reservoir type carriers and surface-scaffold carriers will explain when a large internal volume is advantageous and when hierarchical capillarity and wicking to the surface dominate performance. The outcome will be a quantitative basis for choosing carriers that balance capacity with controlled delivery at the crack interface, and for defining the crack-width range within which each carrier type is most effective.

By addressing these research gaps, the field can progress towards reliable, scalable, and sustainable self-healing concrete systems suitable for a wide range of infrastructure applications. The demonstrated potential of natural fibres—particularly jute—suggests that bio-based, environmentally friendly materials are viable alternatives to traditional synthetic carriers and may play a key role in the development of next-generation cementitious composites.